Titre: Title:	High Barrier Water-Based Polymer/Clay Nanocomposite Coating
Auteur: Author:	Fatma Ben Dhieb
Date:	2019
Type:	Mémoire ou thèse / Dissertation or Thesis
Référence: Citation:	Ben Dhieb, F. (2019). High Barrier Water-Based Polymer/Clay Nanocomposite Coating [Thèse de doctorat, Polytechnique Montréal]. PolyPublie. https://publications.polymtl.ca/4010/

POLYTECHNIQUE MONTRÉAL

affiliée à l'Université de Montréal

High Barrier Water-Based Polymer/clay Nanocomposite Coating

FATMA BEN DHIEB

Département de génie chimique

Thèse présentée en vue de l'obtention du diplôme de *Philosophiæ Doctor*

Génie chimique

Août 2019

POLYTECHNIQUE MONTRÉAL

affiliée à l'Université de Montréal

Cette thèse intitulée :

High Barrier Water-Based Polymer/clay Nanocomposite Coating

présentée par **Fatma BEN DHIEB**

en vue de l'obtention du diplôme de *Philosophiæ Doctor*

a été dûment acceptée par le jury d'examen constitué de :

Nick VIRGILIO, président
Abdellah AJJI, membre et directeur de recherche
Frej MIGHRI, membre et codirecteur de recherche
Seyed Hesamoddin TABATABAEI, membre et codirecteur de recherche
Marie-Claude HEUZEY, membre
Suprakas SINHA RAY, membre externe

DEDICATION

To my mother

ACKNOWLEDGEMENTS

I would like first to show my deepest gratitude to Professor Abdellah Ajji, my supervisor, for giving me the opportunity to work on this project. The trust he placed in me helped me to grow professionally and I had always something to learn from our conversations.

My co-directors Pr. Frej Mighri and Dr. Hesam Tabatabaei have been of great support and even though we didn't meet often, their expertise and advices helped advancing this work.

I can't thank enough our team members, Ebrahim Jalali Dil, Claire Cerclé, Redouane Boutrouka and Richard Silverwood who helped me in so many aspects of this project with their expertise and the interesting discussions that we had.

During this period at Polytechnique I met wonderful people that became friends, among them some of my group colleagues, Hanan, Hoda, Hajer, Mounia, Zohreh, Zahra, Nury, Nusrat and Shiva with whom I shared so many great memories and to whom I am thankful for the moral support.

Other than my group, I have met amazing people at Polytechnique specially Navid, Julien, Mario, Charles, Ivan and Matthieu. Having them around made some tough days easier with their contagious cheerfulness.

I'm grateful also to my family, for their constant encouragement and specially my mother, she gave me confidence and believed in me. She also knew every time how to make my worries look so tiny.

Last but not least, I'm grateful for my partner who gave me strength to overcome my issues. He always had good advices for my project and have been my rock during all these years.

RÉSUMÉ

Face au besoin urgent de matériaux recyclables, il existe un intérêt croissant pour l'amélioration des emballages existants tels que les emballages multicouches. Cet emballage contient différentes couches de polymères, chacune répondant à un besoin différent, comme la barrière aux gaz, les propriétés mécaniques et la qualité du scellage. Pour assurer la barrière à l'oxygène, la couche barrière est généralement un polymère très peu perméable tel que l'alcool éthylène vinylique (EVOH) et le nylon. Cela présente toutefois des inconvénients tels que le coût et la non recyclabilité de l'emballage.

Une alternative intéressante pour remplacer cette couche est l'utilisation d'un revêtement haute barrière. À cette fin, le revêtement nanocomposite a été étudié dans cette thèse. La Montmorillonite (MMT) a été choisie comme charge en raison de sa disponibilité et de son prix abordable. Afin de mieux comprendre l'effet des polymères sur les propriétés de l'argile dans un revêtement nanocomposite, quatre polymères ont été choisis pour étudier les revêtements à base de liaisons hydrogène ; l'oxyde de polyéthylène (PEO), le polyvinylpyrrolidone (PVP), le chitosane (CS) et l'alcool polyvinylique (PVA).

En utilisant la technique de dépôt couche par couche (LbL), deux structures différentes, bicouche et quadricouche, ont été étudiées, qui diffèrent par le nombre de couches de l'unité répétitive (deux et quatre respectivement). Pour la structure bicouche, PVA, PEO et PVP ont été utilisés avec la MMT, tandis que dans la structure quadricouche, deux couches de CS ont été ajoutées à l'unité répétitive. L'avantage d'utiliser ces trois polymères (PEO, PVP, PVA) est la différence au niveau de leurs structures et leur liaison hydrogène avec la MMT qui permet une comparaison intéressante de leurs effets sur les propriétés de l'argile et sur la perméabilité.

Outre la barrière de ces revêtements, les propriétés de la MMT ont été étudiées en utilisant la diffraction des rayons X pour calculer l'espacement entre les couches et la spectroscopie infrarouge pour déterminer son orientation. Selon les résultats obtenus, le polymère choisi pour la structure LbL affecte l'orientation et l'intercalation de l'argile. Pour souligner l'importance de la région interfaciale dans les nanocomposites ayant une concentration élevée en charge, les données expérimentales de perméabilité ont été comparées à certains modèles de perméabilité existants et, à partir de ces résultats, une modification du modèle de Nielsen a été suggérée.

Dans la première partie de la thèse, le revêtement LbL a été appliqué par trempage, ce qui n'est pas couramment utilisé dans l'industrie. Pour préparer l'industrialisation de ce procédé, la technique 'Doctor Blade' a été choisie. L'avantage d'utiliser cette technique, est sa similarité avec les procédés industriels et le meilleur contrôle sur le volume de revêtement déposé que le trempage. Pour cette partie de la thèse, des revêtements de PVA-MMT ont été déposés par LbL avec les deux techniques. Pour réduire leur perméabilité, les deux revêtements ont été réticulés avec du glyoxal et du glutaraldéhyde. Les propriétés barrières ont été déterminées pour différentes valeurs de l'humidité relative afin d'évaluer l'impact de la technique de revêtement sur la barrière à l'oxygène.
La morphologie du film et les propriétés de l'argile ont également été caractérisées. Étant donné que les agents de réticulation sont généralement soumis à des limitations concernant leur utilisation dans des emballages alimentaires, une approche différente a été étudiée pour réduire la perméabilité à l'oxygène. Elle consiste à augmenter la concentration de la solution de PVA, ce qui améliore considérablement la barrière à l'oxygène, même pour une humidité relative élevée. Un résultat différent a été obtenu avec l'augmentation de la concentration de la solution de MMT, car elle détériorait la perméabilité, que ce soit pour une humidité relative faible ou élevée. Cette partie a donc montré l'impact de la technique de revêtement sur les propriétés du revêtement.

La réticulation étant souvent considérée pour améliorer la barrière à l'oxygène, la dernière partie de ce travail a été consacrée à l'étude de la cinétique de réticulation. Deux types de revêtements ont été déposés par LbL sur un substrat de PET, PVA et PVA-MMT. Pour comprendre le mécanisme de réticulation, ces revêtements ont été réticulés avec du glyoxal pour différentes périodes de temps et leur perméabilité a été déterminée. Les résultats de perméabilité pour ces temps de réticulation ont permis l'identification des étapes de réticulation. La réaction de réticulation étant réversible, un environnement acide a été adopté pour étudier la cinétique de la réaction et déterminer la constante de réaction apparente. La caractérisation FTIR de ces revêtements a conduit à une corrélation entre les coefficients de perméabilité et l'intensité des pics FTIR pour une réaction avec et sans l'ajout d'un acide.

ABSTRACT

With the urgent need for recyclable materials, there's a growing interest for the improvement of existing packaging like the multilayer packaging. This package has different layers of polymers, each one fulfilling a different need like gas barrier, mechanical properties and saleability. To ensure the barrier to oxygen, the barrier layer, is generally a high barrier polymer like ethylene vinyl alcohol (EVOH) and Nylon. This, however, has some drawbacks like the cost and the non recyclability of the package.

One interesting alternative to replace this layer is the use of a high barrier coating. To this aim, a nanocomposite coating was the focus of this thesis. Montmorillonite (MMT) was chosen as the filler due to its availability and affordable price. To provide a deeper understanding of the effect of polymers on the properties of clay in a nanocomposite coating, four polymers were chosen to study hydrogen bonding based coatings; polyethylene oxide (PEO), polyvinylpyrrolidone (PVP), chitosan (CS), and polyvinyl alcohol (PVA). Using the Layer by Layer (LbL) deposition technique, two different structures, bilayer and quadlayer were investigated, which differ in the layers number of the repetitive unit (two and four respectively). For the bilayer structure, PVA, PEO and PVP were used with MMT while in the quadlayer structure, two layers of CS were added to the repetitive unit. The advantage of using these three polymers (PEO, PVP, PVA) is that their different structures as well as their different type of hydrogen bonding with MMT, allow an interesting comparison of their effect on clay properties and the nanocomposite permeability.

Beside the barrier of these coatings, MMT properties were investigated using X-ray diffraction for calculating the interlayer spacing and infra red spectroscopy to determine its orientation. According to the obtained results, the chosen polymer for the LbL structure, affects the clay orientation and intercalation. To highlight the importance of the interfacial region in nanocomposites, with high filler loading, experimental permeability data were compared to some existing permeability models and based on those results, a modification of Nielsen's model was suggested.

In the first part of the thesis, LbL coating was applied by dipping which is not commonly used in industry. To prepare for the scale up of this process, a blading technique was chosen using a Doctor Blade. The advantage of using blade coating is its similarity with industrial processes and the better control of the deposited coating volume than dipping. For this part of the thesis, PVA-MMT coatings were deposited by LbL with blade and dip coating. To reduce their permeability, both

coatings were crosslinked with glyoxal and glutaraldehyde. The barrier properties were determined for different values of relative humidity (RH), to evaluate the impact of the coating technique on the oxygen barrier. The film morphology and the clay properties were also characterized. Since crosslinkers are usually subject to limitations regarding their use in food packaging, a different approach was investigated to reduce oxygen permeability. It consisted in increasing the concentration of the PVA solution which improved considerably the oxygen barrier even for high RH. A different result was obtained with the increase of MMT solution concentration as it increased the permeability whether for low or high RH.
This part showed, thus, the importance of the coating technique in shaping the coating properties.

Since crosslinking is often considered for improving oxygen barrier, the last part of this work was dedicated to the study of crosslinking kinetic. Two types of coating were deposited by LbL on a PET substrate, PVA and PVA-MMT. To understand the crosslinking mechanism, these coatings were crosslinked with glyoxal for different times and their permeability was determined. The permeability results for these crosslinking times allowed the identification of the crosslinking steps. As the crosslinking reaction is reversible, acidic environment was adopted for the investigation of the reaction kinetic and determining the apparent reaction rate constant. The FTIR characterization of these coatings, led to a correlation between the permeability coefficients and the intensity of the FTIR peaks for both mild condition and acidic environment reaction.

TABLE OF CONTENTS

LIST OF TABLES

LIST OF FIGURES

LIST OF SYMBOLS AND ABBREVIATIONS

CA	Contact angle
CS	Chitosan
DB	Doctor Blade
GA	Glutaraldehyde
Gly	Glyoxal
LbL	Layer by Layer
MMT	Montmorillonite
PEI	Polyethylene imine
PET	Polyethylene terephthalate
PEO	Polyethylene oxide
PVA	Polyvinyl alcohol
PVP	Polyvinyl pyrrolidone
RH	Relative humidity

LIST OF APPENDICES

CHAPTER 1 INTRODUCTION

Packaged food products require a specific concentration of gas in the package for their storage in order to keep their properties during their expected shelf life. Some of them tolerate only a very low oxygen concentration. Various types of packaging are already in the market with a high barrier to gas. Multilayer packaging, metal and oxide coatings are among the most produced.

Both methods are expensive and in the case of silicon oxide, SiO_x, the package is less flexible and therefore easily subject to the development of flex cracking. Other than this criterion, today's stringent environmental measures have led to an increased demand for recyclable packaging material.

Incorporating fillers into the polymer to improve its properties has gained in popularity, especially with biodegradable polymers. Affordable and available fillers like clay and nanocellulose, have seen an increasing interest during these last decades. This approach has been intensively studied for films prepared by casting and extrusion. While an improvement has been observed, incorporating clay is limited mainly by a maximum concentration beyond which the mechanical properties of the film deteriorate due to the accumulation of clay platelets. The minimum permeability observed for the oxygen barrier was around 10^{-21} (m^2 s^{-1} Pa^{-1}) for the extrusion and 5.71 10^{-22} (m^2 s^{-1} Pa^{-1}) for casting [1], whereas nanocomposite coatings have resulted in better properties and a high gas barrier. Those coatings are interesting for packaging industry. With such thin coatings to replace barrier polymers in multilayer structures, the package can be recycled.

For these coatings to be integrated in the package, the resulting permeability must be similar or lower than the permeability of high barrier polymers like polyvinyl alcohol (PVA) (0.2 cm^3. µm/(m^2.day.atm))

This permeability can be reduced further using the method of successive deposition of polymer layers (Layer by Layer, LbL), which results in coated films with a high oxygen barrier in addition to the excellent exfoliation of clay platelets. This method, however, can not be applicable to all polymers, as it is limited to polymers able to establish hydrogen bonds or electrostatic interaction.

The main objective of this work is to produce a high barrier nanocomposite coating with the LbL technique in order to improve the recyclability of multilayer structures.

To achieve this goal, a fundamental study of the hydrogen bonding in nanocomposite coating was first conducted and LbL was used to deposit coatings by dipping the substrate in the polymers and clay solutions. Two types of assemblies, bilayers and quadlayers, were of interest and three polymers (PVA, PEO, PVP) were deposited along with clay or with clay and chitosan on PET substrate. The effect of their interaction with clay and their structure on permeability and clay properties were investigated. The obtained permeability was also compared to the prediction of known permeability models. This dipping technique was then compared to blading by focusing only in PVA-MMT coatings. Crosslinking with two dialdehydes, glyoxal and glutaraldehyde was first studied to reduce the permeability. The hydrophobicity and morphology of the coatings surface were also investigated. The composition of those coatings was then tailored in order to compare the obtained permeability to the one of crosslinked coatings. For the final part, the crosslinking reaction of PVA with glyoxal in a LbL coating was of interest. The reversibility of this reaction was studied for both PVA and PVA- MMT coatings and FTIR characterization was done to develop a correlation between the permeability and the FTIR absorption intensity. This correlation represents an important step in the study of this reaction kinetic.

This work is summarized in three articles that have been published or submitted to a scientific journal and this thesis consists of the following sections:

- Chapter 2 provides a literature review that covers the main topics of this thesis and a description of the originality of this work and its main and specific objectives.
- The selected materials, the adopted methodology and the characterization techniques are described in chapter 3. It's followed by a brief description of the articles organization in chapter 4.
- The main achievements of this work are given in the format of three scientific papers in chapters 5,6 ad 7
- A critical discussion of this work and its main issues is presented in chapter 8.
- Finally, the conclusions of this work and the recommendations for future work on nanocomposite coatings are presented in chapter 9.

CHAPTER 2 LITERATURE REVIEW

2.1 Reducing permeability in packaging

2.1.1 Permeability of a package

The main function of a package is the control of the needed concentration of gas inside it, required to reach the expected shelf life of the product. Some sort of food like vegetables need breathable packaging, that permits the diffusion of a high concentration of oxygen whereas others like dry fruits tend to lose their characteristic properties with the exposure to small amount of oxygen. Thus, the starting point to design a package is the required shelf life. The selected materials and their thickness define the permeability:

$$P = \frac{Q.L}{A.t.\Delta p} \tag{2.1}$$

With L and A, the thickness of the material and the surface area through which gas permeates. This permeability coefficient represents the permeated gas quantity Q, during a time t with a certain pressure difference Δp.[2] Besides the packaging material, the permeability depends also on the permeant gas, as the solubility and the diffusion coefficients, S and D respectively, vary according to the permeant gas and the polymer:

$$P = S.D \tag{2.2}$$

D is specific to the permeant gas – polymer pair and varies from 10^{-8} to 10^{-13} cm^2/s for solid polymers whereas S is a thermodynamic parameter that indicates the sorption capacity of a polymer for a certain molecule.[3]

D and S follow Arrhenius law which implies that temperature is a very important parameter to be determined when testing permeability. According to Fick's second law, the concentration of the diffusing permeant is linked to the D coefficient and the diffusing rate at the unsteady state.

$$\frac{\partial C}{\partial t} = D\,\frac{\partial^2 C}{\partial x^2} \tag{2.3}$$

This equation can have a simplified solution, equation 2.4. By fitting of the curve of flux as function of time, Figure 2.1, D and P can be determined and S calculated with equation 2.2[4]:

$$J(t) = \frac{Pp}{l}[1 + 2\sum_{n=1}^{\infty}(-1)^n \exp(-\frac{D\pi^2 n^2 t}{l^2})] \quad (2.4)$$

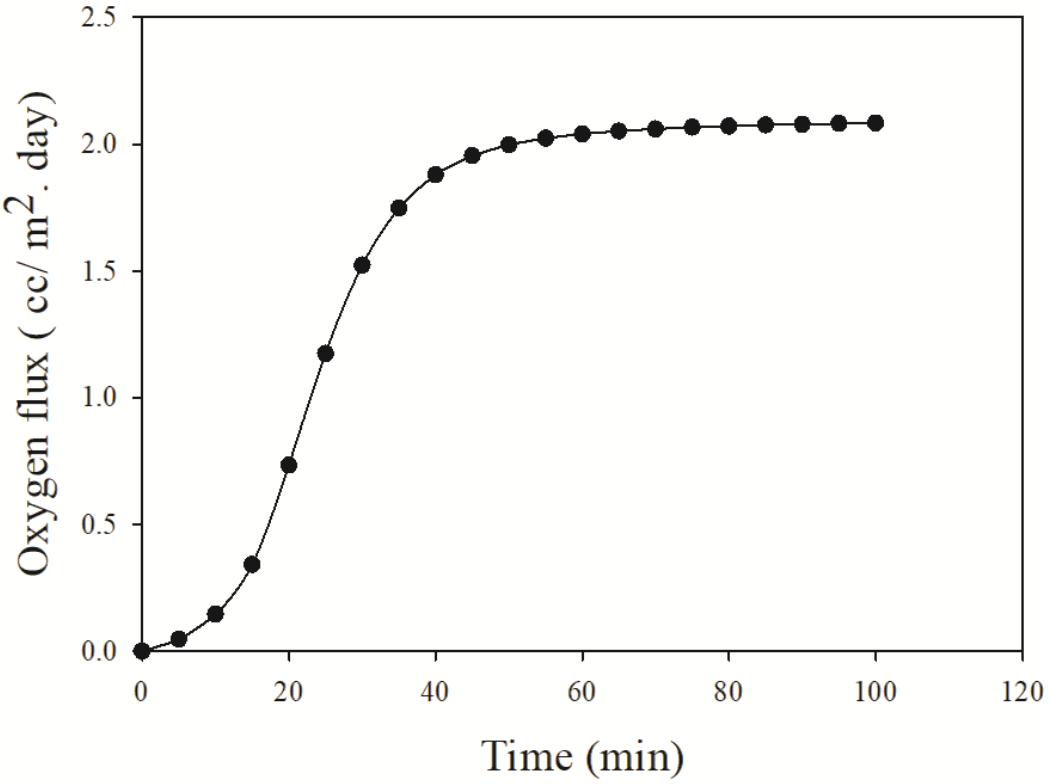

Figure 2.1 Experimental data flux of a coated PET film

2.1.2 Conventional methods for reducing permeability

2.1.2.1 Multilayer structure

To have layers of polymers, a multilayer structure can be obtained by lamination or coextrusion. Lamination is the joining of polymers layers, which can also include paper or aluminium foil. A water or solvent based adhesive is used for adhesive lamination. It's applied by a wet or a dry-bonding process. For the former, the adhesive is applied in between the layers and then dried in an oven to evaporate the solvent while for the latter, the adhesive is applied to one of the substrates, dried, and then the second substrate is added to the laminated structure. A solid adhesive, mixture

of polymers and waxes, is also used for lamination. In this case, it's melted and then applied in between the layers to laminate them while cooling. For extrusion lamination, a polymer is used in the same manner as the solid adhesive except that it's extrusion melted.[2]

Coextrusion: it can be processed by casting or film blowing. In either case, polymers are melted simultaneously in separate extruders and then injected through a die with separate exits that brings them together as sheets without mixing them. To avoid delamination of the resulting product due to poor polymers compatibility, a tie layer is used to increase the adhesion in between layers.[5]

Multilayers structure is extensively used to produce a variety of product for food packaging. The main advantage of such structure is that the final properties of the package are the sum of the properties of all the layers which explain its popularity. An example of such structure is the package for stuffed pasta, produced by Reifenhäuser Kiefel Extrusion GmbH, represented in Figure 2.2. The barrier properties are due to the ethyl vinyl alcohol (EVOH) layer, the mechanical properties to the low-density polyethylene (LDPE) layers and since many barrier polymers lose their efficiency with humidity, polyethylene layers act as water barrier.

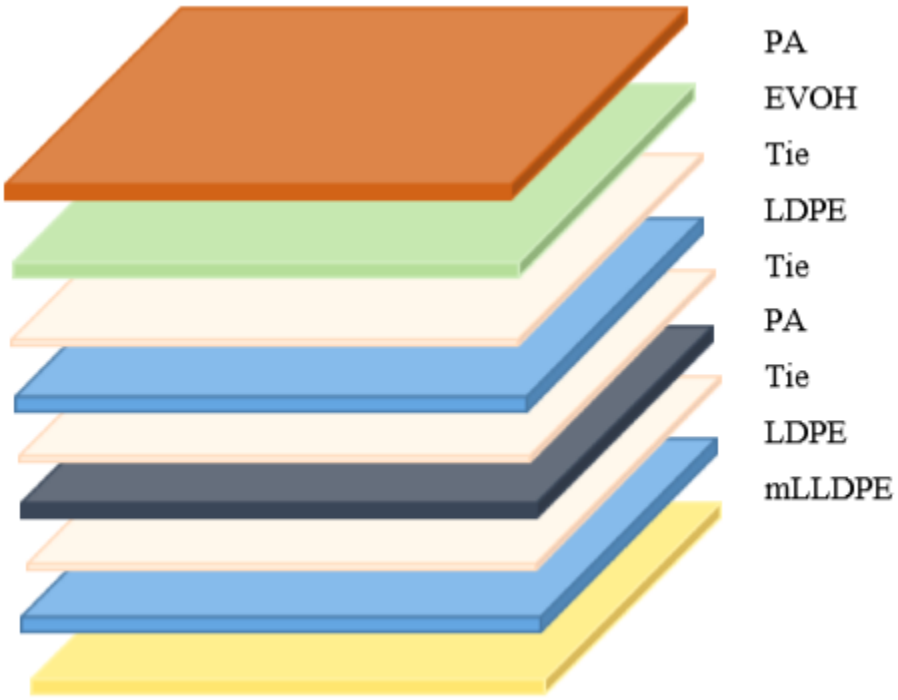

Figure 2.2 9-Layer structure of a multilayer package from Reifenhäuser Kiefel Extrusion GmbH

These barrier properties depend closely on the polymer's structure which can change according to many factors like polarity, crystallinity and chains orientation. The polarity of a polymer is due to the interactions between chains (hydrogen bonds for example) resulting in a compact structure. For semi crystalline polymers, crystalline parts are impermeable which increase the oxygen barrier. Some of the high oxygen barrier polymers are reported in Table 2.1.

Table 2.1 Oxygen permeability of some high barrier polymers

Polymers	Permeability (cm^3 cm/cm^2 s Pa)	References
Ethyl vinyl alcohol (EVOH)	$0.000105\ 10^{-13}$	6
Liquid crystal polymer (LCP)	$0.00023\ 10^{-13}$	7
Poly (m-xylene adipamide) MXD6	$0.000765\ 10^{-13}$	8
Polyethylene naphtalate (PEN)	$0.008\ 10^{-13}$	9
Polyacrylonitrile (PAN)	$0.00015\ 10^{-13}$	
Polyamide 6 (PA6)	$0.0285\ 10^{-13}$	
Polyvinylidene chloride (PVDC)	$0.004\ 10^{-13}$	

Even though the multilayer structure has a polymer layer specific to oxygen barrier, the permeability of the package is determined by considering all the layers:

$$\frac{L_T}{P_T} = \sum \frac{L_i}{P_i} \tag{2.5}$$

With L_T, P_T the thickness and permeability of the package respectively and L_i, P_i are the thickness and permeability of each layer.

2.1.2.2 **Use of fillers**

Among the alternatives to improve mechanical properties and the gas barrier of the film is the addition of a filler. This nanocomposites are usually obtained by solution casting, melt processing or in situ polymerization.[10] Fillers can be used with different process and allow a remarkable improvement of the nanocomposite properties even with small amounts. Nanoclay had been extensively studied for the last decades, more precisely, since the work of a Toyota research team, in 1980 [1] that showed its potential. The reduction of permeability with the incorporation of the filler is due to the tortuosity in the film. This describes the path of the diffusing molecule through the nanocomposites. Due to the fillers, this path becomes sinuous increasing thus the diffusion time which decrease the permeability, Figure 2.3.

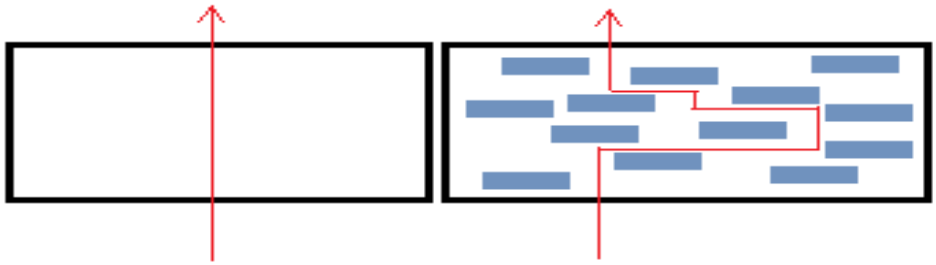

Figure 2.3 Simulation of the path of a penetrant particle in a nanocomposite and a neat polymer

This tortuosity, τ is usually described as inversely proportional to the permeability ratio[11]:

$$\frac{P_n}{P_0} = \frac{1-\emptyset}{\tau} \tag{2.6}$$

With P_n the permeability of the nanocomposite, P_0 the permeability of the neat polymer and $\emptyset$ the volume fraction of the filler.

2.1.2.3 **Polymer blends**

Blending polymers to obtain a high barrier material consists mainly in mixing a high barrier polymer with one or more polymers. Such structure enables achieving the desired properties with a reasonable cost. Among the known miscible blends, there is polystyrene-poly (vinyl methyl ether) (PS/PVME) and poly (vinylidene fluoride)-poly- (methyl methacrylate) (PVDF/PMMA). Some blends, even though immiscible thermodynamically, still have interesting properties. Those are the compatible blends, a good example is the high impact polystyrene, PS, (rubber as dispersed phase

in PS) and acrylonitrile, butadiene and styrene polymers (ABS).[12] As the big majority of polymer blends is immiscible, compatibilization is an important part of the process. The compatibilizer is located at the interface and has usually in its structure, a block miscible with one of the polymer and a second block miscible with the other polymer.[13]

2.1.2.4 **Coatings**

To reduce oxygen permeability, metal oxide and nanocomposite coatings are often used. Metal oxide coatings are extensively used since decades, due to the excellent barrier achieved, while the interest in nanocomposite coatings started much later, with the increasing awareness about ecofriendly material and the importance of recyclability.

To achieve a high oxygen barrier, metal and metal oxide coatings are usually applied to a polymeric substrate. Similar performance is also achieved by silicon oxides, that result in a transparent, thermally stable with a high gas barrier coating, that can lower considerably the permeability of the polymer substrate as well as its permeability to water vapor.[14] This is due to the low free volume in the coating and its covalent bonding with the substrate (Si-C and Si-O-C).[15] The deposition technologies for these coatings are mainly physical vapor deposition (PVD) and chemical vapor deposition (CVD). Volatile precursors are used for the CVD process and are decomposed by photons, heat or plasma. For polymers, that are thermally sensitive, plasma is usually applicable (plasma enhanced CVD (PECVD)) so that coating deposition can take place at a lower temperature. For the PVD, thermal evaporation or impact process are used to transform the particles to the gaseous state. Those particles are then deposited on a substrate under vacuum with a pressure usually lower than 0.1 mbar.[13] [16] These coatings have two types of defects, microdefects and nanodefects. Microdefects are pinholes , microcracks,[17] or uncoated areas for PE substrates due to a high surface roughness.[15] Nanodefects are responsible for the gas permeability increase and are due to the non equilibrium thermodynamic nature of these techniques. [18]

2.2 Nanocomposite coatings

2.2.1 Coating techniques

For gas barrier packaging material, nanocomposites coatings are a cheaper, more ecofriendly alternative than thin metal oxide films and high barrier polymer layer. Several techniques are used to deposit those coatings, among them roll, spray, spin, dip coating and doctor blading. All these techniques enable the deposition of coatings from the nanocomposite's solution after the solvent evaporation.

- Spin coating: The principle of this technique is maintaining the rotation of the substrate, while one or different polymers are injected sequentially onto the surface. This fast rotation allows the formation of thin films, faster than with dipping technique and gives a uniform coating[19] with a very orderly internal structure.[20]
- Spray coating: To enable spraying, the material is usually molten or dissolved in an appropriate solvent.[21] It's then projected with a nozzle on the substrate surface. Several spraying techniques are used, among them thermal, warm and vacuum plasma spraying.
- Roll to roll coating: the coating material is passed to the application roll by an auxiliary roll and the substrate is coated by going around a support roll and passing between this latter and the application roll.
- Gravure coating: An engraved roll is used for this technique and its cavities are filled with the coating material. Once the excess removed from the roll with a blade, the substrate is coated by passing between this roll and a pressure roll.[22]
- Doctor blading: This technique has little to no waste as the nanocomposite solution is spread on the substrate with a blade moving at a constant speed. The distance between the blade and the roll tailors the coating thickness. This technique can be transferable to a reel-to reel system with the condition of a high solution viscosity (100- 20 000 mPa s).[23]
- Dip coating: This technique consists in dipping the substrate in the desired coating solution and pulling it up at a certain speed, which controls the coating thickness.[24]

Depending on the choice of the technique, the properties of the film vary. Char et al compared the morphology and wettability of dip coated and spin coated films for a hydrogen bond assembly.

They concluded that a grainy aspect of the films was obtained with immersion while they were smoother with the spin coating.[25] A wide variety of fillers is used for polymer based coatings, like oxides, metallic particles, clay, carbon nanotube (CNT), graphene oxide,[26] nanocellulose and cellulose nanocrystal. Other than the properties of the matrix and the fillers, the permeability of a coating depends also on its thickness, roughness and density.[18]

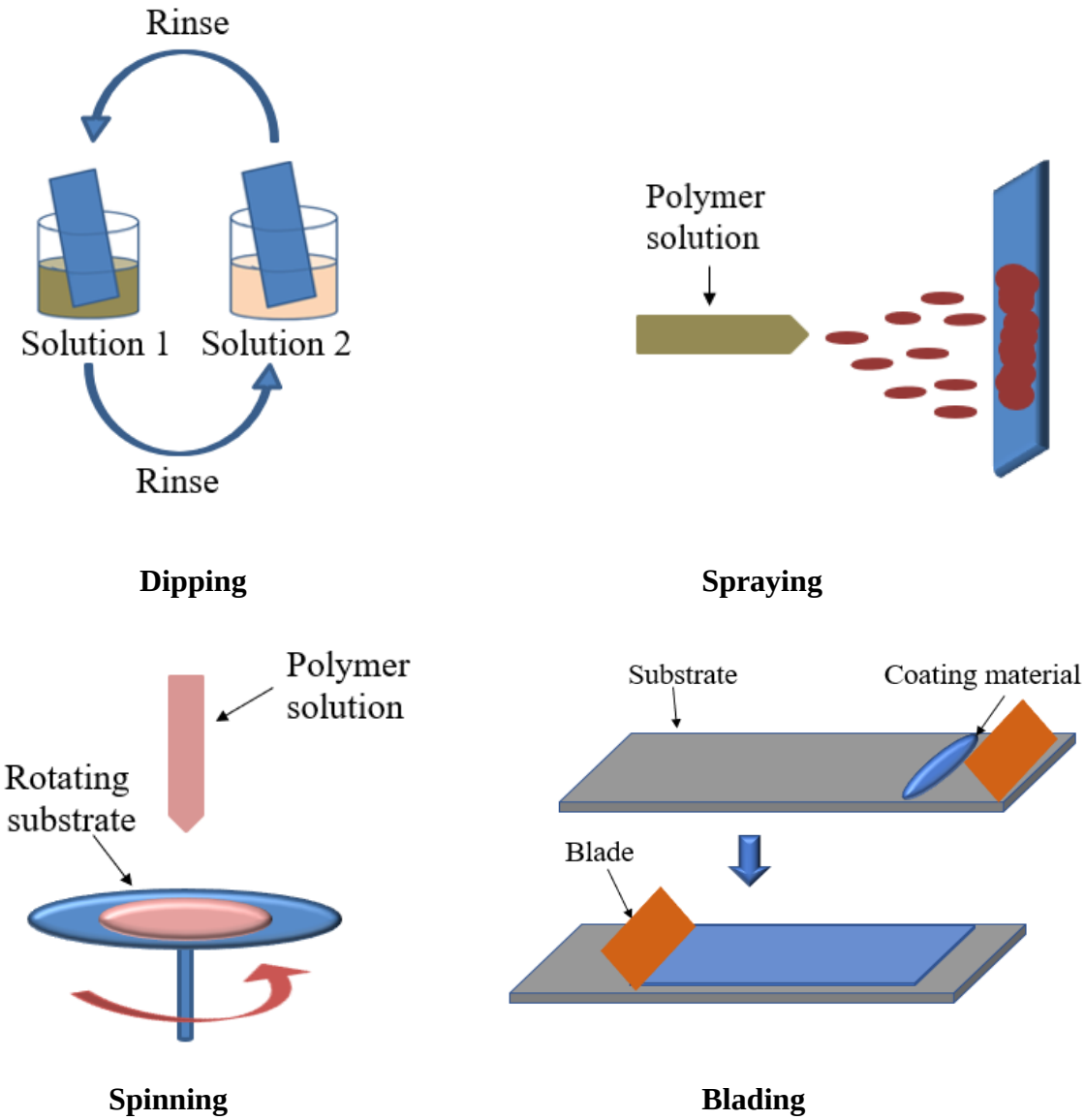

Figure 2.4 Some coating techniques

2.2.2 **Clay**

2.2.2.1 Clay structure

The smectites are among the most used clays as their high aspect ratio improves drastically the matrix properties. Among these clays, Montmorillonite showed great results. It's structured as a stack of several platelets[27] separated by an interlayer spacing of around 12 Å[28] filled with exchangeable cations. Each of this platelet has two layers of tetrahedral sandwiching an octahedral layer.[27] These platelets have on their surface oxygens linked to Si, which makes hydrogen bonding with intercalating polymers possible. Clay can be intercalated with polymers if there's enough affinity. In the case of a good interaction with the matrix and with the right process, these platelets can even exfoliate and become completely independent of their stack. Nanocomposites have better properties with exfoliated clay, but it's not evident to reach this state for many processes and for a high clay loading in the matrix. Clay properties that affect tortuosity are its volume fraction, intercalation state, the quality of its dispersion and its orientation.

2.2.2.2 Clay orientation

The clay orientation is usually investigated with Small Angle X ray Scattering (SAXS)[29] and FTIR spectroscopy. To determine clay orientation with infrared analysis, a polarizer is used to record three spectra in the transmission mode. These spectra have three different directions: vertical machine direction, S_M, horizontal transverse direction S_T and horizonal direction with the film tilted by an angle φ with respect to the machine direction (MD), S_{NT}.

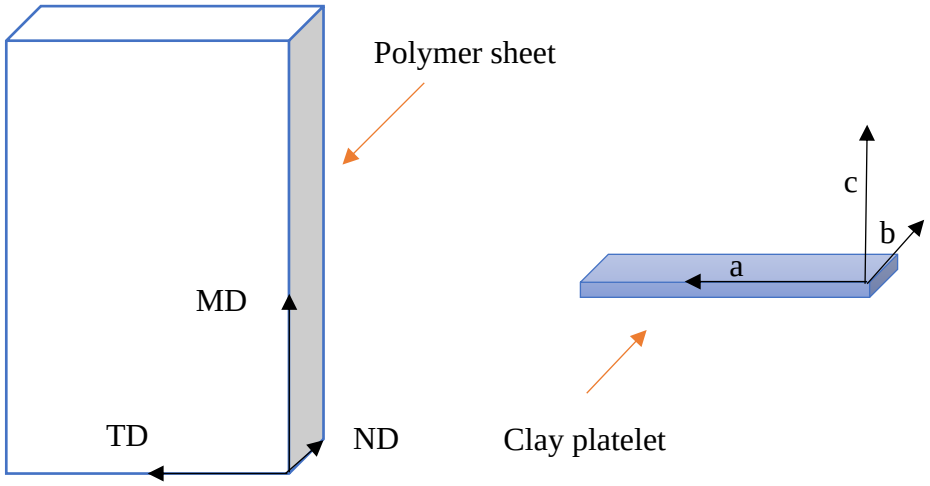

Figure 2.5 Illustration of the polymer and filler axes

The Montmorillonite (MMT) has four characteristic peaks at 1080, 1025, 1048, 1120 cm^{-1} [30] corresponding to the stretching of Si-O. Three of these peaks (1025, 1048 and 1120 cm^{-1}) are related to the basal oxygen, which is the oxygen at the surface of the clay platelets. The peak at 1080 cm^{-1} is specific to the apical oxygen, located at the internal edge of the tetrahedral sheet and with a Si-O bond perpendicular to the platelet plane. [31]

To determine the orientation, one of the needed spectra, S_N, is calculated with equation 2.7. [32]

$$S_N = \frac{S_{NT}(1-\frac{sin^2\varphi}{n^2})^{1/2} - S_T(1-\frac{sin^2\varphi}{n^2})}{sin^2\varphi/n^2} \quad (2.7)$$

The φ angle is 45 ° and the MMT refractive index n is 1.503 [33]. The last spectrum to be calculated, S_0, represents the average of the three spectra S_M, S_N and S_T. As S_n characterizes the normal direction to MMT platelets, the following Herman's orientation function [30], is used to calculate the orientation :

$$f_{CN} = 0.5(\frac{A_N}{A_0} - 1) \quad (2.8)$$

With A_N and A_0, the band intensities in the S_N and S_0 spectra related to the apical oxygen with a vibrational transition moment normal to the platelets and lies along the c-axis. $(\frac{A_N}{A_0})$ is referred to

as D, the dichroic ratio. For a better quantification of this orientation, the average clay orientation angle can be calculated, once the f_{CN} value is known, equation 2.9*:*

$$f_{CN} = \frac{3\langle cos^2\theta\rangle - 1}{2} \quad (2.9)$$

Clay orientation can be tailored by the used process and the choice of the matrix. Extrusion blow molding and blown films have usually a higher orientation than other techniques like compression molding or casting.[34] Even without compatibilization f_{CN} is around 0.8 for some blown samples[30] and it can be affected by the draw ratio (DR) (varies from 0.6 to 0.749 when the DR increases from 1 to 5).[35] Having a perfectly oriented and exfoliated clay is one of the challenges for clay-based nanocomposites. This can be achieved with the LbL technique that results in thin films with a high gas barrier competitive to the conventional materials.[36]

2.2.3 Layer by layer coating technique

This technique relies on the presence of interaction between polymers, usually electrostatic interactions or hydrogen bonding, so that their alternated deposition on a substrate results in a multilayer structure. This structure can also consist of polymers and nanoparticles. Clay nanoparticles, in particular, have been widely used in LbL as polyanions and have resulted in a clay-polymer structure with strong bonds, similar, in some cases, to nacre structure.[37] This technique has several advantages over conventional coating methods, mainly the simplicity of the process and the equipment, the ability to apply it to different shapes and the tunable thickness.[38] The only requirement for the deposition of this multilayer structure is the presence of interactions with the substrate, these films can therefore be produced on any surface and various fillers can be used like nanoparticles of oxide or clay platelets.[39] Many substrates are therefore corona treated to have a charged surface.[40] In other cases, a primer layer is first deposited on the substrate to improve the adherence of the LbL structure to the substrate. A Polyethylene imine (PEI) solution is often used as a primer. [41] The films obtained by LbL are characterized by a high barrier to oxygen but limited by their sensitivity to moisture as many studied polymers are water soluble. Laminating these films with a moisture-resistant film is often applied to preserve the oxygen barrier even at 95% relative humidity.[42] Since the first LbL films made by Decher in the 1990s, these films have been studied for several uses such as packaging, biomaterials, drug delivery and electrolytic

batteries.[43] Common coating techniques can be applied to LbL process with possible modification of some of them.[38, 44] The deposition of a nanocomposite coating by LbL is the same as depositing an all polymer LbL coating. The substrate is alternately dipped in the filler and the polymer solutions. The characterization of the LbL morphology showed an interpenetrative structure of the layers and mainly two type of structures, the "ladder like" and "scrambled egg".[45] The former is a more ordered structure due to equal charge compensation between layers.

2.3 Hydrogen bonding in LbL assembly

Interaction in between layers in LbL assemblies, vary according to the used material. Electrostatic interactions and hydrogen bonding for instance, are more common than the other types of interaction like hydrophobic or Van Der Waals forces.[38] LbL assemblies based on hydrogen bonding were introduced in 1997 by Rubner, Stockton et al.[38] Its main advantage is its applicability to a wide variety of polymers with good properties needed for many applications like packaging. Compared to electrostatic interactions, hydrogen bonding reduces the LbL films rigidity.[43, 46-47] An example of stiff LbL films is the polyethylene imine (PEI) /polyacrylic acid (PAA) assembly, which was modified by replacing PEI with polyethylene oxide (PEO) to have a film with similar behavior to elastomers.[41, 43] PEO, in particulier, have been used for LbL assemblies with various polymers, poly(methyl acrylate) (PMA)[48], PAA[41, 48] and poly(methacrylic acid) (PMAA).[25] Depending on the desired properties, flexible polymers like polyvinyl alcohol (PVA) or more rigid like PVP and chitosan (CS) can be used, Figure 2.8. PVA, in particular, has a high barrier to gas and has an excellent affinity to MMT which results in coatings with impressive mechanical properties.[49] Rigid polymers like polyvinyl pyrrolidone (PVP) and chitosan (CS) are also used for high barrier coatings. PVP in particular showed a highly structured assembly when inkjet printed by LbL alternately with clay,[50] while CS has an increasing interest due to its sustainability and its antimicrobial properties. CS can establish hydrogen bonds as well as electrostatic interactions resulting in a good interaction with various polymers as well as fillers. It has a good gas barrier and filmogenic properties making it attractive for the solution casting process.

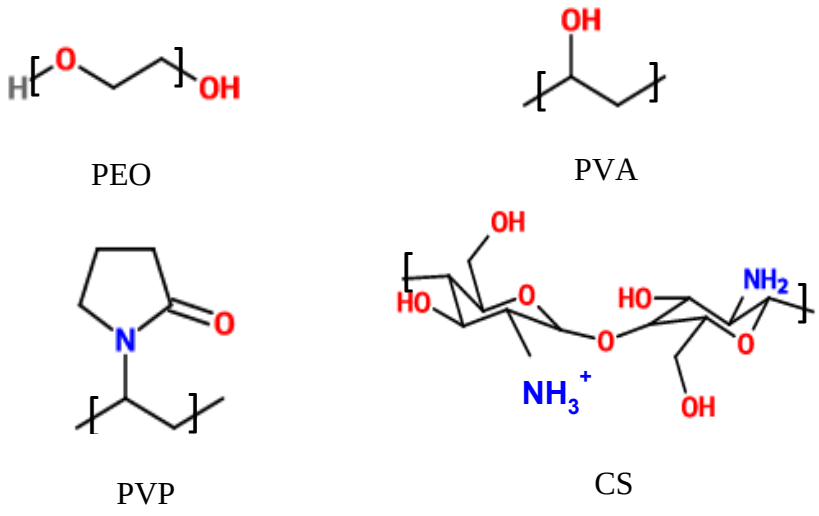

Figure 2.6 Structure of Chitosan, PVA, PVP and PEO

2.4 **Modeling permeability for nanocomposites**

The permeability of a certain gas through a polymer is affected by two parameters, the diffusion coefficient of this polymer and the solubility of the gas in it, equation 2.2. The gas molecules first adsorb on the polymer surface and then, diffuse through it. To diffuse, gas molecules jump into neighboring holes by the formation of a channel between the two holes.[51] According to this description there's a static and a dynamic free volume. The static is related to the properties of the holes in the matrix (number and size) and associated with the gas solubility whereas, the dynamic is dependent on the frequency of channel formation and is associated with the gas diffusivity.[52] In other words, the difference between the diffusion and the solubility coefficients is that the former is a kinetic factor associated to the mobility of the gas molecules in the matrix and the latter is a thermodynamic factor controlled by the affinity between the matrix and the diffusing molecules.[4] The diffusion through a nanocomposite is usually described by the tortuosity which is the reason for the improvement of the gas barrier properties. To describe the effect of the filler on the permeant gas and the matrix properties, many interesting models have been developed, Table 2.2. Nielsen's model is amongst the most used. This model describes the tortuosity as an increase in the gas path by a factor equal to $\frac{L\emptyset}{2W}$, equation 2.10, with L/W the filler's aspect ratio (L, the length and W, the

width of a platelet of filler) and Ø its volume fraction. This model assumes a perfectly oriented filler and an average of L/2 additional distance for each platelet that the diffusing gas molecule encounters while permeating through the nanocomposite. This model showed good permeability prediction for systems with 1% or less of fillers.[53]

$$\frac{P}{P_0} = \frac{1-Ø}{1+\frac{LØ}{2W}} \tag{2.10}$$

The main considered parameters are usually the filler's volume fraction and its aspect ratio. Few models considered also the orientation. Among the most used is the Bharadwaj's model. This latter is a modification of Nielsen's model with an introduction of an orientation parameter S, with three possible values, 0 for random orientation, 1 and -0.5 are for the two extremes, perfect alignment perpendicular to the surface and a vertical orientation, respectively.

$$\frac{P}{P_0} = \frac{1-Ø}{1+\frac{LØ}{2W}(\frac{2}{3})(S+\frac{1}{2})} \tag{2.11}$$

Bharadwaj considered Nielsen's model for the best orientation (S=1). For a vertical orientation, the tortuosity factor is equal to 1, meaning an absence of tortuosity in the nanocomposite.

a)

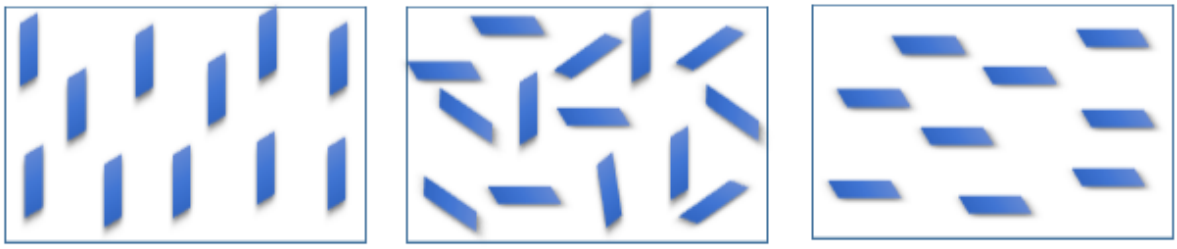

S= - 0.5 S= 0 S= 1

b)

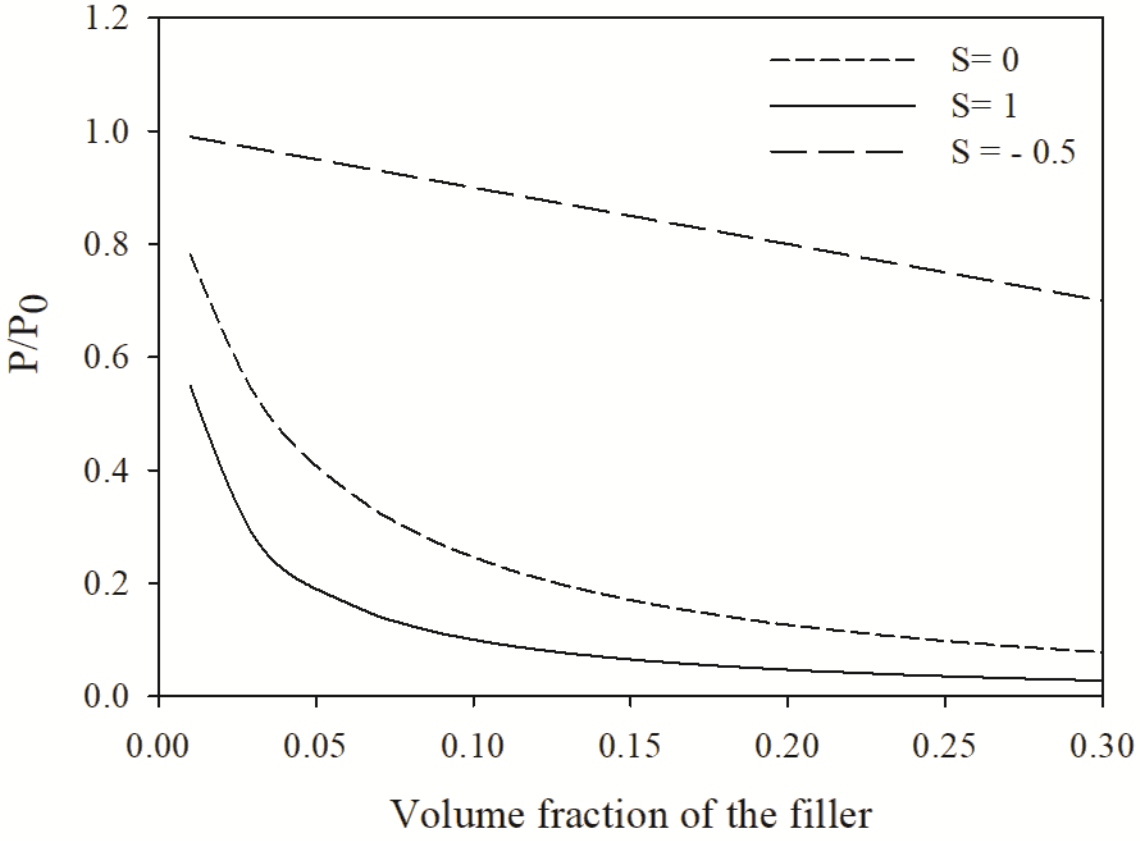

Figure 2.7 a) Clay orientation corresponding to the orientation factor, S[54] b) Variation of permeability ratio with filler orientation

Other models like Sorrentino's, considered more specific parameters for the orientation by using the orientation angle, θ:

$$\frac{P}{P_0} = \frac{1+\beta\emptyset}{(1-\emptyset)+\emptyset\,(\frac{L+2t}{L\sin\theta+2t\cos\theta})^2} \tag{2.12}$$

With β equal to:

$$\beta = \frac{V_s}{V_f}\frac{D_s}{D_0} - \frac{V_s+V_f}{V_f} \tag{2.13}$$

V_s , D_s the volume and the diffusion coefficient of the interface, V_f, the filler volume and D_0 the diffusion coefficient of the unmixed polymer.

By considering the orientation angle, the prediction of the nanocomposite permeability can be more accurate. The angle θ, can be obtained by calculating the Herman's orientation function. In Sorrentino's model, permeability varies considerably with the orientation which makes it a critical parameter to be determined.

The use of a ratio, P/P_0, is intended to limit the parameters of interest to the filler's properties (aspect ratio, volume fraction, orientation...). This, however, can not be always accurate, especially when the filler's percentage in the nanocomposite is high. Fillers like clay interact with the matrix and alter its structure in their vicinity. This is assumed to result in a fraction of the matrix with a higher density than the bulk. Some models like Sorrentino's considered this change by introducing a factor β that takes into account two parameters, a ratio of diffusivities, $\frac{D_s}{D_0}$ and a ratio of volumes, $\frac{V_s}{V_f}$. For such models, the difficulty resides in estimating two factors that are not easily quantifiable. Like Sorrentino, Beall[53] did also consider the interfacial region in its modeling but went further and considered, for the model discussion, three regions around the clay : the compatibilizer (the nearest region to the clay),1-2 nm , the constrained polymer which is the part of the matrix that is affected by the clay, 50-100 nm, and the neat polymer as the third region.

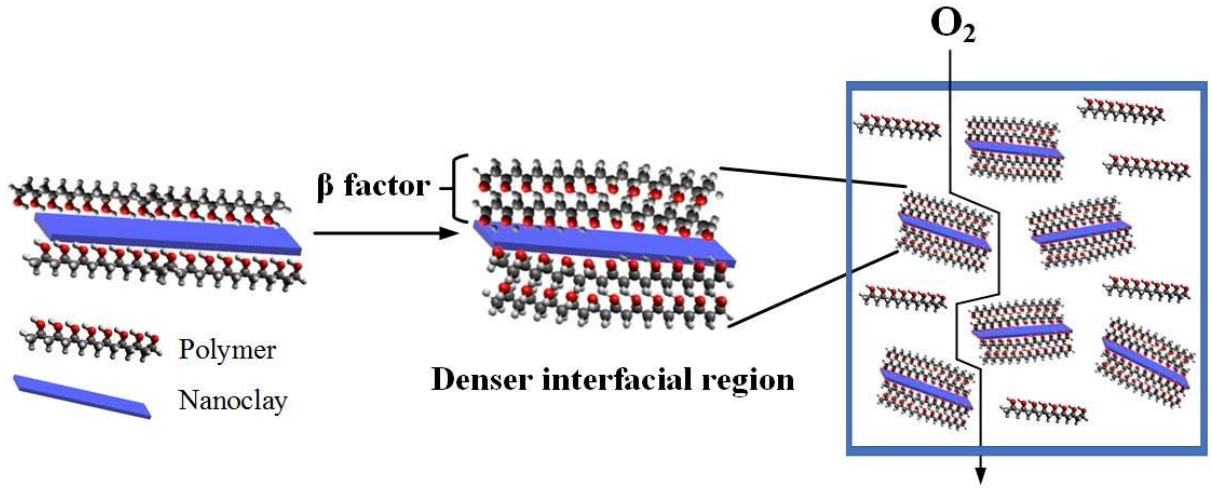

Figure 2.8 Illustration of the interfacial region in a nanocomposite[55]

Like Nielsen's model, numerous models focused on determining the best tortuosity formula. Maxwell's model, for example, considered only the volume fraction of the filler for the tortuosity which led to a linear relationship between the permeability ratio and the volume fraction.

Other models like Gusev and Cussler models assumed a perfect filler orientation and rather stressed the role of the volume fraction in reducing permeability. By considering the quadratic and exponential effect of Ø on the tortuosity, the permeability ratio decreases sharply for Ø > 0.15, Figure 2.11, predicting lower permeability values than Nielsen's model.

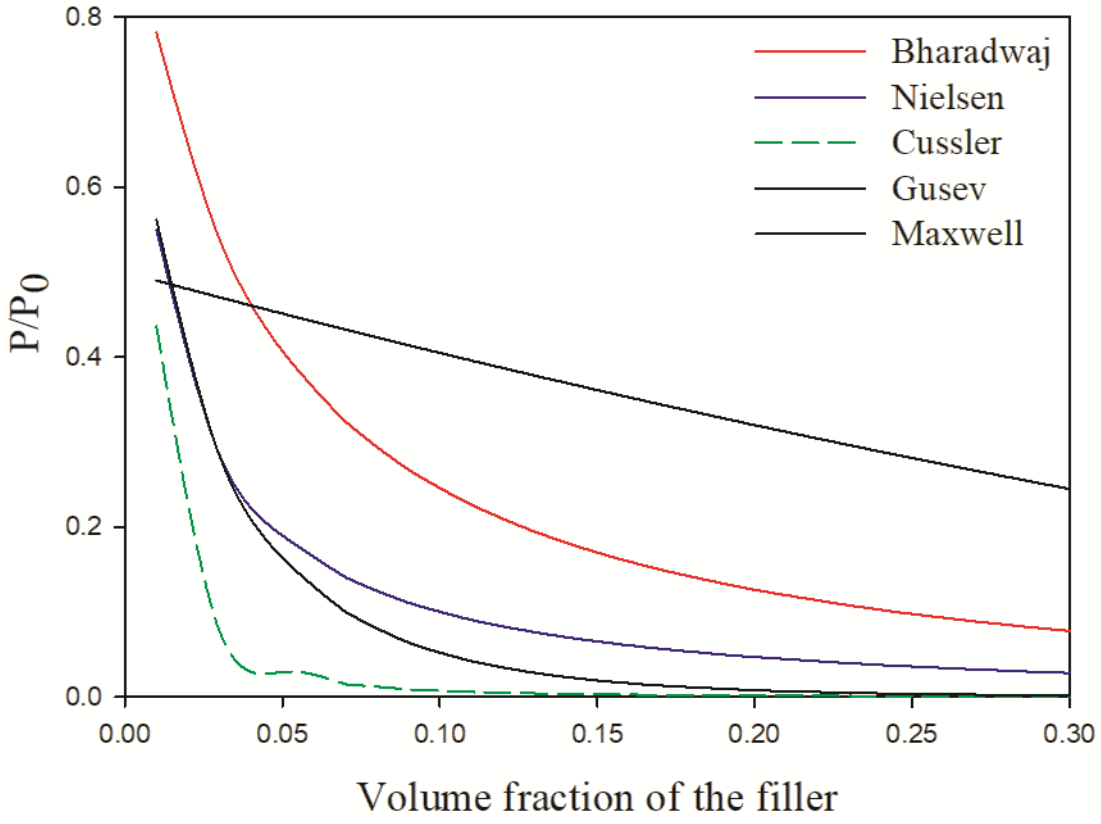

Figure 2.9 Comparison of permeability models

Table 2.2 Equation and considered parameters of some permeability models

Model	Relative permeability formula (P/P_0)	Considered parameters
Bharadwaj [54]	$\frac{1-\emptyset}{1+\frac{L\emptyset}{2W}(\frac{2}{3})(S+\frac{1}{2})}$	S=1 Perfect orientation
Gusev [56]	$exp[-(\frac{L\,\emptyset}{3.47W})^{0.71}]$	Perfect orientation No overlapping
Nielsen [57]	$\frac{1-\emptyset}{1+\frac{L\emptyset}{2W}}$	Perfect orientation
Cussler [58-59]	$\frac{1-\emptyset}{1-\emptyset+\frac{\mu}{4}(\frac{L\emptyset}{W})^2}$	μ=0.5 Randomly spaced flakes μ=0 Regularly spaced flakes and infinitely long in one dimension
Maxwell [60]	$\frac{1-\emptyset}{1+\frac{\emptyset}{2}}$	Dilute suspension
Lape [61]	$\frac{1-\emptyset}{(1+\frac{2\alpha\emptyset}{3})^2}$	Randomly placed aligned filler
Sorrentino [62]	$\frac{1+\beta\emptyset}{(1-\emptyset)+\emptyset\,(\frac{L+2t}{L\sin\theta+2t\cos\theta})^2}$	θ= angle between the thickness direction of a platelet, and the diffusion direction.

2.5 **Crosslinking**

One of the misconceptions about LbL assemblies is that they have a stratified structure with unmixed layers. Several studies have shown that its layers interpenetrate, making its structure more

similar to a miscible blend than to a multilayer structure.[48] This interpenetration makes the crosslinking of LbL assemblies possible. This latter can be a chemical, thermal or a photo crosslinking.[25] Contrary to casting, the crosslinking of LbL assemblies is subsequent to the deposition of the film. Depending on the coating technique, the LbL film can be dipped in the crosslinker solution for dip coating or a crosslinker layer is bladed, sprayed or spinned on the top of the film layers. 1-(3-Dimethylaminopropyl)-3-ethylcarbodiimide hydrochloride (EDC), maleic acid and aldehydes are among the most used crosslinkers. Crosslinking is widely used to reduce films sensitivity to moisture, as free functional groups establish hydrogen bonds with water molecules, present at high relative humidity. The covalent bonding with a crosslinker inhibits this hydrogen bonds and helps preserving the film's properties. This bonding reduces also the permeability to gas as less free volume is available for the diffusion of gas molecule. Crosslinking can also stabilize some polymers by reducing their sensitivity to pH. EDC, for instance, initiates the creation of amine bonds between amine groups of PAH and carboxylic groups of PMA which reduces the free charged groups in the film and thus the sensitivity to pH.[63]

Aldehydes are very reactive crosslinkers and react mainly with amine and hydroxyl groups to establish covalent bonds.

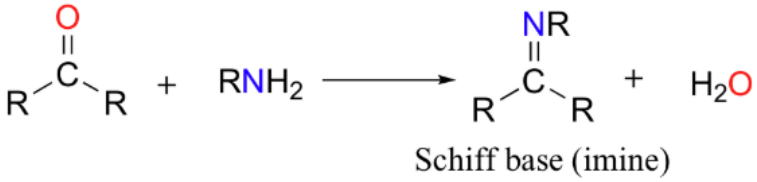

Figure 2.10 Schiff base reaction

Schiff bases were discovered by Hugo Schiff. They are the product of the condensation of carbonyl compounds and primary amines, Figure 2.12. They are used to stabilize oxidized metals and their metal chelates are known for their selectivity to some metal ions.[64]

On the other hand, crosslinking polymers with hydroxyl groups is a two steps reaction. In the first step, the carbonyl group is replaced by two hydroxyl groups, and one of them reacts with a hydroxyl group of the polymer to result in a hemi acetal, unstable intermediate, hard to isolate. In the second step, the free hydroxyl group of the aldehyde reacts with another group of the polymer adjacent to

th the first, which forms the acetal. Study of the catalytic constant of this reaction showed that this second step is the limiting one.[65]

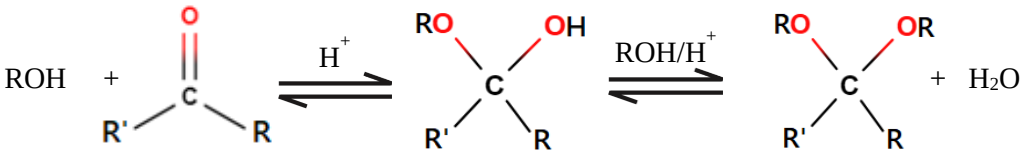

Figure 2.11 Acetal reaction

Crosslinking of PVA

The studied PVA crosslinking reactions with aldehydes are usually homogeneous,[66-67] as a crosslinker solution is added to the polymer solution. Based on previous studies of the kinetic of crosslinking with aldehydes, a second order reaction to describe it, equation 2.14, is generally accepted. [68]

$$-\frac{dC_a}{dt} = KC_pC_a \qquad (2.14)$$

With C_a, the aldehyde concentration, C_p, the polymer concentration and k, the reaction rate constant. Kormanovskaya studied the crosslinking of PVA with formaldehyde and among other interesting results, it was suggested that the crosslinking of two adjacent hydroxyl groups is a one step reaction. [69] This interpretation came as a result of a higher rate of interaction for aldehyde with PVA and 1.3-glycols than with monohydric alcohols.

Without the addition of an acid, this reaction becomes reversible which leads to non proportional variation of the crosslinking degree with the crosslinker/ PVA ratio.[70]

The characterization of the crosslinking reaction of PVA by glyoxal with FTIR showed mainly a variation in the hydroxyl groups density and the C-O bonding when increasing the ratio crosslinker/PVA.[67]

LbL films crosslinking was extensively studied and showed interesting results. Podsiadlo et al. [49] crosslinked a LbL assembly of PVA- MMT with glutaraldehyde (GA) and obtained a crosslinked film with higher brittleness, stiffness and strength. The same results were also obtained by Patro et al.,[26] for LbL films of PVA/Laponite-Graphene oxide. In this latter case, different crosslinking

times with GA were tried and a deterioration of the film properties was observed for a crosslinking time higher than 1 hour.

Crosslinking time is not often discussed for LbL technique as it's only applicable for techniques like dipping, where the film's contact time with the crosslinker can be controlled. In other techniques like spraying, spinning or blading, this contact time is mainly controlled by the drying step.

As a conclusion of this literature review, recyclable alternatives are now in high demand for packaging material and nanocomposite coatings seem to be part of the solution. Applying promising techniques like LbL to deposit them is currently investigated by many research groups. Such technique results in a high filler loading in the coating and an excellent oxygen barrier. To overcome some of its drawbacks like the sensitivity to moisture of the coatings, they can be crosslinked with dialdehydes. A fundamental study of these coatings is required to have a better understanding of the properties of the filler and its impact on the polymer so that to choose better the component of a coating. Also, crosslinking the LbL coating is widely used but no study has tackled its kinetic.

2.6 Objectives

The main objective of this work is to develop a water-based coating with a high oxygen barrier for its application in packaging. To reach this objective, specific objectives of this work are summarized as follows:

- To establish a fundamental understanding of the effect of the polymer structure and affinity to clay on the orientation and intercalation of the clay platelets in a nanocomposite coating based on hydrogen bonding and deposited by LbL.

- To investigate the effect of two coating techniques, blading and dipping, on the permeability to oxygen of nanocomposite coatings at high relative humidity, their effect on the crosslinking efficiency with glyoxal and glutaraldehyde and the resulting surface hydrophobicity obtained for crosslinked and no coatings.

- To study the crosslinking kinetic of PVA with glyoxal by determining the reversibility steps, the apparent reaction rate constant for non reversible crosslinking and the effect of MMT on this kinetic.

2.7 Originality

Although the nanocomposite coatings have seen an increasing interest for gas permeability reduction, the orientation of fillers like clay in coatings has been characterized in some studies but to our knowledge, no study has focused on the clay orientation in LbL deposited coating and the effect of the intercalated polymer in this orientation. Moreover, a model based on Nielsen's permeability model was suggested to better predict the permeability of LbL nanocomposite coating based on their volume fraction.

Since blading is usually the industrial process for coating, a comparison of this technique to dipping was conducted in the second step of this thesis, by characterizing the coating morphology, the clay properties and the permeability of the obtained coatings.

Our findings showed how the crosslinking efficiency in reducing the sensitivity to moisture varies with the used technique for LbL coating, which, to our knowledge no published work has discussed yet.

Considering the extensive use of aldehyde crosslinking for improving polymers properties, the crosslinking of nanocomposite coatings of PVA and MMT with glyoxal was the focus of the last part of this thesis. Oxygen permeability coefficients of coatings with different crosslinking times were used to shed light on this acetal reaction and its reversibility steps which has not been reported before. In the next step of this study, a linear correlation was established between permeability coefficient and the FTIR absorption intensity. Such correlation simplifies permeability characterization and help further determine the crosslinking kinetic. In the case of non reversible crosslinking, crosslinking kinetic was investigated and apparent reaction rate constants were compared for PVA and PVA-MMT coatings which has never been addressed before for crosslinked LbL coatings.

CHAPTER 3 METHODOLOGY

3.1 Materials

For the studied coatings, three polymers were selected: Polyvinyl alcohol (PVA) (Mw=140 000 – 186 000 g. mol^{-1}), polyvinylpyrrolidone (PVP) (Mw=360 000 g. mol^{-1}) and polyethylene oxide (PEO) (Mw=4 000 000 g. mol^{-1}), all supplied by Sigma Aldrich (Saint Louis, Missouri, USA). They were combined with Chitosan (CS) (Mw=150 000 g. mol^{-1}) (Sigma Aldrich (Saint Louis, Missouri, USA)), for the quadlayer structure. To have a nanocomposite coating, Natural sodium Montmorillonite (MMT) was chosen. It was purchased form BYK (Gonzales, Texas, United States) and have a density of 2.86 g/cm^3. For all deposited coatings a primer layer of polyethylene imine (PEI), supplied by MICA Corporation (Shelton, CT, USA), is first applied to the substrate with a concentration of 0.6wt.%. For the crosslinking of these coatings, glyoxal (Gly, 40% aqueous solution) and glutaraldehyde (GA, 25% aqueous solution) were purchased from Sigma Aldrich (Saint Louis, Missouri, USA) and diluted to a 5% solution.

The chosen substrate is a polyethylene terephthalate (PET) film, with a 16 μm thickness. For the study of orientation with FTIR in the transmission mode, low density polyethylene (LDPE) was used instead of PET to avoid peak saturation. Both substrates were provided by ProAmpac (Terrebonne, Qc, Canada). Depending on the characterization technique two types of silicon plates were used, purchased from EL-Cat Inc. (Ridgefield Park, New Jersey, United States). For FTIR characterization, silicon plates transparent to infra red were used as substrate for the studied coatings whereas one phase polished silicon plates were used for the profilometry characterization as it offered a more solid substrate than PET with a smooth surface, essential for a precise thickness measurements of such thin coatings.

3.2 Solutions preparation

Polymer solutions were prepared with deionized (DI) water and a concentration of 0.1 wt.% was used. MMT with 0.5 wt.% concentration was also prepared with DI and needed longer stirring period.

To dissolve PVA, it was heated for 2 hours at 80 °C with constant stirring. All the polymers and MMT were used as received except for the chitosan that had the solution pH adjusted to 6 with the addition of acetic acid and sodium hydroxide (1M).

3.3 Coatings preparation

3.3.1 Dip coating

Before each coating deposition, a PEI primer layer is deposited. To do so, the substrate is dipped in the PEI solution for 20 min. Once the substrate with the primer layer rinsed and dried, the desired coating is then deposited by dipping the substrate in the polymer or MMT solution, for 1 min, rinsing it for 30s and then drying it. For the first bilayer, the dipping and rinsing times are higher, (5 and 1 min respectively) to have a better coverage.

3.3.2 DB coating

DB coating was simpler than dipping as it doesn't need rinsing and drying steps. As for dipping a primer layer was deposited first on the substrate. For the LbL coating, few milliliters of polymers or MMT were spread each time on the substrate. As it's a small volume deposited for each layer, drying time was very short.

Three types of structures were studied in this work, quadlayer, trilayer and bilayer structures. The difference between them is the number of layers in the repetitive unit. A 10 bilayers coating, for example, has two layers in the repetitive unit meaning a total of 20 layers deposited, whereas a 10 quadlayer coating, has four layers in the repetitive unit, so 40 layers deposited in total.

3.4 Characterization

3.4.1 X-ray diffraction

To determine the interlayer spacing of MMT d(001), a Philips X'pert apparatus was used for the wide-angle X-ray diffraction spectroscopy (XRD) with a copper CuKα radiation source (λ =1.54056 Å). The studied coatings were deposited on silicon substrates and scanned with a 0.02

°/s rate from 2 to 10 degrees. For the crystallinity detection in the polymers, samples were scanned from 2 to 40 degrees.

3.4.2 **Morphology**

3.4.2.1 **AFM**

To obtain samples with a smooth surface for the AFM characterization, polycaprolactone (PCL) was initially melted at 80°C and placed in the silicone molds. The coated films were then embedded into the molten polymer. Hot and cold press were used to obtain compact samples. Those cooled samples had then one extremity crafted in pyramid shape tip with a razor blade. Using a cryo-microtome (Leica-Jung RM 2065) operated at -170°C, the samples were microtomed. The morphology of this smooth cross-section of the coated PET is examined with an Atomic Force Microscopy (AFM) machine (Nanoscope V Dimension Icon/ Fastscan AFM, Bruker, USA) operated in tapping mode in air. To acquire the AFM images, Intermittent Peak Force tapping ™ was used with a 125 μm TESPA-V2 Air probes having a tip radius of 8 nm. Considering that the materials in the molded samples have different modulus, the tapping phase mode was the one used for the analysis of the nanostructure of the studied coatings.

The nanostructures size in the coating as well as the coating thickness were determined using the free ImageJ software. The obtained average values are reported as XX±YY with, XX the average value and YY its standard deviation. The coating roughness was measured at 6 different spots and the average value is reported with its standard deviation. For the microstructure analysis of the surface, phase images of various samples were compared by analyzing 5μm x 5μm scan windows.

3.4.2.2 **Profilometry**

Silicon plates were the substrates for this characterization and Dektak 3030 stylus profilometer was used to determine the coating thickness. For each deposited coating, a part of the silicone plate was left uncoated. A stylus moves over the coated and uncoated regions according to the user-programmed scan speed, length, and stylus force. Once the scan recorded, the uncoated part is set as reference for the thickness calculation.

3.4.3 Permeability

The permeability to oxygen of the coated PET was determined via a MOCON OXTRAN 2/21 (Minneapolis, USA) at 25 °C, 0% relative humidity, and 1 atm pressure, following the ASTM D-3985-81. For the test at 70% RH a MOCON OXTRAN 10X apparatus (Minneapolis, USA) was used at 25°C. For these tests, a mixture of 2% hydrogen (H_2) and 98% nitrogen (N_2) was the carrier gas and a 100% oxygen (O_2) was the test gas.

The Water vapor permeability (WVP) measurements were done at 37.8 °C, 1 atm pressure and 100% RH in accordance with D-6701 ASTM standard using a MOCON PERMATRAN-W Model 101K (Minneapolis, USA).

3.4.4 FTIR analysis

3.4.4.1 Clay orientation

To determine the orientation of the clay in the coatings, a Spectrum 65 FTIR spectrometer from PerkinElmer (Waltham, MA) was used to scan the samples in the range 900 to 1200 cm^{-1} with a resolution of 4 cm^{-1} and an accumulation of 32 scans. A Spectra-Tech zinc selenide wire grid polarizer from Thermo Electron Corp, was used. Using a slide holder, to place the polarizer in one side and the sample in the other side, three spectra were recorded for each sample, in the horizontal transverse direction, S_T, in the vertical machine direction, S_M and in the horizontal direction with the film tilted at an angle φ with respect to the machine direction (MD), S_{NT}. For these FTIR measurements, PET was replaced by LDPE due to peaks saturation with PET.

The MMT Si-O stretching bands are four around 1120 ,1080,1048 and 1025cm^{-1} [30]. Three of these peaks (1025, 1048 and 1120 cm^{-1}) are related to the oxygen at the surface of the MMT platelets (basal oxygen) whereas the peak at 1080 cm^{-1} is specific to the apical oxygen. This oxygen is linked to Aluminium and located at the internal edge of the tetrahedral sheet. It's importance for orientation measurement is due to its bond Si-O that is perpendicular to platelet plane.[31] Based on the obtained spectra, a fourth spectrum, which is the spectrum in normal direction, S_N, is calculated

According to this equation [32]:

$$S_N = \frac{S_{NT}(1-\frac{\sin^2\varphi}{n^2})^{1/2} - S_T(1-\frac{\sin^2\varphi}{n^2})}{\sin^2\varphi/n^2} \quad (3.1)$$

With φ equal to 45 ° and n, the refractive index of MMT with a value of 1.503 [33], the equation can then be rewritten as:

$$S_N = 3.968\ S_{NT} - 3.5\ S_T \quad (3.2)$$

To be able to calculate the Herman's orientation function, the structurally independent spectrum S_0, is also calculated and it's the arithmetic average of S_M, S_N and S_T spectra. Considering c, the normal axis of the clay platelet and S_N the spectrum corresponding to the normal direction, the f_{CN} function characterize then the orientation of platelets in a parallel direction to the coating surface[30]:

$$f_{CN} = 0.5(\frac{A_N}{A_0} - 1) \quad (3.3)$$

A_N and A_0 being the band intensities in the S_N and S_0 spectra corresponding to the apical oxygen. The ratio ($\frac{A_N}{A_0}$) is referred to, as dichroic ratio, D.

3.4.4.2 **Coating characterization**

To characterize the studied coating, the same FTIR spectrometer was used in transmission mode. The coatings were deposited on an infra red transparent silicon plates and were scanned in the range 600 to 4000 cm^{-1} with a resolution of 4 cm^{-1}.

3.4.5 **Contact angle**

Water contact angle measurement were conducted at room temperature with a Contact Angle Goniometer OCA20 from dataphysics. Distilled water was the probe liquid. To calculate the contact angle, the time selected for all the images, was 5 seconds starting from the moment the drop reaches the coating. The reported values are an average of five readings.

CHAPTER 4 ORGANIZATION OF ARTICLES

The main achievements of this work are presented in the form of three scientific papers in the following chapters:

Chapter 5 presents the results of the first paper "*Effect of nanoclay orientation on oxygen barrier properties of LbL nanocomposite coated films*" that has been published in *RSC advances*, in January 2019. In this work, the impact of the polymer structure and its affinity to MMT on the properties of this clay were investigated. Clay orientation was determined by FTIR peak deconvolution and FTIR interactive spectral subtraction for the different structures and its interlayer spacing was determined by XRD. The morphology of a quadlayer assembly was characterized by AFM analysis and the thickness of the studied structures was determined. The permeability of the coatings was also measured for different number of deposited layers. Following the comparison of experimental results to known permeability models, a modified Nielsen's model was proposed to consider the contribution of the interfacial region in reducing permeability, as its fraction becomes considerable in high filler loading nanocomposites.

Chapter 6 presents the second article *"Comparison of crosslinking efficiency in dip and roll deposited coatings on their oxygen barrier"* that has been published in *ACS Omega*, in September 2019. This article's focus was the impact of the coating techniques on the film's properties. PVA-MMT coatings deposited by dipping and blading were crosslinked with glyoxal and glutaraldehyde and their permeability to oxygen was determined for different values of relative humidity as well as their permeability to water vapor. The thickness and roughness of these coatings were also characterized by profilometry and AFM analysis respectively. In a second part, the effect of the coating composition on its oxygen permeability was investigated. The concentration of the PVA solution was increased in order to improve hydrogen bonding in the coating, and for another set of coatings the MMT solution concentration was varied to increase the clay volume fraction in the coating. The hydrophobicity of the surface was determined by water contact angle measurements and the clay interlayer spacing was characterized by XRD

Chapter 7 presents the third article, "*Study of the crosslinking of PVA with glyoxal in LbL nanocomposites"* that has been submitted to *Open Journal of Polymer Chemistry*, in July 2019. In

this paper the crosslinking of PVA based coatings with glyoxal was investigated. PVA and PVA-MMT coatings were crosslinked with glyoxal for different times and their permeability to oxygen was measured. Plotting permeability in function of the crosslinking time enabled the visualization of the different crosslinking steps for the reversible reaction. To determine the crosslinking reaction kinetic, acidic environment was adopted to avoid reversibility. The contact angle to water was determined for the PVA-MMT coatings and FTIR spectroscopy was used in transmission mode to study the variation of the covalent bonding in the coating, for the different crosslinking times. The order of the reaction was determined by fitting and a linear correlation was established between permeability and FTIR absorption intensity.

CHAPTER 5 ARTICLE 1: EFFECT OF NANOCLAY ORIENTATION ON OXYGEN BARRIER PROPERTIES OF LBL NANOCOMPOSITE COATED FILMS

Fatma Ben Dhieb[1], Ebrahim Jalali Dil[1], Seyed H. Tabatabaei[2], Frej Mighri[3] and Abdellah Ajji[1*]

[1] 3SPack NSERC-Industry Chair, CREPEC, Chemical Engineering Department, Polytechnique Montreal, C.P. 6079, Succ. Centre ville, Montreal, QC, Canada H3C 3A7

[2] ProAmpac, Terrebonne, QC, Canada J6Y 1V2

[3] CREPEC, Chemical Engineering Department, Laval University, Quebec, QC, Canada

(*) All correspondence should be addressed to: *abdellah.ajji@polymtl.ca*

(Published in *RSC advances, 8 January 2019)*

Abstract

Layer by layer (LbL) film deposition is an efficient technique used to produce thin coatings with high gas barrier properties. In this study, multilayer composite coatings with hydrogen bonding inter-layer interactions were deposited by LbL on a PET substrate, with an alternate deposition of a nanoclay layer and different intercalating polymers layers, namely chitosan (CS), polyethylene oxide (PEO), polyvinylpyrrolidone (PVP) and polyvinyl alcohol (PVA). The investigated coatings had two different structures, quadlayers and bilayers which are different in the number of layers in the repetitive unit (four and two respectively). The alignment of nanoclay platelets and the extent of their intercalation were studied using Fourier transform infrared (FTIR) spectroscopy and X-ray diffraction (XRD). The results showed that the dispersion level and the orientation of nanoclay particles depend considerably on the molecular structure of intercalating polymers and their interactions with nanoclay. An oxygen permeability model, specific to high filler loading composites, was then developed by considering only the aspect ratio and the volume fraction of the nanoparticles.

Keywords: LbL, Orientation, Nanoclay, nanocomposites, Oxygen permeability.

Introduction

Given their light weight, high chemical resistance and low interaction with food, polymers have been considered good candidates for packaging and their wide variety have allowed for a large spectrum of properties. Nevertheless, the constant demand for better oxygen barrier packaging motivated research toward improving the barrier properties of polymers. This depends mainly on the diffusivity of gas molecules and their solubility in the polymer.[1]Incorporation of additives such as nanoclay is among the investigated alternatives to improve the properties such as the oxygen barrier [2-4]. The impermeable structure of clay coupled with a large aspect ratio, increase tortuosity along the path of a gas molecule through the polymer, which consequently reduces gas permeability. The relative permeability is inversely proportional to tortuosity, τ [5].

$$\frac{P}{P_0} = \frac{1-\phi}{\tau} \tag{5.1}$$

where, P_0 is the permeability of the non-filled polymer and ϕ is the volume fraction of the filler. Tortuosity can vary considerably with the aspect ratio of nanoclay, its volume fraction, intercalation and orientation. This latter trait has been extensively investigated for melt processed films [6-7-8]. In addition to the direct effect of nanoclay on tortuosity, it can also indirectly affect the tortuosity by altering the crystallinity and orientation of polymer crystallites[9]. For instance, a preferred orientation of nanoclay and crystallites along the machine direction have been previously reported in the literature and is attributed to the shear stress in the die and the large elongational stress at the die exit [10-11]. Therefore, it can be seen that, besides dispersion, controlling nanoclay orientation is critical to the final nanocomposites properties[12]. Recently layer by layer (LbL) coating has emerged as a new method to produce much thinner nanocomposite coatings with high oxygen barrier properties[13-14], since the lack of clay exfoliation and its aggregation, hinder the use of clay with conventional processes, e.g. extrusion[15]. High clay concentration can be achieved with this technique, enabling, thus, a good oxygen barrier[16-22]. Many types of clay are used for coating (hectorite, synthetic mica, Vermiculite (VMT), Montmorillonite (MMT), …) as they improve gas barrier and mechanical properties. MMT, for instance was extensively studied for LbL coatings. With its charged oxygens and hydroxyl groups on the surface it can establish hydrogen bonds and electrostatic interactions with polymers. Among different aspects of LbL nanocomposites, the

effects of nanoclay dispersion and *d*-spacing on oxygen barrier properties, mechanical properties and transparency are the most commonly studied aspects in the literature. LbL is a simple technique relying on interaction between layers. This could be based on electrostatic interactions between charged polymers, hydrogen bonding, Van der Waals forces or hydrophobic interactions [23]. Among them, the most studied ones are electrostatic [18] and hydrogen bonding [24-25] interactions. Properties of the LbL assembled films depends considerably on the type of these interactions. For electrostatic interactions based coatings, polymers such as poly(acrylic acid), PAA, polyethyleneimine, PEI[26-27], polyvinylamine, PVAm [18], polyacrylamide, PAM [22] have been used and resulted in very dense films. Hydrogen bonding interactions, on the other hand, allow a more flexible structure that can withstand mechanical strains while maintaining their oxygen barrier [28]. Chitosan (CS), polyethylene oxide (PEO), Polyvinylpyrrolidone, PVP, and polyvinyl alcohol (PVA) are among the most common polymers used for hydrogen bonding based coatings which will be used in this study. Chitosan is from a renewable source, recognized as having good barrier properties and forms film easily (from solutions). PVA has a considerable density of functional groups and establishes strong hydrogen bonds. Contrary to PVA, PVP has a rigid structure allowing a more linear growth of LbL film and, similar to chitosan, it can readily form films. PEO has a linear, non-branched structure with different functional group than PVA and PVP. These differences allow studying the effect of molecular structures on the properties of the film samples. The operating parameters for the LbL technique have been extensively studied to determine their effect on the resulting film properties. For instance, the pH[19], the deposition time [17] and the application of different procedures such as removing the drying step [29] were key factors in improving the film properties by tuning the density and the behavior of the resulting layers.

To characterize these properties, many methods have been adopted, particularly thermal analysis to determine the thermal transition temperature[25, 30], ellipsometry to measure the layers thickness[16, 21, 31-32 ,] quartz crystal microbalance, QCM-d, to track the mass change with each layer [33-34] and gas transmission measurement to evaluate the film permeability. [35]

As LbL technique allows achieving good dispersion even at high nanoclay contents, nanoclay coatings produced by this technique show good oxygen barrier properties[16-22]. It is known that the tortuosity of the path of the gas molecule is strongly related to nanoclay orientation in the deposited

layers. However, despite the significant potential of LbL coatings, there is little information about the clay orientation. [15]

Since nanocomposites properties, such as oxygen permeability, are considerably dependent on tortuosity, the study of clay orientation and intercalation will be carried out for two types of assemblies, bilayer and quadlayer. For the selected coatings, orientation will be determined using FTIR measurements and by using two different quantification methods. As the used polymers (PVA, PEO, PVP and CS) have different potentials to establish hydrogen bonding interactions,[35-40] the obtained results will allow to investigate the effect of different levels of interactions of polymers and nanoclay through the study of the properties of the coatings such as density and oxygen permeability as well as nanoclay dispersion. The experimental results will be then compared with permeability models and a modification of some of those models will be discussed.

5.1 Experimental

5.1.1 Materials

Natural sodium montmorillonite (MMT) platelets (Cloisite NA+), nanoclay, with density of 2.86 g/cm^3 were supplied by BYK (Gonzales, Texas, United States) and used as received. Chitosan (Mw=150 000 g. mol^{-1}), PEO (Mw=4 000 000 g. mol^{-1}), PVP (Mw=360 000 g. mol^{-1}) and PVA (Mw=140 000 – 186 000 g. mol^{-1}) (Figure 5.1) were supplied by Sigma Aldrich (Saint Louis, Missouri, USA).

Different substrates were used according to the characterization technique or the type of test conducted: silicon platelets were used for XRD and profilometry characterization and were purchased from EL-Cat Inc. (Ridgefield Park, New Jersey, United States). Polyethylene terephthalate (PET), 16 μm thickness, (supplied by ProAmpac (Terrebonne, QC, Canada)) was mainly used for permeability tests and AFM characterization and low density polyethylene (LDPE) (supplied also by ProAmpac) served as substrate only for FTIR analysis.

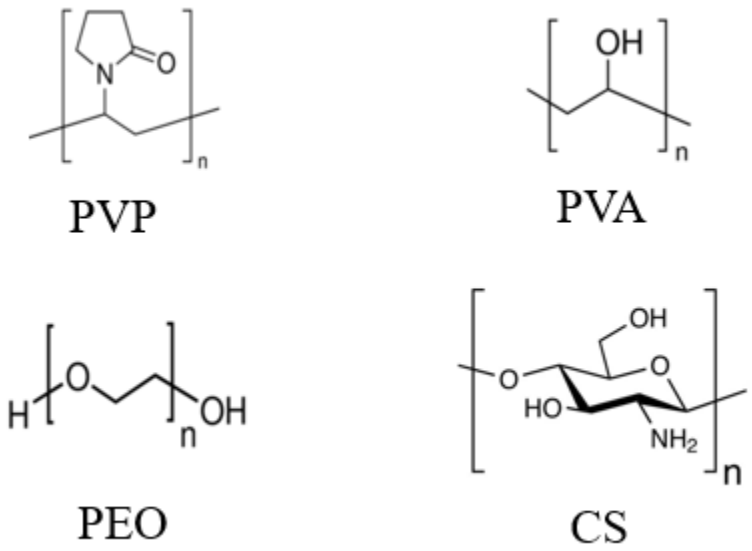

Figure 5.1 Molecular structures of PVP, PVA, PEO and CS.

5.1.2 Preparation of thin coatings

All the solutions were prepared with deionized (DI) water and had the same concentration of 0.1%wt except for MMT (0.5%wt). PVA solution was heated at 80 °C for 2 hours and the pH of chitosan solution was adjusted to 6 by adding acetic acid and 1 molar sodium hydroxide (NaOH). In order to generate a primer layer, all cleaned substrates were initially dipped into a PEI solution (0.6% in DI water) for 20 min and then rinsed with DI water. The coating deposition of each layer consists of three steps, dipping in polymer or MMT solution, rinsing with DI water and drying. Figure S.1 shows schematics of the coating cycle for a quadlayer and bilayer assemblies. For the first deposited bilayer or quadlayer, dipping was done for 5 min and then the sample was rinsed for 1 min. For the following layers, dipping and rinsing times were reduced to 1 min and 30 s, respectively.

5.1.3 Characterization of Coatings

5.1.3.1 Fourier Transform Infrared Spectroscopy (FITR)

In order to investigate orientation of the nanoclay platelets in the thin coatings, infrared analysis was elaborated using a Spectrum 65 FTIR spectrometer from PerkinElmer (Waltham, MA) with a

resolution of 4 cm^{-1} and a 32 scans accumulation within wavenumber range of 900 to 1200 cm^{-1}. All experiments were performed using a Spectra-Tech zinc selenide wire grid polarizer from Thermo Electron Corp. Three types of spectra were recorded with the polarizer; in the vertical machine direction, S_M, in the horizontal transverse direction, S_T and in the horizontal direction with a tilted film at an angle φ with respect to the machine direction (MD), S_{NT}. In order to avoid peaks saturation and overlapping, LDPE was used as substrate. Montmorillonite has four Si-O stretching bands around 1080,1025, 1048,1120 cm^{-1} [7]. The peaks at 1025, 1048 and 1120 cm^{-1} are associated with oxygen at the surface of the clay platelets (basal oxygen) and the peak at 1080 cm^{-1} corresponds to apical oxygen. This latter peak is the oxygen at the internal edge of the tetrahedral sheet, linked to Aluminum and having its Si-O bond perpendicular to platelet plane.[41] The spectrum in the normal direction, S_N, can be calculated with the following equation [42].

$$S_N = \frac{S_{NT}\left(1-\frac{\sin^2\varphi}{n^2}\right)^{1/2} - S_T\left(1-\frac{\sin^2\varphi}{n^2}\right)}{\sin^2\varphi/n^2} \quad (5.2)$$

Considering φ equal to 45 ° and n, the refractive index of Montmorillonite equal to 1.503,[43] the equation can then be simplified to:

$$S_N = 3.968\ S_{NT} - 3.5\ S_T \quad (5.3)$$

The structurally independent spectrum S_0, represent the arithmetic average of the three spectra, S_M, S_N and S_T.

Since orientation of clay platelets can be characterized by the orientation of their plane normal, these can be calculated with the following Herman's orientation function:[7]

$$f_{CN} = 0.5\left(\frac{A_N}{A_0} - 1\right) \quad (5.4)$$

where, A_N and A_0 are the band intensities in the S_N and S_0 spectra corresponding to the peaks whose vibrational transition moment lies along the c-axis, normal to the platelets plane. The ratio $\left(\frac{A_N}{A_0}\right)$ is referred as dichroic ratio, D.

5.1.3.2 **X- Ray Diffraction spectroscopy**

A Philips X'pert apparatus was used to carry out wide angle X-ray diffraction (WAXD) spectroscopy. Measurements were done using a copper CuKα radiation source (λ =1.54056 Å). Coatings deposited on silicon wafers were scanned from 2 to 10 degrees at a rate of 0.02 $°s^{-1}$. The MMT interlayer spacing (d_{001}) was determined using the Bragg's law and the diffraction angle at the maximum intensity peak in XRD patterns

5.1.3.3 **Oxygen transmission rate**

The permeability to oxygen was measured *via* a MOCON OXTRAN 2/21 (Minneapolis, USA) at 25 °C, at 0% relative humidity, and 1 atm pressure, in accordance with the ASTM D-3985-81.

5.1.3.4 **Morphology of coatings**

Coatings deposited on silicon substrate were tested using a Dektak 3030 profilometer to determine their average thickness and calculate their roughness.

In order to prepare the surface for AFM analysis, PCL was first melted at 80°C and then the film was embedded into the molten PCL. The sample was cooled to room temperature and crafted in a pyramid shape tip using a razor blade. The sample was then microtomed using a cryo-microtome (Leica-Jung RM 2065) operated at -170°C. The morphology of the cross-section of coated layers was then examined using an Atomic Force Microscopy (AFM) machine (Nanoscope V Dimension Icon/ Fastscan AFM, Bruker, USA) operated in tapping mode in air. All AFM images were acquired using Intermittent Peak Force tapping ™ using 125 μm TESPA-V2 Air probes with tip radius of 8 nm. Due to the difference in the modulus of the materials in the molded sample, tapping phase mode was used in the analysis of the nanostructure of the coated layer.

The thickness of the coated layer and the size of nanostructures in the layer were determined using the free ImageJ software. The average values are reported as XX±YY where XX is the average value and YY shows the standard deviation.

5.2 Results and discussion

5.2.1 Properties of clay

5.2.1.1 Orientation

The fitting method was used to determine the orientation of the clay platelets. The dichroic ratio (D), was calculated with the area of the peaks after deconvolution, as illustrated in Figure S.2 for a PVA quadlayer. The dichroic ratio was based on the two peaks area of the apical oxygen at the wavenumber of 1080 cm^{-1} and was equal to the ratio of their sum in the S_N spectrum on their sum in the S_0 spectrum. This value is proportional to the orientation of clay perpendicularly to the normal vector of the coating. The chosen function to fit the peaks was PearsonVII, as it confers an intermediate shape between Lorentzian and Gaussian, adjustable with a shape factor parameter. Two of the four orientation peaks corresponding to Si-O stretching were split in two peaks, according to Cole et al.[6]. The MD and transverse direction (TD) spectra were perfectly superposed because of a similar orientation in both directions.

To corroborate these results, a spectral subtraction method, Figure S.3, was used. The dichroic ratio corresponds to the subtraction factor necessary to eliminate the apical oxygen peak (1080 cm^{-1}) [7].

The obtained values of orientation function with both methods are not the same for most of the assemblies, as shown in Figure 5.2, probably due to uncertainties in the deconvolution procedure, but are sufficiently close to ascertain the range of the results obtained.

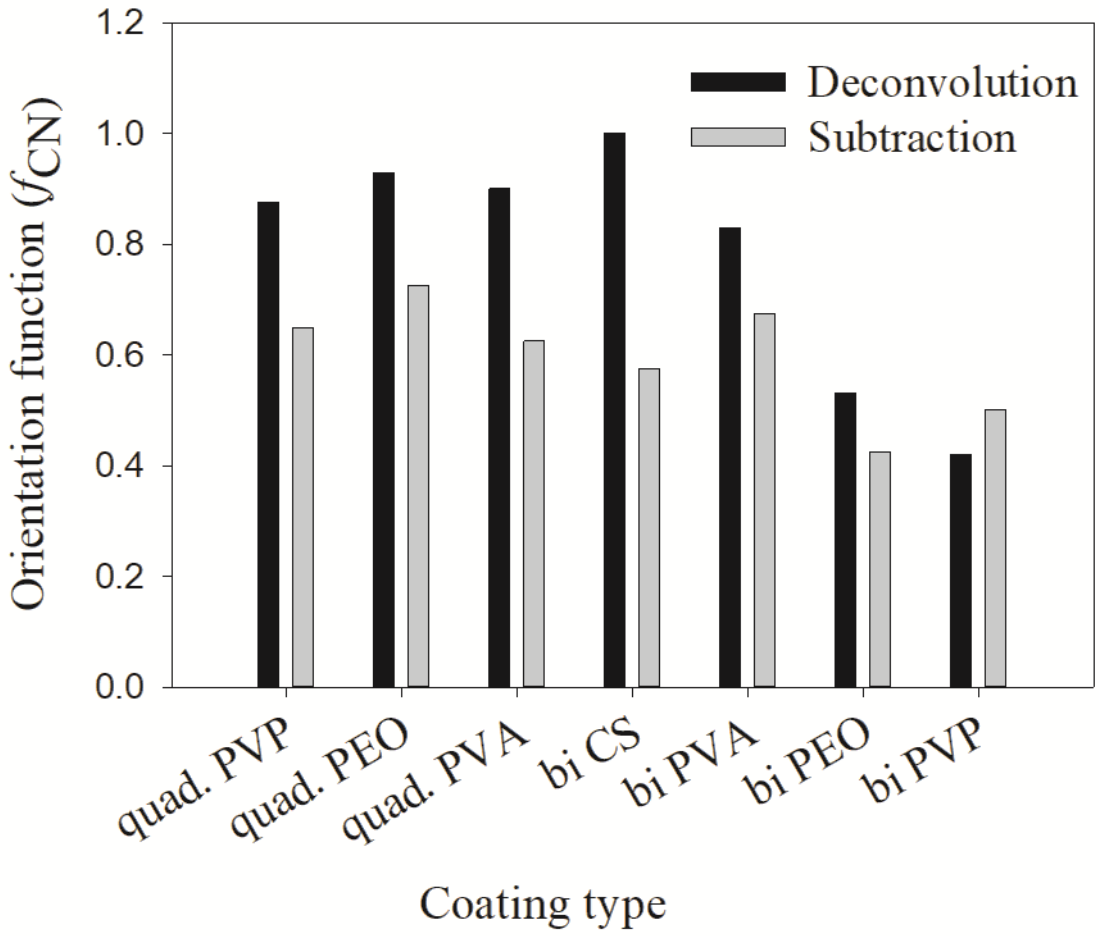

Figure 5.2 Herman orientation function, $f_{CN,}$ determined by subtraction and deconvolution.

It's known that the sum of orientation functions in different directions should be zero[7]. In the case of the deconvolution method, this sum is considerably greater than zero due to the effect of different parameters such as shape factor, peak width and center upon the final results. On the other hand, the obtained results from the subtraction method show a sum close or equal to zero for all the assemblies (Figure 5.3). Based on the aforementioned discussion, the subtraction method will be used in the following discussions for the rest of the paper.

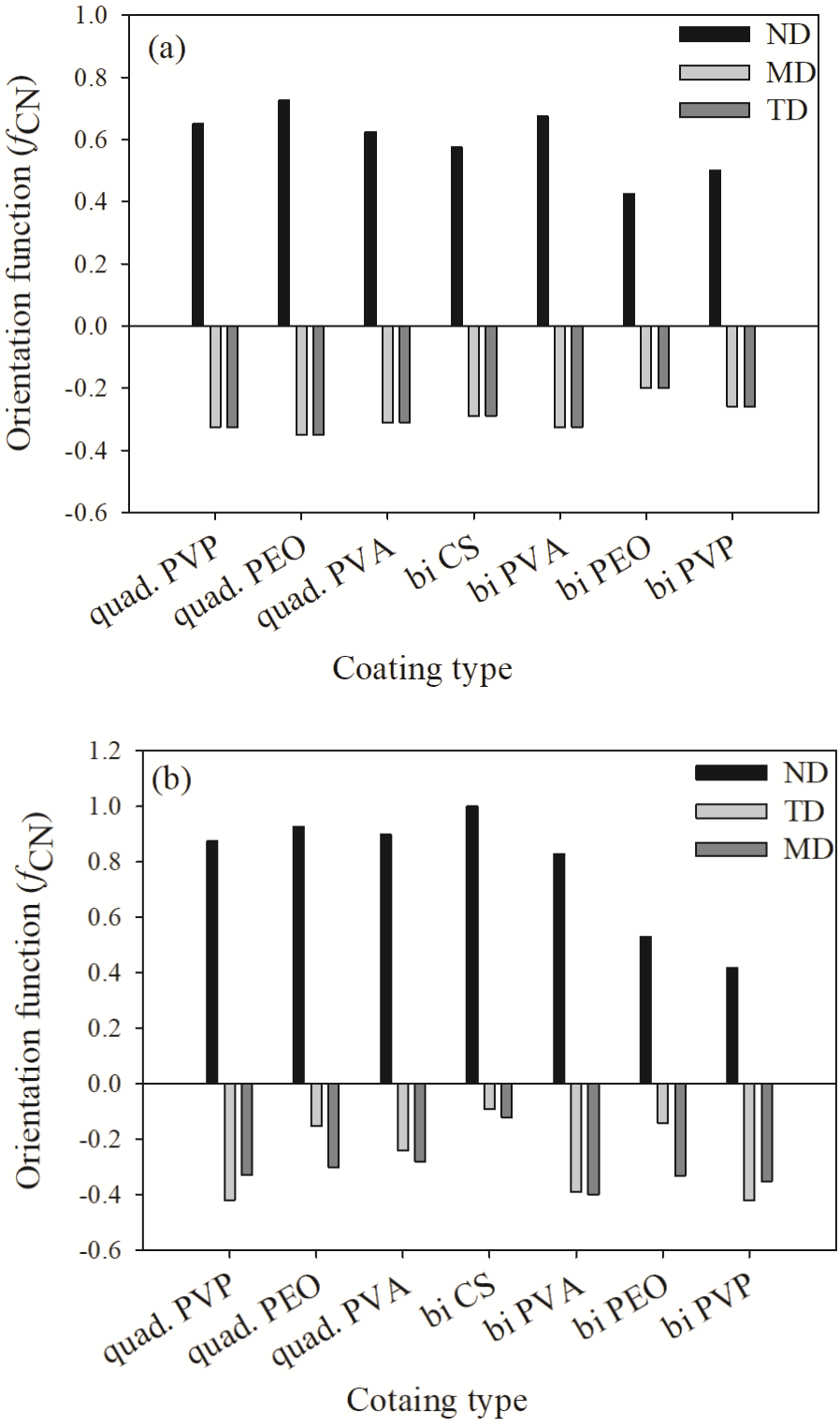

Figure 5.3 Herman orientation functions of the studied assemblies determined by subtraction (a) and deconvolution (b).

It is well known that shear forces during melt processing of nanocomposites tend to orient clay platelets in the machine direction [7].This, however, is not the case for the coatings deposited with the LbL method. For this technique, clay platelets interact freely in solution with the polymers deposited on the substrate. Bearing in mind that MMT platelets establish hydrogen bonding as well as the electrostatic interactions, due to its hydroxyl groups and oxygen, the main difference in clay orientation for the studied assemblies would be at the level of the established hydrogen bonds, in their strength and density. When compared with the orientation function for the different polymers (PVP, PEO and PVA) and the two types of assemblies, bilayer and quadlayer, a similar trend is observed for each polymer (Figure 5.3) with an improvement of orientation for the quadlayer. For the bilayers assemblies, Hermans orientation function has a higher value in the case of the PVA bilayers followed by CS, PVP and PEO bilayers. This can be interpreted by a high affinity of PVA and MMT resulting in a denser structure constraining thus MMT to a certain orientation. Contrary to PEO, CS and PVP have cyclic groups in their structure, stiff enough to avoid entanglement and deposit in an orderly manner, hence constraining MMT to an ordered deposition as well. This CS structure explains the improvement of orientation for the quadlayers structure compare to bilayers. As CS layers alternate the PVA and MMT layers in the PVA quadlayers, the high interaction of PVA with MMT is disrupted causing a slight decrease in orientation.

5.2.1.2 **Nanoclay Dispersion**

Unlike orientation, nanoclay dispersion is extensively studied in nanocomposites, due to its significant role on the dispersion state of nanoparticles. Interlayer spacing of nanoclay has been studied using WAXD spectroscopy of nanocomposites and the neat nanoparticles. As it can be seen in Figure 5.4, the obtained results indicate that MMT interlayer spacing (1.23 nm) increased in all studied assemblies, however, the intercalation level of nanoclay tactoids depends considerably on the polymer type and assembly.

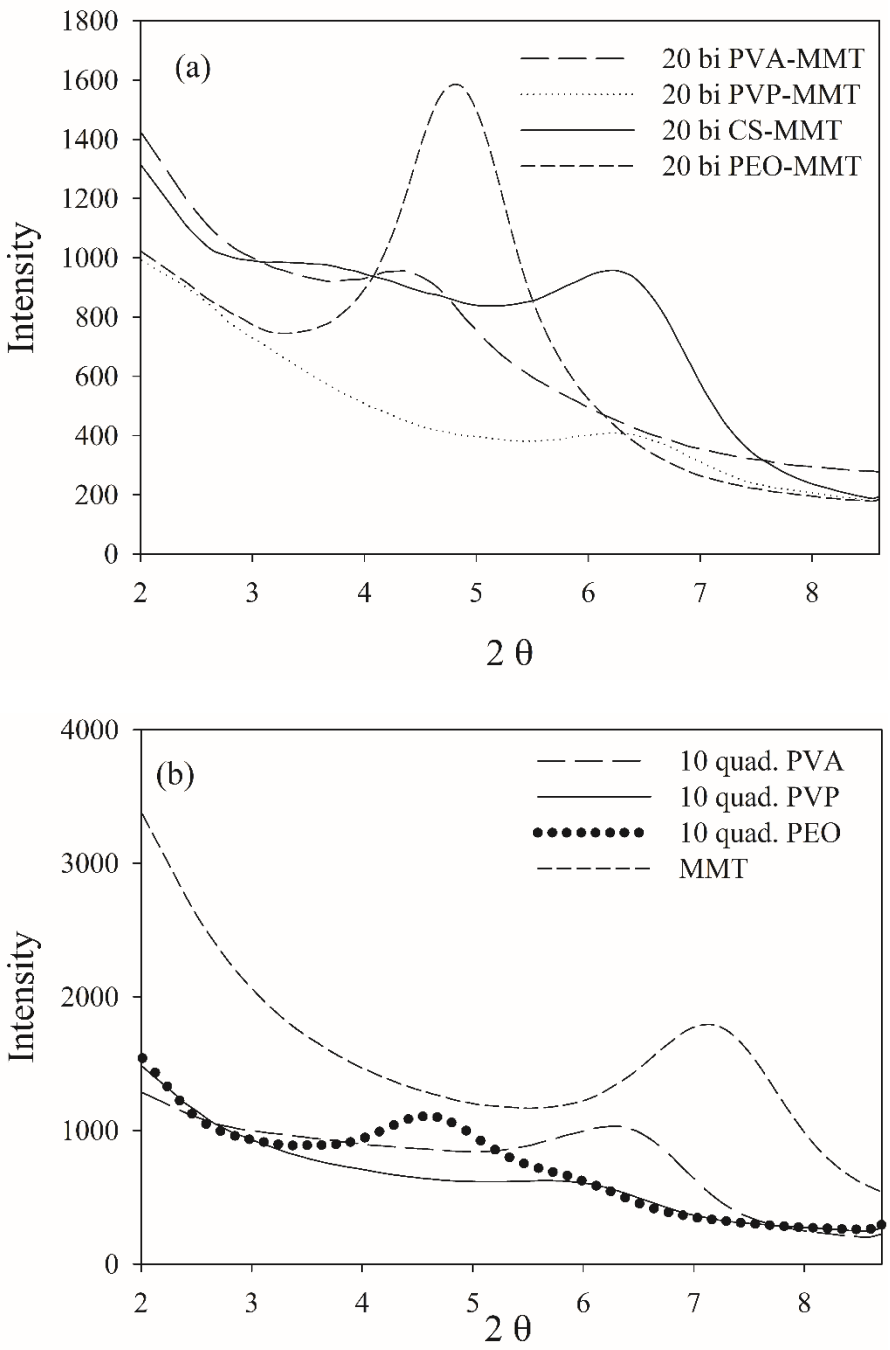

Figure 5.4 Wide angle X-ray spectra of the studied assemblies, a: bilayers and b: quadlayers.

The affinity between polymers and nanoclay is better understood with nanoclay intercalation in the bilayers. As discussed, PVP, PEO and PVA established hydrogen bonds with MMT implying that their intercalation in the clay interlayer spacing depends on the extent of hydrogen bonding. Chitosan and PVP bilayers have the lowest intercalation, meaning a more stacked clay platelets

than PEO and PVA bilayers. This weak intercalation may be explained by the presence of cyclic groups in both polymers which imparts rigidity to the polymer chain. The better intercalation in the PVA bilayers compare with the PEO is due to the higher reactivity of its functional groups.

Considering that the rigidity of chitosan hinders its diffusion[4], one can infer that nanoclay intercalation, for a quadlayer assembly, depends mainly on the diffusion of polymers through the chitosan layers. As MMT is trapped between chitosan layers, nanoclay intercalation should not be much different for the three quadlayers. However, it can be seen that the level of nanoclay intercalation depends on the polymer type in the three quadlayers assemblies. This supports previous studies suggesting that LbL assemblies have interpenetrated structures [44-47].

PEO and PVP quadlayers have almost the same intercalation of the bilayers with a slight increase, whereas PVA quadlayers have a decrease in the interlayer spacing compare to the bilayers due to the interference of CS in the interaction with MMT (Table 5.1).

The main difference between quadlayer and bilayer structures is the interaction between the polymer layers. In a bilayer, the polymer interacts mainly with clay whereas in a quadlayer, the interaction between adjacent polymers is the predominant one. A study of the morphology of the assemblies could shed more light on those interactions.

5.2.2 Coating morphology

The thickness of the assemblies was measured by profilometry, Figure S.4. For the three quadlayers, the increase in the thickness is linear related to the number of layers. However, the slope of the increase in thickness depends on the type of polymer. PVA resulted in a thinner coating, most probably due to a higher density of established hydrogen bonding with CS and MMT, while PVP led to thicker coatings which, could be attributed to a considerable fraction of free volume in the coating.

Table 5.1 summarises some physical properties and crystallography of the studied assemblies measured by FTIR, profilometry and XRD. For the same number of layers, the bilayers are thicker which is probably due to the higher nanoclay content of these structures. Indeed, with lower amount

of nanoclay, the quadlayers have more interaction and inter-diffusion between the polymer layers, resulting in a thinner structure compare to bilayer assemblies.

Table 5.1 Physical properties and crystallography of the studied assemblies.

Multilayers / Properties		PEO	PVA	PVP	CS	PVA	PVP	PEO
		6 quadlayers			12 bilayers			
Orientation function (f_{CN})		0.725	0.625	0.65	0.575	0.675	0.5	0.425
Thickness (μm)		0.266	0.236	0.309	0.33	0.37	0.5	0.48
Crystallo.	2theta	4.63	6.46	5.97	6.47	4.44	6.43	4.83
	d-spacing (Å)	19	13.67	14.78	13.64	19.89	13.73	18.26

The nanostructure of the coating was examined using AFM imaging. Figure 5.5 A and B show the typical nanostructure of a PVA quadlayer coating.

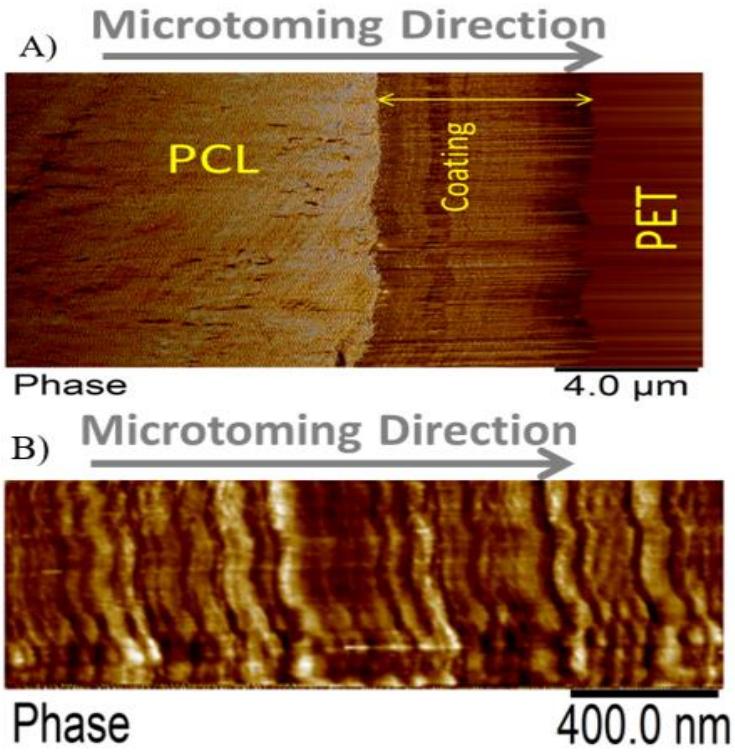

Figure 5.5 Atomic Force Microscopy (AFM) images of a PVA quadlayer coating. The cross section scanned at low (A) and high (B) magnification illustrates the layered structure of the coating.

The periodic multilayer structure is composed of two different materials shown as a darker and a brighter phase, Figure 5.5. The darker phase in the AFM image indicates a longer contact time between the tip and the surface which could be due to the softness or higher level of interactions of the surface with the tip. As the AFM tip used in this study is made of silicon, a better interaction between MMT nanoparticles and the tip is expected.

The nature of the darker phase can also be examined using the height profile over different regions of coated layer, Figure 5.6. The results indicate that the darker phase has always a lower height compared with the other phase. Considering that the thermal expansion coefficient of silica based material is at least ten times lower than that of polymers such as PVA[48-49], both lower height and darker color leads to the conclusion that the darker phase should be the nanoclay layer.

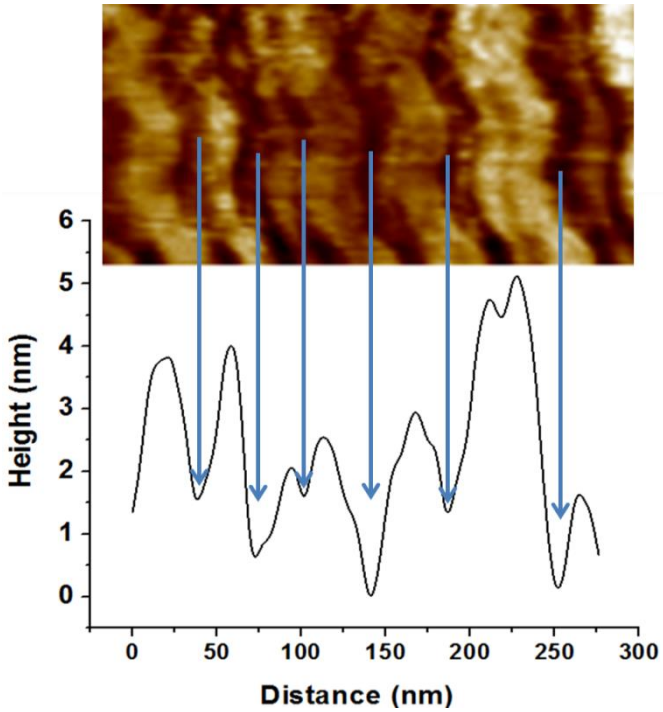

Figure 5.6 Height profile of the coating.

Image analysis results indicate a layer thickness of 31±11 nm for the darker phase and 52±25nm for the brighter phase. The greater standard deviation of the brighter phase indicates a broader distribution for the thickness of this layer. During coating preparation, a four-layered sequence was deposited, CS/ PVA/ CS/MMT but, only two layers can be observed with AFM. These results further corroborate our previous results indicating PVA diffusion through the chitosan layer. As Chitosan and PVA are miscible [50] and PVA layer is trapped between chitosan layers, only one phase represents all of the polymers' layers.

5.2.3 **Permeability to oxygen**

The better understanding of nanoclay properties as well as polymer interactions in the prepared assemblies allow a much deeper interpretation of oxygen permeability results. As discussed previously, the main difference between bilayer and quadlayer assemblies is the polymers interaction in the quadlayers. The importance of this interaction is clearly perceived through the difference in permeability between the two types of assemblies (Figure5.7). Both types of coatings reduce considerably the neat PET permeability, 156 cc.mil/m^2.day.

In contrast with PVA, both PVP and PEO quadlayer assemblies have four times less permeability than bilayers; this result correlates well with those of Priolo and al.[16] and further supports the idea of a better oxygen barrier with higher spacing between clay layers. Considering that bilayer coatings are thicker than quadlayers, as shown in Table 5.1, the latter have clearly better intermolecular interaction due to the presence of CS layers that allow more hydrogen bonding in the films, resulting in a better oxygen barrier.

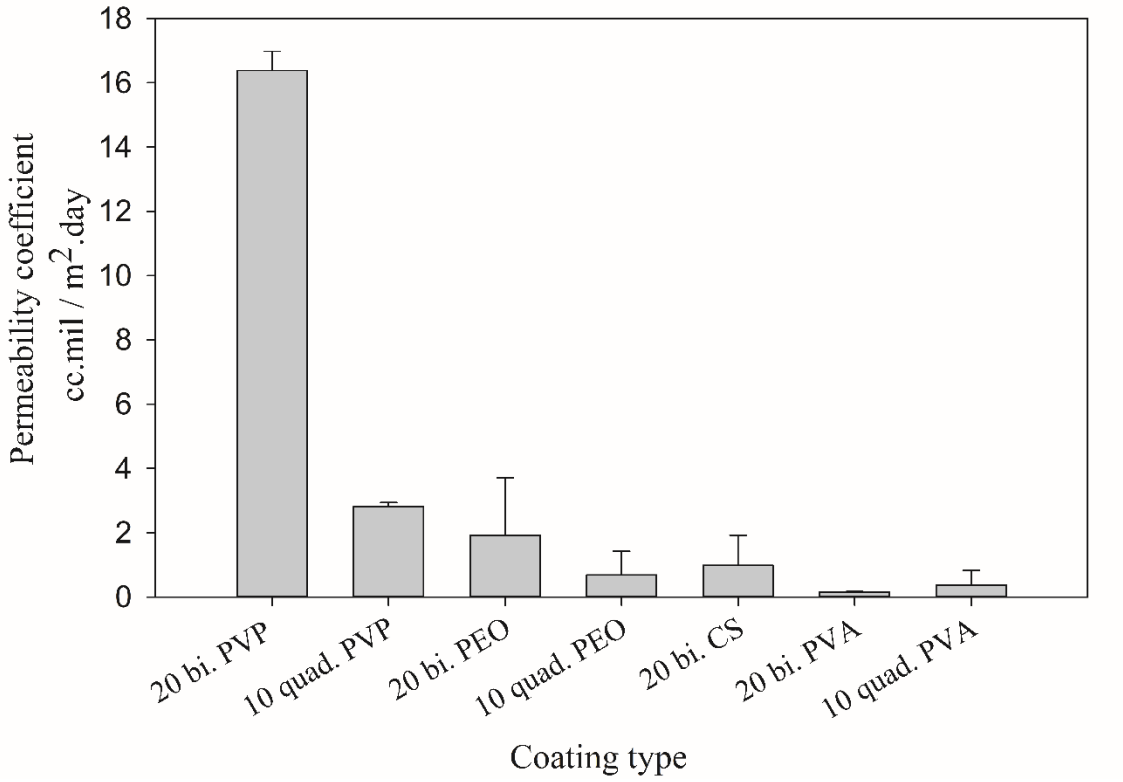

Figure 5.7 Oxygen permeability for bilayer and quadlayer assemblies.

The PVA bilayer, however, has a better barrier than the quadlayer. PVA is known for its significant interaction with nanoclay, resulting in thin coatings with appreciable mechanical properties [38, 51]. The incorporation of CS can create more free volume in the coating since it has a rigid structure, which, even with good electrostatic interactions and hydrogen bonding, results in more free volume compare with the PVA-MMT bilayers. This would explain the lower intercalation and orientation in the case of PVA quadlayers compare to the bilayers.

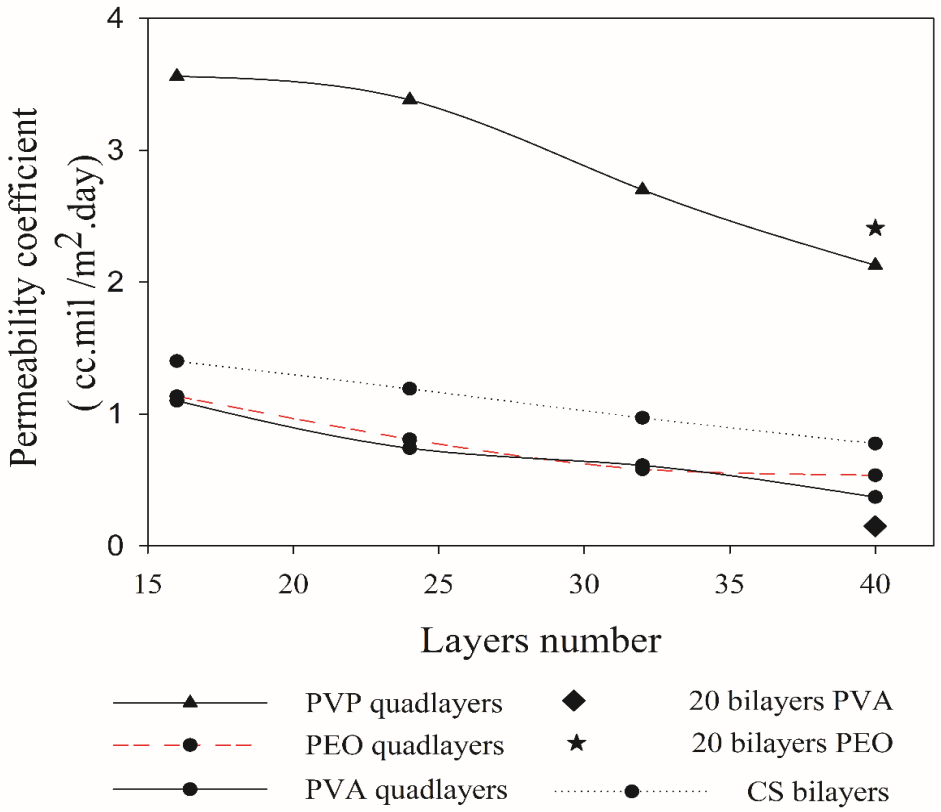

Figure 5.8 Oxygen permeability as a function of the number of deposited layers for four types of assemblies.

Despite the better intercalation with PVP compare to PVA for the quadlayers assemblies, the permeability to oxygen of the PVP quadlayers is much higher, Figure 5.8. This implies that the intermolecular interaction has more impact on the oxygen barrier than clay intercalation.

Permeability models

Different models presented in Table 5.2 have been used for estimating the relative permeability of nanocomposites. Based on the effect that the clay properties (aspect ratio, orientation and volume fraction), its dispersion and the barrier property of neat polymers have on the gas barrier efficiency of the nanocomposites coatings,[52] these models considered the aspect ratio, L/W (with L, the length and W, the width of a nanoclay platelet), along with the volume fraction (ϕ) and the orientation factor (S) as parameters affecting tortuosity. In addition to the models presented for polymer nanocomposites, some empirical and analytical models have been proposed in literature to predict

the permeability of thin film composite (TFC) membranes and mixed matrix membranes (MMMs) which are mainly extensions of Maxwell model.[53-57]

As an example, a trilayer assembly of CS-PVA-MMT on a PET substrate was studied and the relative permeability, P/P_0, was the ratio of the trilayer CS-PVA-MMT permeability coefficient to the one of CS-PVA bilayer on a PET substrate. Only the permeability of the LBL coatings was considered by calculating according to the relationship between the permeability and thickness of a multilayer film:[58]

$$\frac{P_L}{\sum l_i} = \frac{1}{\sum(l_i/P_i)} \tag{5.5}$$

where P_L stands for the total permeability of a multilayer, l_i and P_i are the thickness and permeability for a given layer i respectively.

The different nanoclay parameters were obtained experimentally. The representative weight fraction of MMT was determined using TGA as the final residue at 800 ºC. The nanoclay volume fraction was calculated according to TGA and profilometry results; and the measured ϕ and f_{CN} were 0.25 and 0.65 respectively, while a 166 aspect ratio was used in this study[59].

Table 5.2 Permeability models and their predicted values for filled polymer systems.

Model	Relative permeability formula (P/P_0)	Considered parameters	Predicted relative permeability
Bharadwaj [60]	$\frac{1-\emptyset}{1+\frac{L\emptyset}{2W}(\frac{2}{3})(S+\frac{1}{2})}$	S=1 Perfect orientation	0.044
Gusev [61]	$exp[-(\frac{L\emptyset}{3.47W})^{0.71}]$	Perfect orientation No overlapping	0.00296
Nielsen [62]	$\frac{1-\emptyset}{1+\frac{L\emptyset}{2W}}$	Perfect orientation	0.03448

Cussler [63-64]	$\frac{1-\emptyset}{1-\emptyset+\frac{\mu}{4}(\frac{L\emptyset}{W})^2}$	μ=0.5 Randomly spaced flakes μ=0 Regularly spaced flakes and infinitely long in one dimension	0.0009
Maxwell [65]	$\frac{1-\emptyset}{1+\frac{\emptyset}{2}}$	Dilute suspension	0.281

Among these models, only Bharadwaj didn't consider a perfect orientation. Bharadwaj revised Nielsen's model by introducing the contribution of nanoclay orientation in tortuosity. The order parameter, S, in this model is defined as:

$$S = \frac{1}{2}\langle 3\cos^2\theta - 1\rangle \tag{5.6}$$

With θ as the angle between the direction of the normal unit vectors of the coating and the nanoclay platelets. The angular brackets designate the average for all the clay platelets in the coating.[60] In his model, Bharadwaj considered three possible orientations, perpendicular where S=-1/2, a perfect orientation with S=1 and an intermediate situation representing a random orientation with S=0.

With this model, the lowest achievable P/P_0 for this coating is equal to 0.057, when a perfect orientation (S=1) is considered, which is not the case of this LbL coating.

With a 25 vol% nanoclay, the measured permeability ratio, P/P_0 was 0.00142 (a reduction of 99.85%). Given such a percentage, models considering dilute suspensions such as Maxwell's are the ones to diverge the most from the permeability of LbL deposited coatings. Lower values are obtained with Gusev and Cussler models, since aspect ratio and volume fraction effects on permeability are more accentuated by considering an exponential and a quadratic effect respectively. Gusev's model is, however, mathematical without a physical approach, making thus Nielsen and Cussler models the closest models to the experimental data to be considered, Figure 5.9.

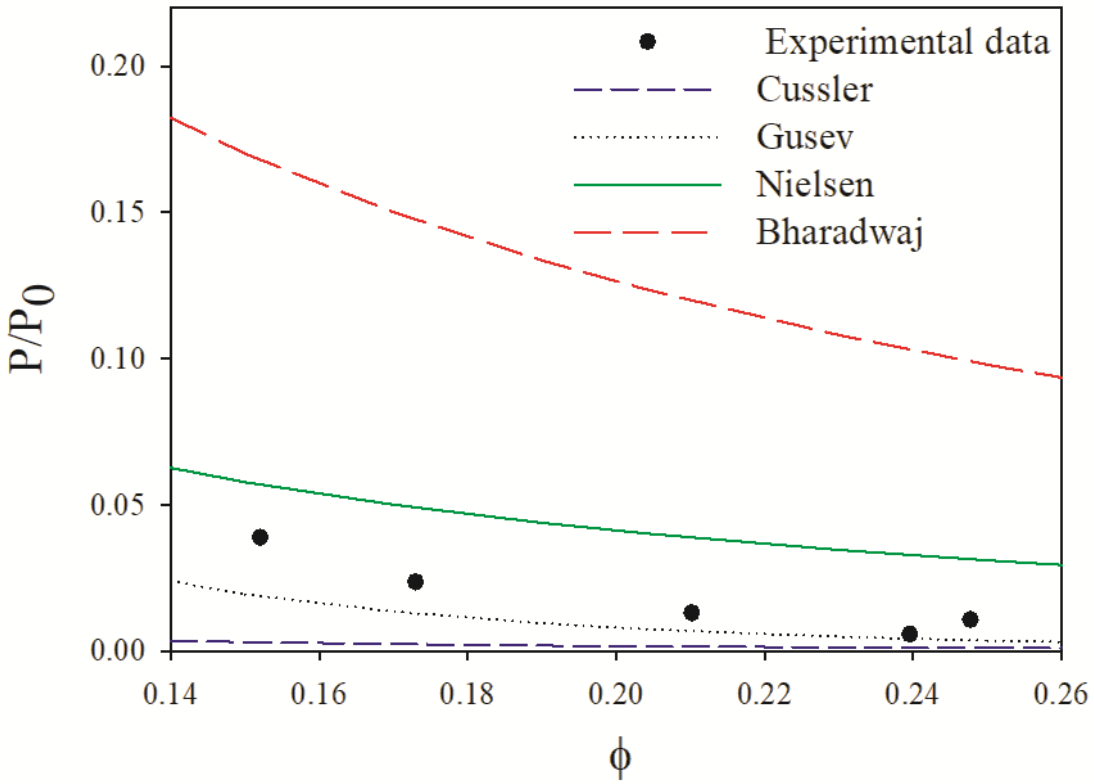

Figure 5.9 Experimental data compared with permeability models.

By considering the P/P0 ratio in permeability models, the properties of the matrix are assumed unaltered by the addition of fillers. However the polymer- clay interaction results in an interface region around the clay platelets characterized by a higher density than the bulk.[66] Due to the high volume fraction of clay in LbL coatings, the volume fraction of this interface becomes considerable. As the studied nanocomposite coatings lack crystallinity, Figure S.5, impermeable domains are limited to the volume fraction of clay and the interface. The increase of this fraction can be expressed as an increase in the clay volume fraction by a factor β. By considering the interfacial region, Nielsen's model can be rewritten as follow:

$$\frac{P}{P_0} = \frac{1-\beta\phi}{1+\frac{L}{2W}.\beta\phi} \tag{5.7}$$

A value of 2, obtained by fititing, for the β factor, reduces the RSS from 0.0043 to 0.0015. This same modification for Bharadwaj's model, decreases the RSS ten times (from 0.06 to 0.0058),

Figure 5.10. This modification can't be applied to Cussler's model as the predicted values are lower than the experimental ones.

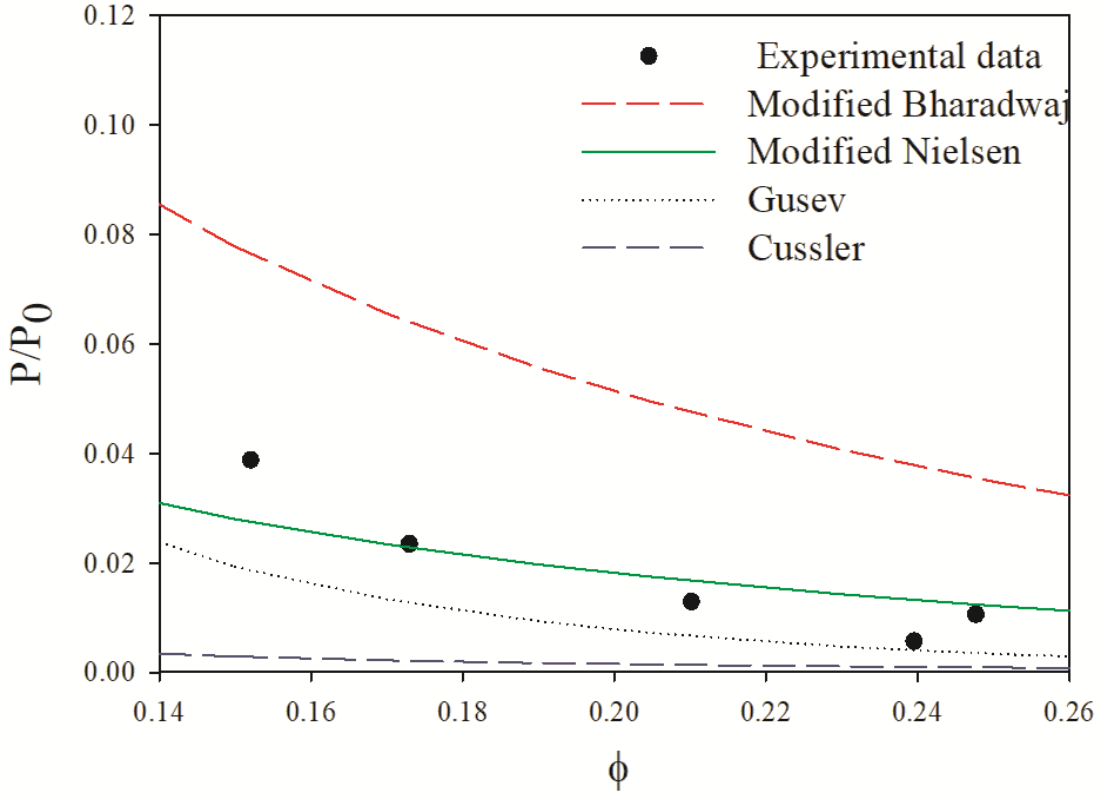

Figure 5.10 Comparison of the experimental data to various models

5.3 Conclusion

In this work, the orientation of nanoclay platelets in hydrogen bonding based LbL assemblies was investigated and its influence on coatings' properties was discussed in detail. The obtained results highlight that LbL assembled coatings don't show a perfectly oriented nanoclay and its orientation is highly affected by the polymer's physical properties. To have a better understanding of the tortuosity in an LbL film, experimental data were compared to permeability models and the impact of the polymer filler interaction in permeability was highlighted. As the purpose from this study is to have a better understanding of the tortuosity in an LbL film, it was only based on one type of filler. Further work will be conducted to study other types of LbL coatings.

5.4 Acknowledgement

The authors gratefully acknowledge the financial support of 3SPack NSERC Industrial Research Chair by the Natural Science and Engineering Council of Canada (NSERC) and ProAmpac Inc. Company.

REFERENCES

1. Choudalakis, G.; Gotsis, A. D., Permeability of polymer/clay nanocomposites: A review. *Eur Polym J* **2009,** *45* (4), 967-984.
2. Picard, E.; Vermogen, A.; Gerard, J.; Espuche, E., Barrier properties of nylon 6-montmorillonite nanocomposite membranes prepared by melt blending: Influence of the clay content and dispersion stateConsequences on modelling. *J. Membr. Sci.* **2007,** *292* (1-2), 133-144.
3. Oguzlu, H.; Tihminlioglu, F., Preparation and Barrier Properties of Chitosan-Layered Silicate Nanocomposite Films. *Macromol Sy* **2010,** *298* (1), 91-98.
4. Laufer, G.; Kirkland, C.; Cain, A. A.; Grunlan, J. C., Oxygen barrier of multilayer thin films comprised of polysaccharides and clay. *Carbohydr. Polym.* **2013,** *95* (1), 299-302.
5. Selke, S. E. M., *understanding plastics packaging technology*. Hanser publishers: Munich, 1997.
6. Cole, K. C., Use of infrared spectroscopy to characterize clay intercalation and exfoliation in polymer nanocomposites. *Macromolecules* **2008,** *41* (3), 834-843.
7. Cole, K. C.; Perrin-Sarazin, F.; Dorval-Douville, G., Infrared spectroscopic characterization of polymer and clay platelet orientation in blown films based on polypropylene-clay nanocomposite. *Macromolecular Symposia* **2005,** *230* (1), 1-10.
8. Tabatabaei, S. H.; Ajji, A., Crystal structure and orientation of uniaxially and biaxially oriented PLA and PP nanoclay composite films. *Journal of Applied Polymer Science* **2011,** *124*, 4854–4863.
9. Varlot, K.; Reynaud, E.; Kloppfer, M. H.; Vigier, G.; Varlet, J., Clay-reinforced polyamide: Preferential orientation of the montmorillonite sheets and the polyamide crystalline lamellae. *J Polym Sci Pol Phys* **2001,** *39* (12), 1360-1370.
10. Tabatabaei, S. H.; Ajji, A., Structure-orientation-properties relationships for polypropylene nanoclay composite films. *J Plast Film Sheet* **2011,** *27* (1-2), 87-115.
11. Bartczak, Z.; Rozanski, A.; Richert, J., Characterization of clay platelet orientation in polylactide-montmorillonite nanocomposite films by X-ray pole figures. *European Polymer Journal* **2014,** *61*, 274-284.
12. Fereydoon, M.; Tabatabaei, S. H.; Ajji, A., Properties of co-extruded nanoclay-filled aliphatic nylon (PA6)/linear low-density polyethylene and aromatic nylon (MXD6)/ linear low-density polyethylene multilayer films. *J Plast Film Sheet* **2014,** *31* (1), 45-77.
13. Priolo, M. A.; Holder, K. M.; Guin, T.; Grunlan, J. C., Recent Advances in Gas Barrier Thin Films via Layer-by-Layer Assembly of Polymers and Platelets. *Macromol. Rapid Commun.* **2015,** *36* (10), 866-79.
14. Cui, Y. B.; Kumar, S.; Kona, B. R.; van Houcke, D., Gas barrier properties of polymer/clay nanocomposites. *Rsc Adv* **2015,** *5* (78), 63669-63690.
15. Malwitz, M. M.; Lin-Gibson, S.; Hobbie, E. K.; Butler, P. D.; Schmidt, G., Orientation of platelets in multilayered nanocomposite polymer films. *J Polym Sci Pol Phys* **2003,** *41* (24), 3237-3248.
16. Priolo, M. A.; Holder, K. M.; Greenlee, S. M.; Stevens, B. E.; Grunlan, J. C., Precisely Tuning the Clay Spacing in Nanobrick Wall Gas Barrier Thin Films. *Chem Mater* **2013,** *25* (9), 1649-1655.

17. Xiang, F.; Tzeng, P.; Sawyer, J. S.; Regev, O.; Grunlan, J. C., Improving the gas barrier property of clay-polymer multilayer thin films using shorter deposition times. *ACS Appl Mater Interfaces* **2014,** *6* (9), 6040-8.
18. Tzeng, P.; Maupin, C. R.; Grunlan, J. C., Influence of polymer interdiffusion and clay concentration on gas barrier of polyelectrolyte/clay nanobrick wall quadlayer assemblies. *J. Membr. Sci.* **2014,** *452*, 46-53.
19. Laufer, G.; Kirkland, C.; Cain, A. A.; Grunlan, J. C., Clay-chitosan nanobrick walls: completely renewable gas barrier and flame-retardant nanocoatings. *ACS Appl Mater Interfaces* **2012,** *4* (3), 1643-9.
20. Holder, K. M.; Priolo, M. A.; Secrist, K. E.; Greenlee, S. M.; Nolte, A. J.; Grunlan, J. C., Humidity-Responsive Gas Barrier of Hydrogen-Bonded Polymer-Clay Multilayer Thin Films. *J Phys Chem C* **2012,** *116* (37), 19851-19856.
21. Priolo, M. A.; Gamboa, D.; Holder, K. M.; Grunlan, J. C., Super gas barrier of transparent polymer-clay multilayer ultrathin films. *Nano Lett* **2010,** *10* (12), 4970-4.
22. Jang, W. S.; Rawson, I.; Grunlan, J. C., Layer-by-layer assembly of thin film oxygen barrier. *Thin Solid Films* **2008,** *516* (15), 4819-4825.
23. de Villiers, M. M.; Otto, D. P.; Strydom, S. J.; Lvov, Y. M., Introduction to nanocoatings produced by layer-by-layer (LbL) self-assembly. *Advanced drug delivery reviews* **2011,** *63* (9), 701-15.
24. Gaidukov, S.; Danilenko, I.; Gaidukova, G., Characterization of Strong and Crystalline Polyvinyl Alcohol/Montmorillonite Films Prepared by Layer-by-Layer Deposition Method. *International Journal of Polymer Science* **2015,** *2015*, 1-8.
25. Lutkenhaus, J. L.; McEnnis, K.; Hammond, P. T., Tuning the glass transition of and ion transport within hydrogen-bonded layer-by-layer assemblies. *Macromolecules* **2007,** *40* (23), 8367-8373.
26. Priolo, M. A.; Gamboa, D.; Grunlan, J. C., Transparent Clay−Polymer Nano Brick Wall Assemblies with Tailorable Oxygen Barrier. *ACS Applied Materials & Interfaces* **2010,** *2* (1), 312-320.
27. Hagen, D. A.; Box, C.; Greenlee, S.; Xiang, F.; Regev, O.; Grunlan, J. C., High gas barrier imparted by similarly charged multilayers in nanobrick wall thin films. *Rsc Adv* **2014,** *4* (35), 18354-18359.
28. Holder, K. M.; Spears, B. R.; Huff, M. E.; Priolo, M. A.; Harth, E.; Grunlan, J. C., Stretchable gas barrier achieved with partially hydrogen-bonded multilayer nanocoating. *Macromol. Rapid Commun.* **2014,** *35* (10), 960-4.
29. Guin, T.; Krecker, M.; Hagen, D. A.; Grunlan, J. C., Thick growing multilayer nanobrick wall thin films: super gas barrier with very few layers. *Langmuir : the ACS journal of surfaces and colloids* **2014,** *30* (24), 7057-60.
30. Vidyasagar, A.; Sung, C.; Gamble, R.; Lutkenhaus, J. L., Thermal Transitions in Dry and Hydrated Layer-by-Layer Assemblies Exhibiting Linear and Exponential Growth. *ACS nano* **2012,** *6* (7), 6174-6184.
31. Yang, Y. H.; Haile, M.; Park, Y. T.; Malek, F. A.; Grunlan, J. C., Super Gas Barrier of All-Polymer Multilayer Thin Films. *Macromolecules* **2011,** *44* (6), 1450-1459.
32. Martin, C.; Jean, B., Nanocellulose/polymer multilayered thin films: tunable architectures towards tailored physical properties. *Nord Pulp Pap Res J* **2014,** *29* (1), 19-30.
33. Gates, S. J.; Shukla, A., Layer-by-Layer Assembly of Readily Detachable Chitosan and Poly(acrylic acid) Polyelectrolyte Multilayer Films. *J Polym Sci Pol Phys* **2017,** *55* (2), 127-131.
34. Aulin, C.; Karabulut, E.; Tran, A.; Wagberg, L.; Lindstrom, T., Transparent nanocellulosic multilayer thin films on polylactic acid with tunable gas barrier properties. *ACS Appl Mater Interfaces* **2013,** *5* (15), 7352-9.
35. Xiang, F.; Ward, S. M.; Givens, T. M.; Grunlan, J. C., Structural tailoring of hydrogen-bonded poly(acrylic acid)/poly(ethylene oxide) multilayer thin films for reduced gas permeability. *Soft matter* **2015,** *11* (5), 1001-7.

36. L. Fang; Goh, S. H., Miscible Chitosan/Tertiary Amide Polymer Blends. *Journal of Applied Polymer Science* **2000,** *76*, 1785–1790
37. Shuguang Cao; Yanqiao Shi; Chen, G., Blend of chitosan acetate salt with poly(N-vinyl-2pyrrolidone): Interaction between chain-chain. *Polymer Bulletin* **1998,** *41*, 553–559.
38. Patro, T. U.; Wagner, H. D., Layer-by-layer assembled PVA/Laponite multilayer free-standing films and their mechanical and thermal properties. *Nanotechnology* **2011,** *22* (45), 455706.
39. Sun, J.; Su, C.; Zhang, X.; Yin, W.; Xu, J.; Yang, S., Reversible swelling-shrinking behavior of hydrogen-bonded free-standing thin film stabilized by catechol reaction. *Langmuir : the ACS journal of surfaces and colloids* **2015,** *31* (18), 5147-54.
40. Yang, S.; Zhang, Y.; Zhang, X.; Guan, Y.; Xu, J.; Zhang, X., From cloudy to transparent: chain rearrangement in hydrogen-bonded layer-by-layer assembled films. *Chemphyschem* **2007,** *8* (3), 418-24.
41. Farmer, V. C., *The Infrared Spectra of Minerals* Mineralogical Society of Great Britain and Ireland: London, 1974; Vol. 4.
42. Cole, K. C.; Depecker, C.; Jutigny, M.; Lefebvre, J. M.; Krawczak, P., Biaxial deformation of polyamide-6: Assessment of orientation by means of infrared trichroism. *Polym Eng Sci* **2004,** *44* (2), 231-240.
43. j. brandrup; e. h. immergut; grulke, e. a., *Polymer Handbook (Fourth Edition)*. Wiley: New York, 1999.
44. Picart, C.; Mutterer, J.; Richert, L.; Luo, Y.; Prestwich, G. D.; Schaaf, P.; Voegel, J. C.; Lavalle, P., Molecular basis for the explanation of the exponential growth of polyelectrolyte multilayers. *Proc. Natl. Acad. Sci. U.S.A* **2002,** *99* (20), 12531-5.
45. Schmitt, J.; Grunewald, T.; Decher, G.; Pershan, P. S.; Kjaer, K.; Losche, M., Internal Structure of Layer-by-Layer Adsorbed Polyelectrolyte Films - a Neutron and X-Ray Reflectivity Study. *Macromolecules* **1993,** *26* (25), 7058-7063.
46. Decher, G., Fuzzy nanoassemblies: Toward layered polymeric multicomposites. *Science* **1997,** *277* (5330), 1232-1237.
47. Lösche, M.; Schmitt, J.; Decher, G.; Bouwman, W. G.; Kjaer, K., Detailed structure of molecularly thin polyelectrolyte multilayer films on solid substrates as revealed by neutron reflectometry. *Macromolecules* **1998,** *31* (25), 8893-8906.
48. Becker, P.; Scyfried, P.; Siegert, H., The lattice parameter of highly pure silicon single crystals. *Zeitschrift für Physik B Condensed Matter* **1982,** *48* (1), 17-21.
49. Nagura, M.; Matsuzawa, S.; K., Y.; H., I., Tacticity Dependence of Molecular Motion in Crystal of Poly(vinyl alcohol). *Polym J.* **1982,** *14* (1), 69-72.
50. Jayaraju, J.; Keshavayya, J.; Rai, S. K.; Basavaraju, K. C., Miscibility Studies on Chitosan/Poly(vinyl alcohol) Blends. *Journal of Macromolecular Science, Part A* **2008,** *45* (4), 271-275.
51. Podsiadlo, P.; Kaushik, A. K.; Arruda, E. M.; Waas, A. M.; Shim, B. S.; Xu, J.; Nandivada, H.; Pumplin, B. G.; Lahann, J.; Ramamoorthy, A.; Kotov, N. A., Ultrastrong and stiff layered polymer nanocomposites. *Science* **2007,** *318* (5847), 80-3.
52. Moler, M. W.; Kunz, D. A.; Lunkenbein, T.; Sommer, S.; Nennemann, A.; Breu, J., UV-Cured, Flexible, and Transparent Nanocomposite Coating with Remarkable Oxygen Barrier. *Advanced Materials* **2012,** *24* (16), 2142-2147.
53. Mahajan, R.; Koros, W. J., Mixed matrix membrane materials with glassy polymers. Part1. *Polym Eng Sci* **2002,** *42* (7), 1420-1431.
54. Song, Q.; Nataraj, S. K.; Roussenova, M. V.; J. C. Tan; D. J. Hughes; W. Li; P. Bourgoin; M. A. Alam; A. K. Cheetham, S. A. A.-M.; E. Sivaniah, Zeolitic imidazolate framework (ZIF-8) based polymer nanocomposite membranes for gas separation. *Energy Environ. Sci.* **2012,** *5* (8), 8359-8369.

55. S. A. Sabzevari; Sadeghi, M.; Mehrabani-Zeinabad, A., Multi-Structural Model for Prediction of Effective Gas Permeability in Mixed-Matrix Membranes. *Macromol. Chem. Phys.* **2013,** *214* (20), 2367-2376.
56. S. A. Hashemifard; A. F. Ismail; Matsuura, T., A new theoretical gas permeability model using resistance modeling for mixed matrix membrane systems. *J. Membr.Sci.* **2010,** *350* (1), 259-268.
57. K. L. Lee; Baker, R. W.; H. K. Lonsdale, Membranes for power generation by pressure-retarded osmosis. *J. Membr.Sci.,* **1981,** *8* (2), 141–171.
58. Siracusa, V., Food Packaging Permeability Behaviour: A Report. *International Journal of Polymer Science* **2012,** *2012*, 1-11.
59. Ploehn, H. J.; Liu, C. Y., Quantitative analysis of montmorillonite platelet size by atomic force microscopy. *Industrial & Engineering Chemistry Research* **2006,** *45* (21), 7025-7034.
60. Bharadwaj, R. K., Modeling the barrier properties of polymer-layered silicate nanocomposites. *Macromolecules* **2001,** *34* (26), 9189-9192.
61. Gusev, A. A.; Lusti, H. R., Rational design of nanocomposites for barrier applications. *Adv. Mater.* **2001,** *13* (21), 1641-1643.
62. Nielsen, L. E., Models for the Permeability of Filled Polymer Systems. *Journal of Macromolecular Science: Part A - Chemistry* **1967,** *1* (5), 929-942.
63. Chuanfang Yang; W.H. Smyrl; Cussler, E. L., Flake alignment in composite coatings. *Journal of Membrane Science* **2004,** *231* 1–12.
64. E.L.Cussler; Hughes, S. E.; William J. Ward, I.; Aris, R., barrier membranes. *Journal of Membrane Science* **1988,** *38*, 161-174.
65. Maxwell, J. C., *A Treatise On Electricity and Magnetism*. Dover Publications, Inc.: New York, 1881; Vol. 1.
66. Sorrentino, A.; Tortora, M.; Vittoria, V., Diffusion behavior in polymer-clay nanocomposites. *Journal of Polymer Science Part B: Polymer Physics* **2006,** *44* (2), 265-274.

CHAPTER 6 ARTICLE 2: COMPARISON OF CROSSLINKING EFFICIENCY IN DIP AND ROLL DEPOSITED COATINGS ON THEIR OXYGEN BARRIER

Fatma Ben Dhieb[1], Seyed H. Tabatabaei[2], Frej Mighri[3] and Abdellah Ajji[1*]

[1] *3SPack NSERC-Industry Chair, CREPEC, Chemical Engineering Department, Polytechnique Montreal, C.P. 6079, Succ. Centre ville, Montreal, QC, Canada H3C 3A7*

[2] *ProAmpac, Terrebonne, QC, Canada J6Y 1V2*

[3] *CREPEC, Chemical Engineering Department, Laval University, Quebec, QC, Canada*

(*) All correspondence should be addressed to: *abdellah.ajji@polymtl.ca*

(Published in *ACS Omega*, 16 September 2019)

Abstract

Coating techniques are key factors in determining coated film properties. In the present study, nanocomposite coating of polyvinyl alcohol (PVA) and a nanoclay, Montmorillonite, were deposited layer by layer using roll (doctor blade, DB) and dip coating techniques, in an effort to compare the impact of these techniques on crosslinking efficiency and oxygen barrier of the coated films. The barrier properties at different relative humidities were tested, and the extent of nanoclay intercalation as well as the films' morphology was investigated. Barrier was further improved by crosslinking the coating with glyoxal and glutaraldehyde. Both techniques gave similar results but with a higher impact of relative humidity in roll coated films. Better results were achieved by tailoring the composition of those coatings to favor a higher density of hydrogen bonding in the coating.

Keywords: LbL, roll and dip, Nanocomposites, oxygen permeability, crosslinking

Introduction

High oxygen barrier materials are in increasing demand for food packaging. Numerous food products have a shelf life that could be shortened due to an inadequate gas barrier of the package. Several technologies have been adopted to enhance the oxygen barrier. Silicon oxide (SiO_x) coating results in a transparent coated film that is microwavable and has a low oxygen permeability as well as a good resistance to water vapor.[1-2] Its weak adhesion to plastic substrates and ease of cracking [3-4] however limits its use in packaging. To have more flexible films, multilayer polymer films were adopted in packaging. This structure enables achieving the required properties (mechanical, saleability, etc.) while maintaining a desirable appearance. Their processing, however, is complicated and their potential recycling, cost, and final possible barrier are limiting factors. Blends also have been extensively studied to produce barrier materials with a possible recycling of used polymers. High barrier polymers like ethylene vinyl alcohol (EVOH) and poly(vinyl alcohol) (PVA) are used as the dispersed phase to reduce the permeability of the matrix. Such structure is cheaper than a multilayered one and reduces the sensitivity to moisture of some high-barrier polymers. The main challenge of blending, though, is the compatibilization of the phases, as most of the polymers are immiscible.

Adding fillers to polymers has gained popularity as an affordable way to reduce polymer permeability[5] and enhance its mechanical properties.[6] It is mainly used with solution casting and extrusion, but a high filler loading cannot be reached, as the resulting agglomeration alters the composite's properties.

The high aspect ratio of clays, such as montmorillonite (MMT) (more than 100[7]), slows the diffusion of oxygen molecules through the polymer by increasing their diffusing path, known as tortuosity.

To improve this tortuosity, the filler's volume fraction and its aspect ratio are usually the considered parameters.[8-9]

The filler's orientation has also an important impact on tortuosity, as demonstrated by Bhardwaj's permeability model,[10] even though it is not usually considered for the modeling of nanocomposite permeability. A vertically orientated fillers, for example, would not improve the tortuosity in the film as does a perfectly horizontally oriented one.

An important factor to be considered when manufacturing nanocomposites is the chosen technique, considering its impact on these fillers' properties. Polymer/clay nanocomposites, for instance, are often prepared by solution and melt intercalation. The main drawback is the clay platelets agglomeration during the processing[11] that limits the amount of clay that can be incorporated in the nanocomposites, particularly in the melt state. This may result in an oxygen barrier not high enough for many applications. For a better barrier and acceptable film transparency, a good clay dispersion and intercalation must be achieved.

In some packaging applications, there is an increasing demand for alternative high-barrier materials due to the growing awareness about recyclability. Such materials could be obtained with nanocomposite coatings, as they result in a thinner structure than melt processed or cast nanocomposites films and an easier recyclability. These coatings have also a better barrier owing to the important fraction of clay that can be achieved. New techniques such as Layer by Layer (LbL) have succeeded in depositing thin nanocomposite coatings with good orientation,[12] dispersion and intercalation of clay platelets. This method consists in the successive deposition of thin layers (polymers and/or nanofiller) on a substrate with numerous types of interlayer interactions to hold these layers together (electrostatic interactions, hydrogen bonding, etc.). Depending on their composition, the thickness of these layers can reach hundreds of nanometers. LbL coatings have a higher gas barrier than conventional metal or mineral oxides coating techniques, as it enables a high clay loading without aggregation.[13]

LbL deposition could be achieved with various processes, such as spin coating,[14] spraying[15-16] and dipping,[17-18] for which scaling up is still a challenge. Another technique that can be applied to LbL thin film deposition is a roll-to-roll process, such as blade coating (DB). This technique, derived from screen-printing, enables the deposition of thin films (hundreds of nanometers) quickly with low material consumption.[19] For LbL nanocomposite coatings, the filler layer can be deposited separately from the polymer and not as a mix, like in the case of single-layer coatings. Due to such alternate deposition, it is possible to have a coating with a considerable amount of filler. [13]

LbL technique is widely applied to water-soluble polymers, which have high sensitivity to moisture. To further improve the oxygen barrier at high relative humidity, there is generally recourse to crosslinking. Dialdehyde crosslinkers (glutaraldehyde (GA), glyoxal (Gly), etc.) are among the most frequently used ones due to their high reactivity and increasing efficiency in

crosslinking water soluble polymers coatings, thus reducing their sensitivity to moisture. [20-21] The focus of this work is on the impact of the chosen coating technique on the oxygen barrier at high relative humidity, which, to our knowledge has not been addressed before.

In this study, LbL coatings of PVA and MMT were deposited on a PET substrate though two techniques, blade and dip coating with the aim of comparing their efficiency in improving the coating's oxygen barrier at high relative humidity. To reduce the sensitivity to moisture, the nanocomposite coatings were crosslinked with two dialdehydes, glyoxal, and glutaraldehyde. The effect of crosslinking on their permeability was investigated and the oxygen permeability of those coatings as a function of the relative humidity was reported. Coatings morphology was analyzed using atomic force microscopy (AFM) and the intercalation of clay platelets was characterized by X-Ray diffraction (XRD).

6.1 Experimental

6.1.1 Materials

PVA (Mw=140 000–186 000 g. mol^{-1}) was purchased from Sigma Aldrich (Saint Louis, Missouri). Natural sodium montmorillonite (MMT) platelets (Cloisite NA^{+}), nanoclay, with a density of 2.86 g/cm^3 were supplied by BYK (Gonzales, Texas) and used as received. Silicon plates, supplied by EL-Cat Inc. (Ridgefield Park, New Jersey) and polyethylene terephthalate (PET) films, supplied by ProAmpac (Terrebonne, Qc, Canada), were used as substrates for LbL deposition. Polyethylene imine (PEI) (5% aqueous solution), supplied by MICA Corporation (Shelton, CT), was used as a primer for all the samples. The crosslinkers, glyoxal (Gly, 40% aqueous solution) and glutaraldehyde (GA, 25% aqueous solution), were purchased from Sigma Aldrich (Saint Louis, Missouri).

6.1.2 Preparation of Thin Films

PVA solutions and MMT suspensions were prepared with deionized (DI) water. PVA solutions were heated at 80 °C for 2 hours. A PEI solution (0.6% in DI water) was used to deposit a primer layer whether blade coated, or dip coated for 20 min and rinsed with DI water.

6.1.2.1 **Dip coating**

The coating deposition cycle is a repetition of dipping in PVA and MMT solutions, rinsing and drying steps, such as illustrated in Figure 6.1a. To increase the coverage of the surface, the dipping time was 5 min for the first bilayer and the rinsing time was 1 min. For the next layers, the dipping and rinsing times were reduced to 1 min and 30 s, respectively. To achieve chemical crosslinking, films were dipped in the GA or Gly solution (5% aqueous solution) after half of the bilayers had been deposited and then at the end, once all the 15 bilayers had been deposited.

6.1.2.2 **Roll (blade) coating**

PVA and MMT layers were deposited alternately by spreading the solution using the doctor blade (Harper Scientific (Charlotte, NC); Figure 6.1 b). As for dipping, a crosslinker layer was applied twice, once half of the bilayers had been deposited and at the end, after the final bilayer.

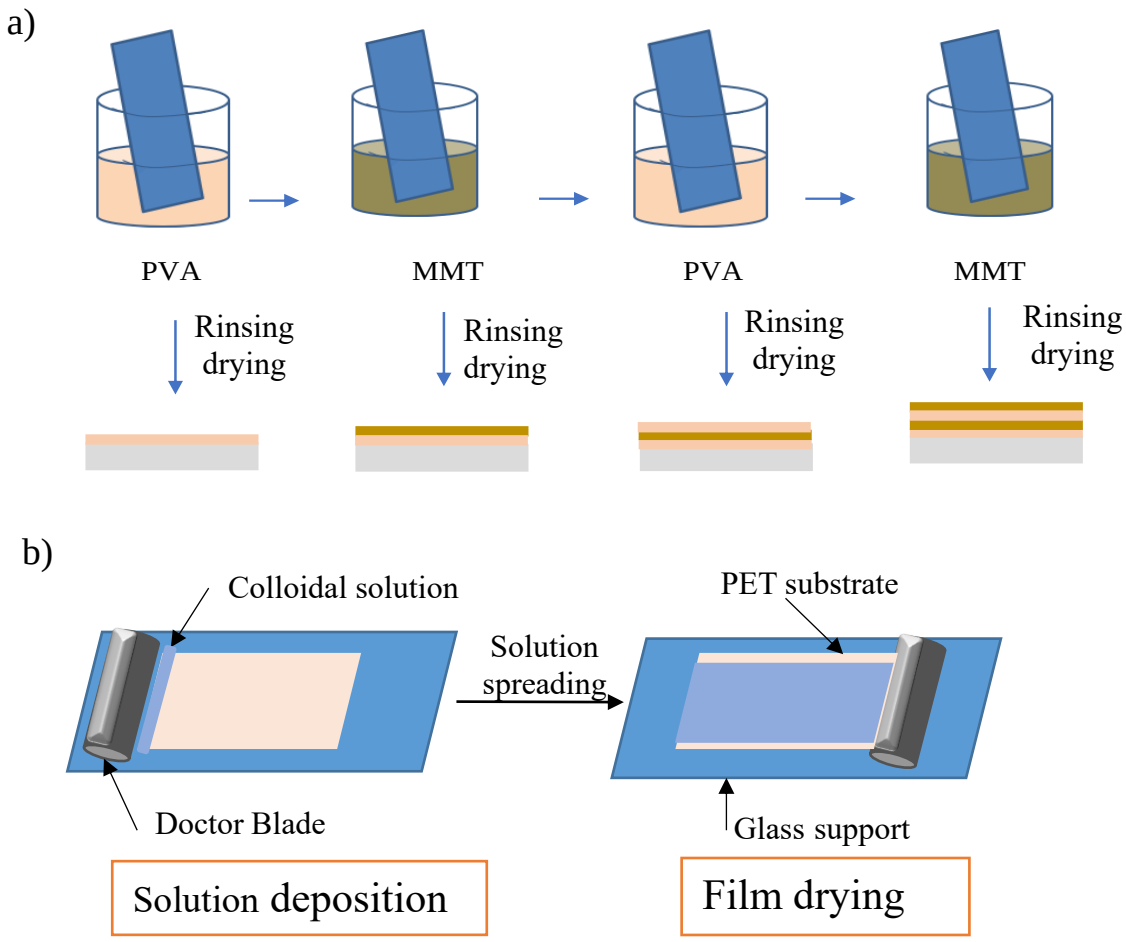

c)

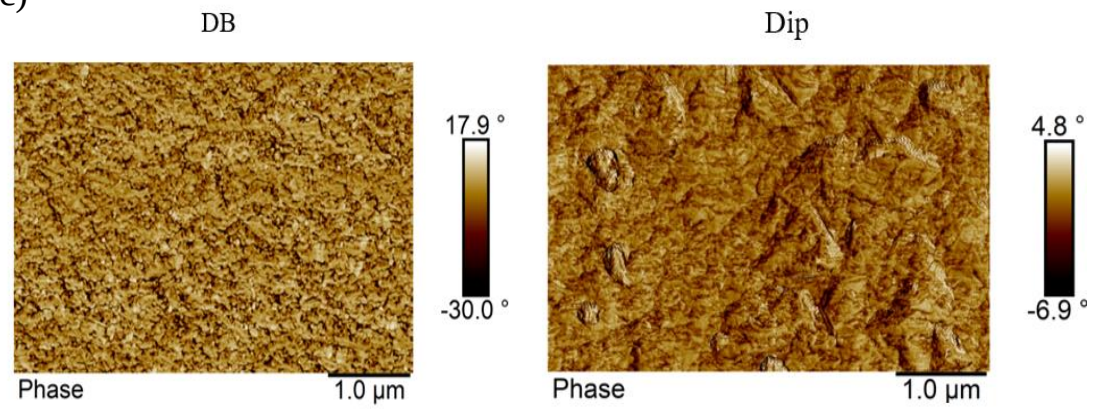

Figure 6.1 Steps of layer-by-layer assembly deposition by a) blade coating and b) dip coating and c) surface morphology of the two coatings

6.2 Characterization

X-ray diffraction (Philips X'pert) was used in the wide-angle mode (wide-angle X-ray diffraction (WAXD)), in the range from 2 to 10° at a rate of 0.02 °/s to determine the MMT interlayer spacing *d* (001) according to Bragg's law. The source is copper Cu Kα radiation (λ =1.54056 Å).

Permeability to oxygen was measured via a MOCON OXTRAN 2/21 (Minneapolis) at 25 °C, 0% relative humidity, and 1 atm pressure, in accordance with the ASTM D-3985-81. For tests with an adjustable relative humidity (RH), a MOCON OXTRAN 10X apparatus (Minneapolis) was used at 25 °C and a RH up to 70%. Water vapor permeability (WVP) was determined at 25°C, via a MOCON PERMATRAN-W Model 101K, for a 100% RH. Water contact angle was measured at room temperature, with distilled water as the probe liquid with a Contact Angle Goniometer OCA20 from dataphysics. The time chosen to calculate the contact angles by the software was 5s after a drop touches the sample surface. Five readings were measured for each sample and an average of these values was reported and used for the results discussion. The thickness of the coatings was determined with a Dektak 3030 profilometer using silicon plates as substrate. Morphology and roughness of the surface of coated layer was examined using an Atomic Force Microscope (AFM) (Nanoscope V Dimension Icon/ Fastscan AFM, Bruker) operated in the tapping mode in air. All of the imaging was acquired using Intermittent Peak Force tapping ™ using 125 µm TESPA-V2 Air probes with the tip radius of 8 nm. The average roughness of the samples was

determined by measuring roughness at 6 different points. The average roughness values are reported with the standard deviations. The surface microstructure was examined by comparing the phase images of different samples for 5μm ×5μm scan windows.

6.3 Results and discussion

Dip coating is a widely used technique for fundamental studies of LbL, whereas blade coating mimics better the industrial coating process and can be helpful in scaling up of the LbL deposition process. Blading technique is faster than dipping, taking approximately half of the time compared to dipping due to fewer steps. This technique is also more cost-effective, as it requires less material for each layer. The use of the DB enables a better control on the deposited volume of material. These techniques result in coatings with different morphologies and properties as discussed in the following sections.

6.3.1 Oxygen and moisture barrier

Oxygen transmission rates (OTR) of PET films coated with LbL deposited assemblies were measured at 23°C and 0% RH. A 15-bilayers coating reduced the neat PET permeability considerably (Table 6.1). This high barrier is due, on one hand, to an important nanoclay loading[13] (>50 wt %) in the LbL coatings, which enhances the tortuosity in the film. On the other hand, the high density of hydroxyl groups in the PVA structure coupled to their strong hydrogen bonding,[22] whether intermolecular or with MMT, can be responsible of a considerable reduction of the free volume in the coatings, thus reducing the permeability.

Blade coating results in a better surface homogeneity than dip coating as illustrated in Figure 6.1c .The hetergeneous surface of dipped coatings is due to the progressive coverage of the substrate with each dipping step, commonly known as island growth.[23] For the first dipping cycles, the substrate surface is partially covered with “islands” of polymers. The homogeneity of the layers as well as a complete coverage of the substrate is eventually obtained with more dipping cycles. This difference in the surface coverage explains the better oxyen barrier of blade-coated films with a permeability almost one third that of dip-coated film at 0% RH.

Neat PET (16 μm) has a higher permeability than conventional barrier polymers like PVA (1.5 cm^3. μm/(m^2.day.atm)).[24] Coating with 15 PVA layers only reduced this permeabilty by 50% with dipping and by 80% with blading (Table 6.1).

Increasing the number of PVA layers (30 instead of 15) futher reduced the permeability by 90 %, whereas adding MMT layers, instead, in a 15-bilayer stucture (15 PVA+ 15 MMT) resulted in the highest reduction, 99%, for both dip and blade coatings. To compare the permeability of a PVA-MMT bilayer coating and a coating with layers of mixed PVA and MMT, a mixture of PVA and MMT was prepared by dispersing MMT in the PVA solution while keeping the same concentration as used for bilayer coating. The permeability of the mix coating was 10 times higher, which is mainly due to the poorer dispersion of MMT and a low intercalation of PVA.

Table 6.1 Oxygen permeability of coated PET and coatings only

	Permeability (cm^3. μm/(m^2.day.atm))	
	Total	coating
PET	3072	-
15 PVA dipped coating	1616.5	34.43
15 PVA bladed coating	405	4.75
30 PVA dipped coating	309	5.65
15 (PVA + MMT) dipped coating	47.59	1.75
15 PVA + 15 MMT dipped coating	8.17	0.48
15 PVA + 15 MMT bladed coating	3.47	0.2

Varying the relative humidity changed the barrier results for the two techniques. By increasing the humidity, the film is in contact with a considerable amount of water molecules that interact with

free hydroxyl groups at the surface. This interaction affects the permeability by altering the free volume in the coating. On one hand, water molecules may disrupt hydrogen bonding by breaking the existing bonds and establishing hydrogen bonds with hydroxyl groups.[20] This implies that a higher density of free hydroxyl groups may increase the permeability. On the other hand, the adsorption of water molecules results in the swelling of the coating,[15] allowing a higher diffusing area for oxygen. Such a swelling can be limited by the presence of well-intercalated MMT platelets in the coating with a strong interaction with the polymer.[25] According to these two points, the better barrier of dipped coating at higher humidity can be related to its lower amount of free hydroxyl groups and its reduced swelling due to the higher amount of MMT in the coating (Figure S.1). WVP results (Table 6.2) confirm this conclusion, as the blade-coated film has a higher permeability to the hydrophilic permeant, i.e. water vapour, implying a higher water adsorption due to the free functional groups.

6.3.2 **Crosslinking**

Crosslinking with Gly and GA reduced the oxygen permeability by 4-5 times for dipping and 2-6 for blading. The better barrier of the Gly crosslinked film may be due to small Gly molecules (Figure 6.2) which enables a faster diffusion through the multilayer structure.

The results are shown in Table 6.2. At high RH, crosslilnking with GA decreased the sensitivity to moisture for both types of coatings. Crosslinking with Gly, however, resulted in two distinct results, with a barrier improvement for dip-coated film and a sharp permeabiltiy increase for blade-coated film. Knowing that permeability in humid conditions depends on the interaction with water, this sharp increase of permeability with Gly could be explained by a higher amount of nonreacted Gly molecule in the film due to the short drying time. The presence of these nonbonded molecules in the coatings may disrupt the established hydrogen bonds. The barrier improvement with crosslinking for the dip and blade coated film crosslinked with GA is the result of the covalent bonding that reduces the fraction of the available hydroxyl groups. The crosslinking mechanism of PVA with dialdehydes has already been discussed in literature,[26-27] and it is described as the establishment of covalent bonds at both crosslinker ends by creating covalent acetal bridges between polymer chains, thus densifiying the coating (thinner coatings with crosslinking, Table 6.2, Figure 6.2).

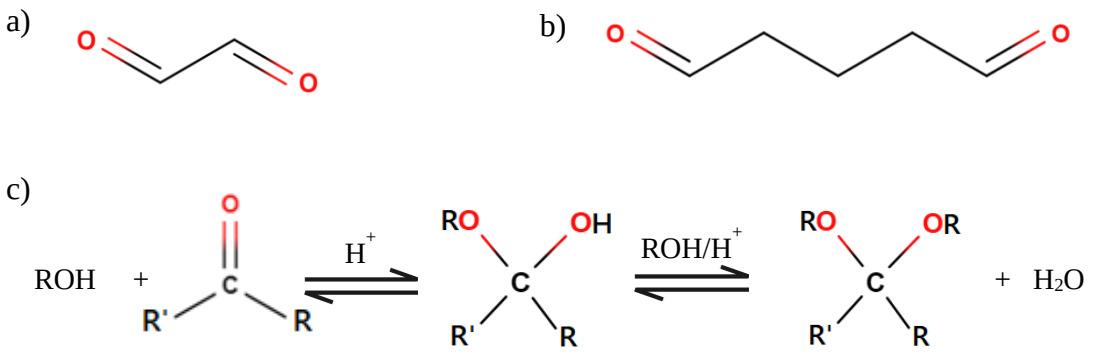

Figure 6.2 Structure of crosslinkers, a) glyoxal, b) glutaraldehyde and c) potential reaction of a dialdehyde crosslinker with PVA

To validate this mechanism for an LbL sructure, FTIR spectra of the crosslinked and no coatings deposited by dipping were compared (Figure 6.3). The vibration band of PVA corresponding to C-O stretching[26, 28] shifted from 1096 cm^{-1} to 1046 cm^{-1},which may be due to inter and intramolecular H-bonding interactions as well as bonding with MMT. The peak intensity increased with crosslinking, with a higher intensity for the Gly crosslinked coating. This change in intensity coupled to the permeability results confirm that crosslinking density is higher with Gly.

The broad peak between 3000-3500 cm^{-1} corresponds to the hydroxyl groups in the coating. With no acid used in the crosslinking reaction, in this study, both reaction steps are reversible. According to the FTIR spectra, there is a higher amount of hydroxyl group in the Gly crosslinked coating compared to the non crosslinked and GA crosslinked coatings. As free functional groups of dialdehyde can be hydroxyl or carbonyl, Gly has more free hydroxyl than GA which is confirmed by the FTIR peak at 1700 cm^{-1} in the GA spectrum, specific to carbonyl groups.

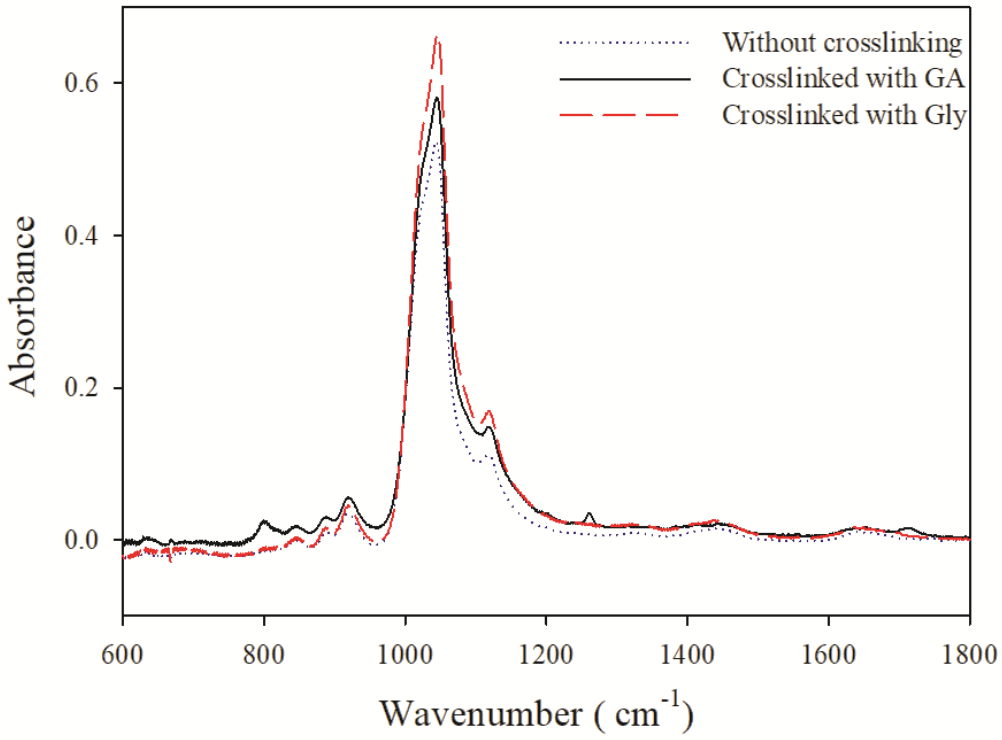

Figure 6.3 FTIR spectra of crosslinked and no PVA- MMT coatings

As for non-crosslinked films, dip-coated films crosslinked with Gly and GA have a better barrier to a hydrophilic permeant (Table 6.2) suggesting that even after crosslinking, blade coated films have a higher density of free functional groups.

Table 6.2 Oxygen permeability at different relative humidity and WVP of coated films

	Oxygen Permeability (cm^3. µm/m^2.day.atm)			WVP 100%RH g/m^2.day	Coating thickness (µm)
Relative humidity	0	40	70		
Dipped coating	8.17	15.65	173.29	49.96	0.964
Bladed coating	3.48	4.66	215.5	53.02	1.02
Dipped coating crosslinked with Gly	1.82	4.16	45.81	49.93	0.92

Dipped coating crosslinked with GA	2.23	4.67	114.16	50.1	0.866
Bladed coating crosslinked with Gly	0.54	0.51	456.3	51.63	0.833
Bladed coating crosslinked with GA	1.71	2.64	55.84	52.16	0.883

To gain information about the hydrophilicity of those coatings, water contact angle (CA) was determined. Dip-coated films had a higher CA with water than blade coated films (Figure 6.4). Blade coated film crosslinked with Gly had the most hydrophilic character, which would explain the sharp increase in its permeability. Since hydrophilicity depends on the composition of the outermost layer[29], the CA is mainly affected by the free hydroxyl groups on the surface that are able to establish hydrogen bonds with water. The higher hydrophilicity of blade-coated films could be explained by a lower crosslinking density as it is limited by the drying time.

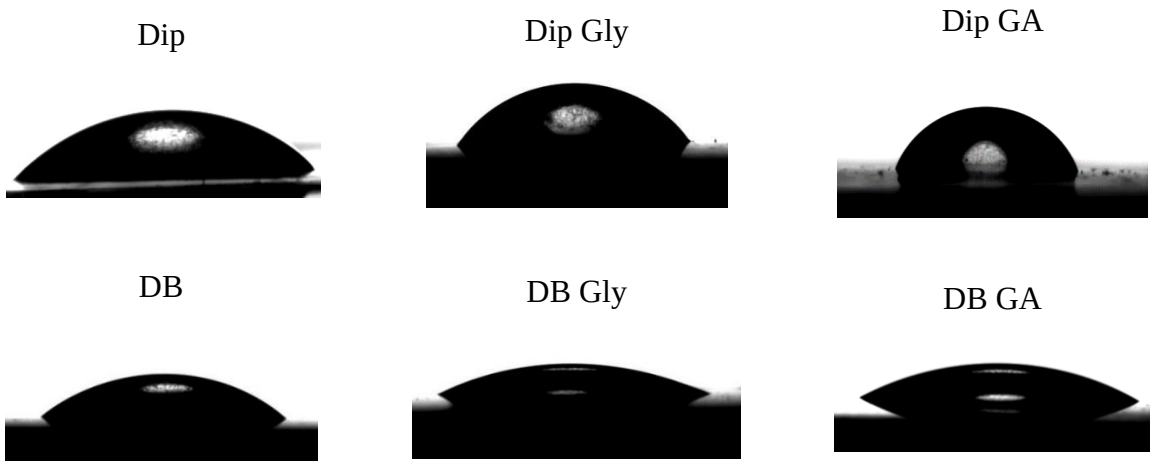

Figure 6.4 Water contact angle of Gly and GA crosslinked blade and dip coated films

The hydrophilicity of those coatings correlates well with the permeability results at 70% RH, Figure 6.5, as dip-coated films have a higher CA and a lower oxygen permeability.

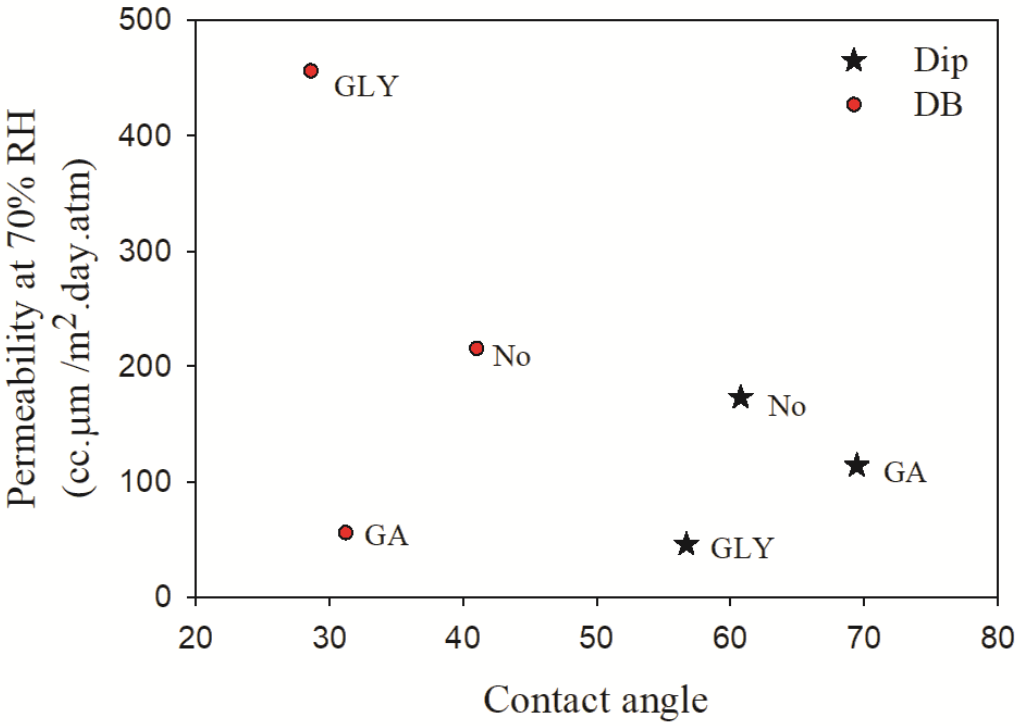

Figure 6.5 Water contact angle and oxygen permeability of the dip and blade coated films at 70%RH without and with GA and Gly crosslinking

Crosslinked coatings with Gly have a similar roughness (37.7±5.4 nm compared to 39.6±8 nm), Figure S.2, even though non crosslinked dipped coating showed a higher roughness (40.4±6 nm compared to 18.8±5.6 nm for bladed coating). Knowing that an incomplete exfoliation of clay and the overlapping of its platelets[30] may affect the coating roughness, clay intercalation and orientation were investigated. The MMT basal spacing of 1.14 nm (2θ peak at 7.73°) increased considerably for both types of coatings, Figure 6.6. The WAXD patterns for the PVA-MMT bilayers deposited by blade and dip coating, show a better nanoclay intercalation for the dip coated films (29.79, 17.89 Å compared to 23.19, 12.92 Å for blading). Considering the affinity between PVA and MMT, the wider interlayer spacing for platelets in dip-coated films may be explained by the better diffusion of PVA between the MMT platelets. The dipping method allows a better mobility of PVA chains as well as a longer time for diffusion. With blading however, the volume of the deposited layers is imposed by the doctor blade and its diffusion is limited by the film's drying.

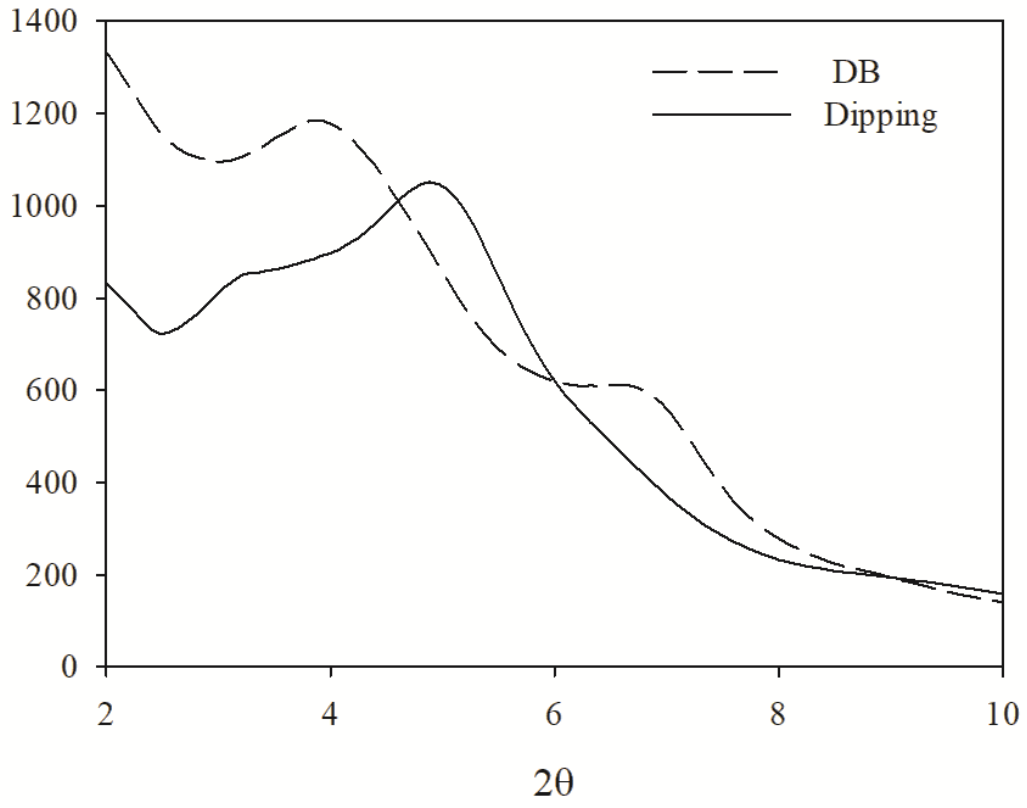

Figure 6.6 Wide-angle X-ray diffraction of PVA-MMT coatings deposited by blade coating and dipping

To compare clay platelets orientation, the Hermans orientation function, f_{CN}, for each type of coating was determined (see supporting information for calculation details). This function ranges from 1 to -1/2, with 1 for an orientation parallel to the surface and -1/2 for vertical platelet orientation. Both techniques resulted in a good clay platelet orientation with a slightly better orientation for blade coating (a value of 0.7 for f_{CN} compared to 0.675 for dipping) as some stress is applied when spreading the solution of PVA or MMT on the substrate.

Clay orientation varies considerably with the used process. Extrusion Blow molding, for instance, results in a better orientation of clay than compression molding or casting.[31] Compressed molded samples of polypropylene and modified clay (Cloisite 20A), have a f_{CN} of around 0.32 when compatibilized and 0.27 without compatibilization.[32] Clay orientation in blown films is considerably higher with a f_{CN} that reaches 0.8 without compatibilization [33] and can be tailored by the draw ratio (DR) (0.6 (DR=1) to 0.749 (DR=5)).[34] Single-layer nanocomposite coatings can also have a similar orientation to LbL coatings. A PVA/Kaolin coating,[35] deposited by a bench coater,

has an orientation value of 0.76. This coating has also a similar permeability to the studied coatings (0.7 ± 0.3 cm^3. μm/ m^2 d. atm (50 % RH)), which is due to its higher thickness (5.9 μm) and crystallinity (40%) as LbL coatings usually lack crystallinity.

6.3.3 Effect of concentration of solutions on permeability

Despite the barrier improvement, crosslinking is an additional coating step that does not generally use environmentally friendly materials. To decrease the moisture sensitivity of the non crosslinked coatings, their composition was tailored. To this end, two approaches were separately considered: the amount of free hydroxyl groups is altered by improving the hydrogen bonding in the coating and the volume fraction of MMT in the coating is increased. This can be achieved by increasing the concentration of the polymer solution and the MMT suspension. For the studied PVA-MMT nanocomposite coating, the concentrations of the polymer solution and the clay suspension affected differently the permeability results. At 0% RH, dipped and bladed coatings showed similar trend of permeability for low PVA solution concentration, as illustrated in Figure 6.7. Bladed coatings showed a slightly better barrier and reached a plateau at 0.3 wt%, whereas the permeability decreased further for dipped coating to reach the same permeability as bladed coating at 0.5 wt%. The same trend is observed at 70% RH, with a plateau in the range of 0.3 - 0.5 wt% for bladed coatings but with a better barrier for dipped coatings.

A higher PVA solution concentration (0.5 wt.%) increased the coating thickness, from 0.964 μm (for a 0.1 wt% concentration) to 1.668 μm, while the percentage per weight of the MMT in the coating was reduced by 4% (Table S1).

This is due to the deposition of the higher amount of PVA, as confirmed by FTIR (Figure S.3) with a higher concentration of hydroxyl groups (3300 cm^{-1}) and C-O bonds (1070 cm^{-1}) in the coating. With the increase in the density of hydroxyl groups, there are more inter and intramolecular hydrogen bondings in the coating, resulting in the shift of the hydroxyl peaks from 3378 to 3359 cm^{-1}.

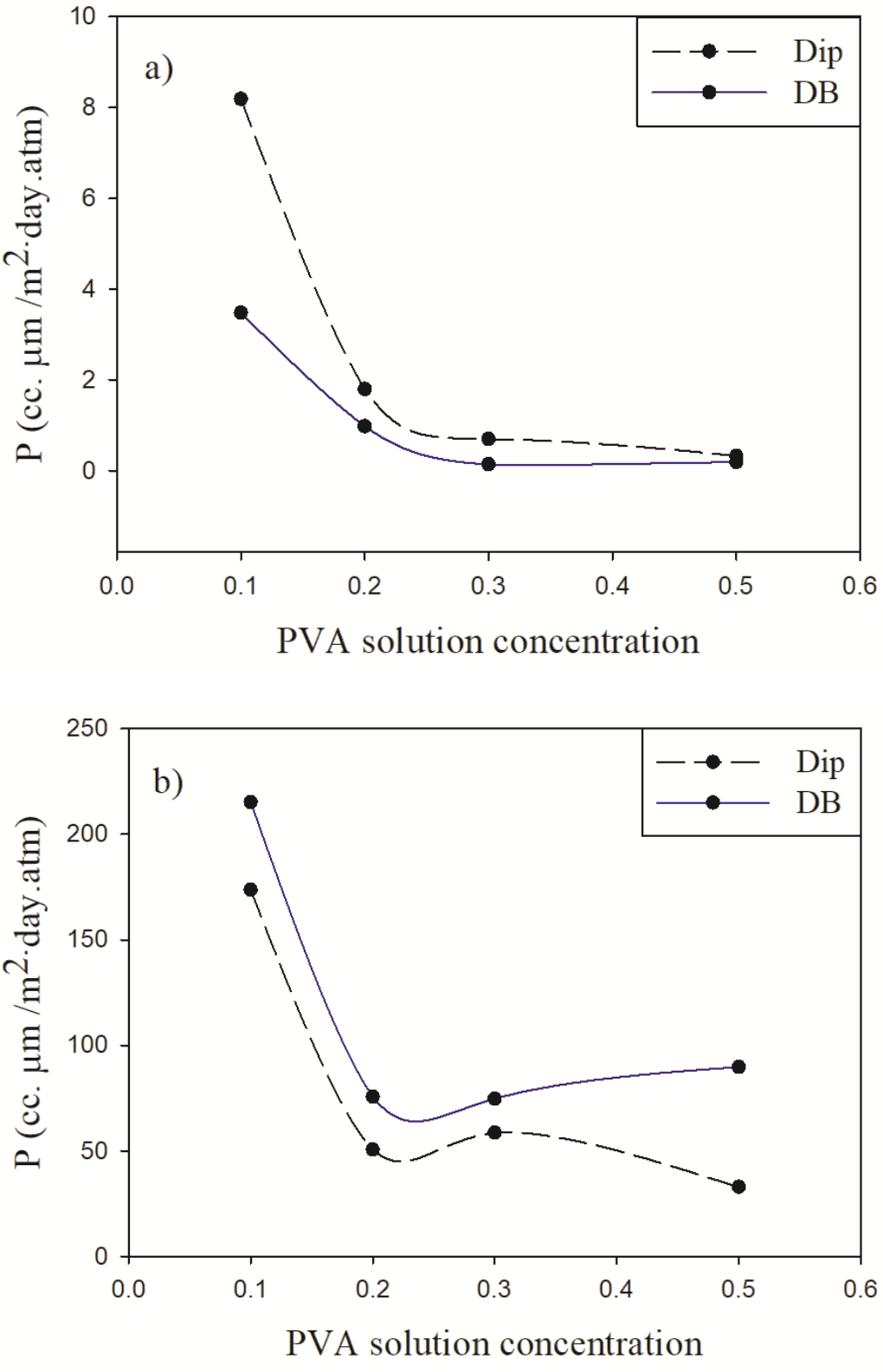

Figure 6.7 Permeability at a) 0 and b) 70 % RH for various PVA concentration

Increasing MMT suspension concentration did not have the same effect on permeability (Figure 6.8a, b). At high and low RH, the permeability of blade-coated films increased remarkably, whereas the permeability of dip-coated films started to increase from the 2 wt% MMT suspension concentration for both RH humidities and did not reach high values as blade-coated films. Contrary to PVA, a high concentration of the MMT suspension did not lead to an improvement of the oxygen barrier. This could be due to platelets agglomeration, thus reducing the tortuosity in the coatings. The high loading of MMT in the film may also hinder the intermolecular hydrogen bonding of PVA, which explains the considerable increase in permeability with the higher concentration of clay suspension (Table S1).

As mentioned previously, the increase of permeability at high RH is due to the established hydrogen bonds between water and free hydroxyl groups and the possible rupture of pre-existing hydrogen bonds. Reducing this permeability was possible with higher concentration of PVA in the film due to a denser intermolecular interaction that lowers the number of available hydroxyl groups to interact with water. The barrier order shifted with the RH for these two techniques. A plausible explanation could be that at dry conditions, the deposited layers of PVA and clay are stuck together thus preventing the permeation of oxygen. At high relative humidity, however, the solubility of water molecule changes the fraction of free volume in the film. Tailoring the concentration of clay and polymer solutions could also shed light on the clay-polymer interface in the coatings. As clay-PVA interaction is based on hydrogen bonding, the more established bonds there are, the more the whole structure is maintained and the less water can penetrate. By increasing PVA concentration, dip coating resulted in the lowest permeability at 70% RH. This confirms that the lower sensitivity of dipped coatings to humidity is due to a higher density of hydrogen bonds.

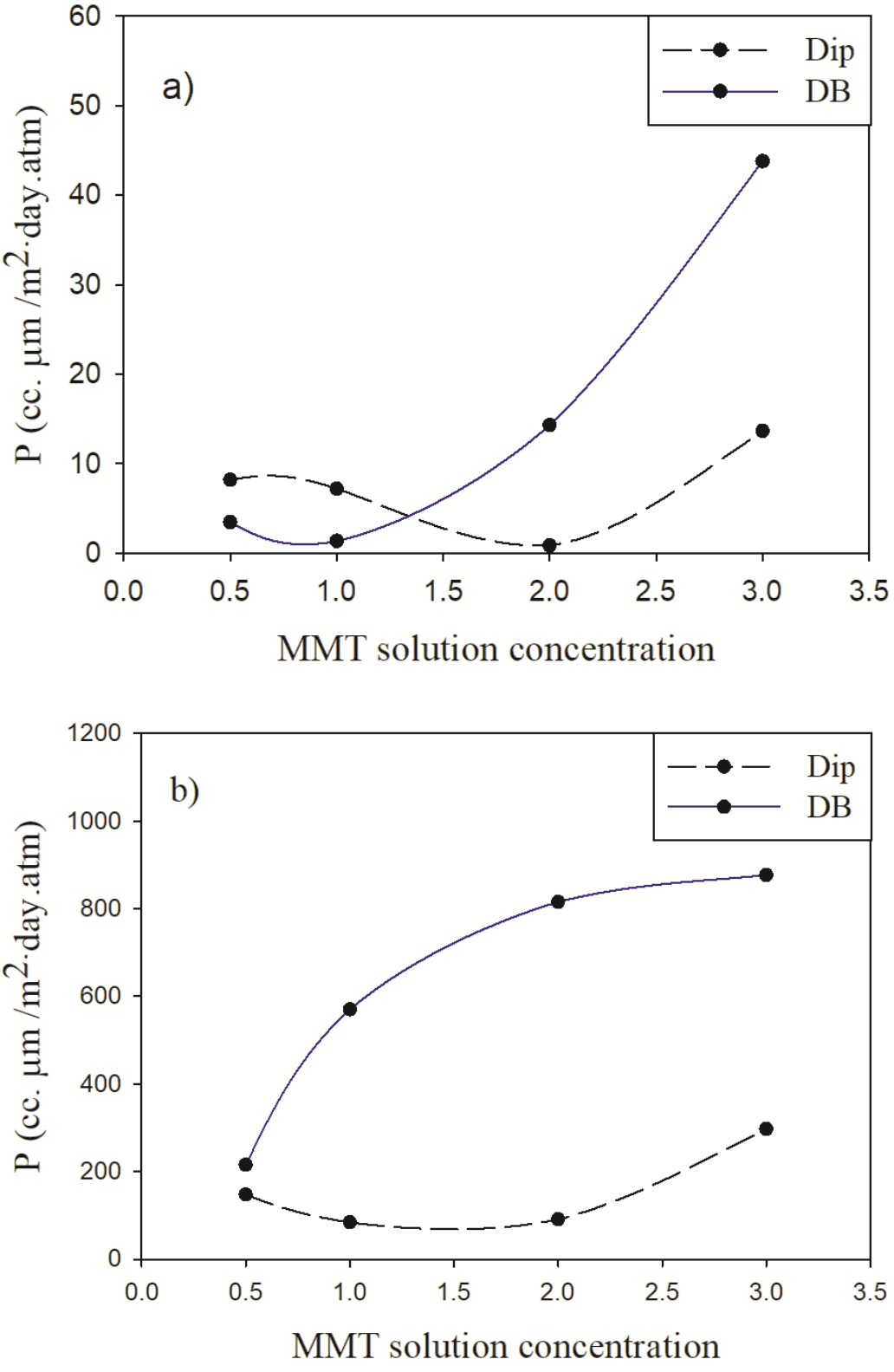

Figure 6.8 Permeability variation with the concentration of the MMT solution for a) 0% and b) 70% RH

6.4 Conclusion

In this study, barrier properties of two types of coating were investigated. Bilayers coatings of PVA and MMT were deposited by the LbL technique on a PET substrate using blade and dip coating. The presence of free hydroxyl groups at the surface caused a high sensitivity to moisture for both coatings. Crosslinking this LbL structure with dialdehydes reduced the oxygen permeability at high relative humidity. Although the permeability was reduced by up to six times, densifying the coating by creating covalent bonds between PVA and the crosslinker was not enough for a better barrier. Limiting free hydroxyl groups interaction with water by increasing hydrogen bonding in the coating turned out to be a better alternative. By Increasing PVA concentration in the coating, oxygen permeability was 26 times lower for dip-coated films and 19 for blade-coated ones. Increasing the volume fraction of clay was also considered as an alternative. Different concentrations of the MMT suspension were used, and the resulting permeability led to the conclusion that MMT concentration had a limit above which clay platelets agglomeration increases the permeability. Finally, our results suggest that the coating technique has a significant impact on the coating surface structure, the extent of interlayer interaction, the clay properties and the permeability of the coatings.

6.5 Acknowledgement

The authors gratefully thank for the financial support from 3SPack NSERC Industrial Research Chair by the Natural Science and Engineering Council of Canada (NSERC) and ProAmpac Inc. Company.

6.6 Supporting information

Calculation details of clay orientation, TGA thermograms of dipped and bladed coatings, AFM surface roughness profiles of dipped and bladed coatings, FTIR spectra of PVA-MMT coatings with different concentrations of PVA solution, coating properties (thickness and MMT%) and permeability for three different composition of the coating.

REFERENCES

1. Bieder, A.; Gruniger, A.; von Rohr, P. R., Deposition of SiOx diffusion barriers on flexible packaging materials by PECVD. *Surf Coat Tech* **2005,** *200* (1-4), 928-931.
2. Lewis, J. S.; Weaver, M. S., Thin-film permeation-barrier technology for flexible organic light-emitting devices. *Ieee Journal of Selected Topics in Quantum Electronics* **2004,** *10* (1), 45-57.
3. Leterrier, Y., Durability of nanosized oxygen-barrier coatings on polymers - Internal stresses. *Progress in Materials Science* **2003,** *48* (1), 1-55.
4. A.W.Ott; Chang, R. P. H., Atomic layer controlled growth of transparent conducting ZnO on plastic substrates. *Mater Chem Phys* **1999,** (58), 132-138.
5. Arora, A.; Choudhary, V.; Sharma, D. K., Effect of clay content and clay/surfactant on the mechanical, thermal and barrier properties of polystyrene/organoclay nanocomposites. *Journal of Polymer Research* **2010,** *18* (4), 843-857.
6. Naoki Hasegawa; Hirotaka Okamoto; Masaya Kawasumi; Usuki, A., Preparation and Mechanical Properties of Polystyrene–Clay Hybrids. *Journal of Applied Polymer Science* **1999,** *74*, 3359-3364.
7. Ploehn, H. J.; Liu, C. Y., Quantitative analysis of montmorillonite platelet size by atomic force microscopy. *Industrial & Engineering Chemistry Research* **2006,** *45* (21), 7025-7034.
8. Nielsen, L. E., Models for the Permeability of Filled Polymer Systems. *Journal of Macromolecular Science: Part A - Chemistry* **1967,** *1* (5), 929-942.
9. EL Cussler; Hughes, S.; Ward, W.; Aris, R., Barrier membranes. *J. Membr. Sci.* **1988,** *38*, 161-174.
10. Bharadwaj, R. K., Modeling the barrier properties of polymer-layered silicate nanocomposites. *Macromolecules* **2001,** *34* (26), 9189-9192.
11. Azeez, A. A.; Rhee, K. Y.; Park, S. J.; Hui, D., Epoxy clay nanocomposites - processing, properties and applications: A review. *Composites Part B-Engineering* **2013,** *45* (1), 308-320.
12. Ben Dhieb, F.; Dil, E. J.; Tabatabaei, S. H.; Mighri, F.; Ajji, A., Effect of nanoclay orientation on oxygen barrier properties of LbL nanocomposite coated films. *Rsc Adv* **2019,** *9* (3), 1632-1641.
13. Cui, Y. B.; Kumar, S.; Kona, B. R.; van Houcke, D., Gas barrier properties of polymer/clay nanocomposites. *Rsc Adv* **2015,** *5* (78), 63669-63690.
14. Soz, C. K.; Yilgor, E.; Yilgor, I., Simple processes for the preparation of superhydrophobic polymer surfaces. *Polymer* **2016,** *99*, 580-593.
15. Tsurko, E. S.; Feicht, P.; Nehm, F.; Ament, K.; Rosenfeldt, S.; Pietsch, I.; Roschmann, K.; Kalo, H.; Breu, J., Large Scale Self-Assembly of Smectic Nanocomposite Films by Doctor Blading versus Spray Coating: Impact of Crystal Quality on Barrier Properties. *Macromolecules* **2017,** *50* (11), 4344-4350.
16. Mundra, P.; Otto, T.; Gaponik, N.; Eychmuller, A., Automated setup for spray assisted layer-by-layer deposition. *The Review of scientific instruments* **2013,** *84* (7), 074101.
17. Richert, L.; Lavalle, P.; Payan, E.; Shu, X. Z.; Prestwich, G. D.; Stoltz, J. F.; Schaaf, P.; Voegel, J. C.; Picart, C., Layer by layer buildup of polysaccharide films: physical chemistry and cellular adhesion aspects. *Langmuir : the ACS journal of surfaces and colloids* **2004,** *20* (2), 448-58.
18. Elzbieciak, M.; Zapotoczny, S.; Nowak, P.; Krastev, R.; Nowakowska, M.; Warszynski, P., Influence of pH on the structure of multilayer films composed of strong and weak polyelectrolytes. *Langmuir : the ACS journal of surfaces and colloids* **2009,** *25* (5), 3255-9.
19. Kergommeaux, A. d.; Fiore, A.; Faure-Vincent, J.; Pron, A.; Reiss, P., Colloidal CuInSe2nanocrystals thin films of low surface roughness. *Advances in Natural Sciences: Nanoscience and Nanotechnology* **2013,** *4* (1), 015004.
20. Vartiainen, J.; Harlin, A., Crosslinking as an Efficient Tool for Decreasing Moisture Sensitivity of Biobased Nanocomposite Films. *Materials Sciences and Applications* **2011,** *02* (05), 346-354.
21. Yang, Y. H.; Haile, M.; Park, Y. T.; Malek, F. A.; Grunlan, J. C., Super Gas Barrier of All-Polymer Multilayer Thin Films. *Macromolecules* **2011,** *44* (6), 1450-1459.

22. Gohil, J. M.; Bhattacharya, A.; Ray, P., Studies On The Crosslinking Of Poly (Vinyl Alcohol). *Journal of Polymer Research* **2005,** *13* (2), 161-169.
23. Picart, C.; Lavalle, P.; Hubert, P.; Cuisinier, F. J. G.; Decher, G.; Schaaf, P.; Voegel, J. C., Buildup mechanism for poly(L-lysine)/hyaluronic acid films onto a solid surface. *Langmuir : the ACS journal of surfaces and colloids* **2001,** *17* (23), 7414-7424.
24. Maes, C.; Luyten, W.; Herremans, G.; Peeters, R.; Carleer, R.; Buntinx, M., Recent Updates on the Barrier Properties of Ethylene Vinyl Alcohol Copolymer (EVOH): A Review. *Polym Rev* **2018,** *58* (2), 209-246.
25. Holder, K. M.; Priolo, M. A.; Secrist, K. E.; Greenlee, S. M.; Nolte, A. J.; Grunlan, J. C., Humidity-Responsive Gas Barrier of Hydrogen-Bonded Polymer-Clay Multilayer Thin Films. *J Phys Chem C* **2012,** *116* (37), 19851-19856.
26. Zhang, Y.; Zhu, P.; Edgren, D., Crosslinking reaction of poly(vinyl alcohol) with glyoxal. *J Polym Res* **2009,** *237* (5), 725-730.
27. Podsiadlo, P.; Kaushik, A. K.; Arruda, E. M.; Waas, A. M.; Shim, B. S.; Xu, J.; Nandivada, H.; Pumplin, B. G.; Lahann, J.; Ramamoorthy, A.; Kotov, N. A., Ultrastrong and stiff layered polymer nanocomposites. *Science* **2007,** *318* (5847), 80-3.
28. Gaidukov, S.; Danilenko, I.; Gaidukova, G., Characterization of Strong and Crystalline Polyvinyl Alcohol/Montmorillonite Films Prepared by Layer-by-Layer Deposition Method. *International Journal of Polymer Science* **2015,** *2015*, 1-8.
29. Liu, C.; Shi, L.; Wang, R., Crosslinked layer-by-layer polyelectrolyte nanofiltration hollow fiber membrane for low-pressure water softening with the presence of SO 4 2− in feed water. *Journal of Membrane Science* **2015,** *486*, 169-176.
30. Cho, C.; Wallace, K. L.; Hagen, D. A.; Stevens, B.; Regev, O.; Grunlan, J. C., Nanobrick wall multilayer thin films grown faster and stronger using electrophoretic deposition. *Nanotechnology* **2015,** *26* (18), 185703.
31. Bartczak, Z.; Rozanski, A.; Richert, J., Characterization of clay platelet orientation in polylactide-montmorillonite nanocomposite films by X-ray pole figures. *European Polymer Journal* **2014,** *61*, 274-284.
32. Galgali, G.; Agarwal, S.; Lele, A., Effect of clay orientation on the tensile modulus of polypropylene-nanoclay composites. *Polymer* **2004,** *45* (17), 6059-6069.
33. Cole, K. C.; Perrin-Sarazin, F.; Dorval-Douville, G., Infrared spectroscopic characterization of polymer and clay platelet orientation in blown films based on polypropylene-clay nanocomposite. *Macromolecular Symposia* **2005,** *230* (1), 1-10.
34. Fereydoon, M.; Tabatabaei, S. H.; Ajji, A., Effect of Uniaxial Stretching on Thermal, Oxygen Barrier, and Mechanical Properties of Polyamide 6 and Poly(m-xylene adipamide) Nanocomposite Films. *Polymer Engineering and Science* **2015,** *55* (5), 1113-1127.
35. Åsa Nyflött; Lars Axrup; Gunilla Carlsson; Lars Järnström; Magnus Lestelius; Moons, E.; Wahlström, T., Influence of kaolin addition on the dynamics of oxygen mass transport in polyvinyl alcohol dispersion coatings. *Nord Pulp Pap Res J* **2015,** *30* (3), 385-392.

CHAPTER 7 ARTICLE 3: STUDY OF THE CROSSLINKING OF PVA WITH GLYOXAL IN LBL NANOCOMPOSITES

Fatma Ben Dhieb[1], Adrián Carrillo García[2], Seyed H. Tabatabaei[3], Frej Mighri[4], Abdellah Ajji[1*]

1 3SPack NSERC-Industry Chair, CREPEC, Chemical Engineering Department, Polytechnique Montreal, C.P. 6079, Succ. Centre ville, Montreal, QC, Canada H3C 3A7

2 Chemical Engineering Department, Polytechnique Montreal, Montreal, QC, Canada

3 ProAmpac, Terrebonne, QC, Canada J6Y 1V2

4 CREPEC, Chemical Engineering Department, Laval University, Quebec, QC, Canada

(*) All correspondence should be addressed to: abdellah.ajji@polymtl.ca

(Submitted to *Open Journal of Polymer Chemistry*, 22 July 2019)

ABSTRACT

Crosslinking is a common practice to improve the barrier properties of polymers. In this study, Montmorillonite (MMT) was used with Polyvinyl alcohol (PVA) to deposit nanocomposite coatings by Layer by Layer (LbL) on a PET substrate and were crosslinked with glyoxal (Gly). Two crosslinking conditions were studied, under mild condition and with an acidic environment. Mild condition was useful to identify the reversibility steps and the optimum crosslinking times while the acidic environment was essential to investigate the crosslinking mechanism, by determining the permeability for different crosslinking times. PVA and PVA-MMT coatings showed a strong correlation between the permeability coefficients for different crosslinking times and the FTIR results.

Keywords: Glyoxal, LbL, nanocomposite, PVA, crosslinking mechanism

INTRODUCTION

Barrier materials are in constant demand for a wide variety of applications, especially for food packaging which has a considerable growth of the flexible packaging market. Polymeric materials are a considerable part of this market and many technologies are currently applied to improve their gas barrier. Among the most popular, the multilayer structured film in which a barrier layer (ethylene vinyl alcohol (EVOH), Nylon…) is usually part of a three to twelve layers structure. Metallic and silicon oxide coatings are also extensively used for high barrier packaging. In addition to this two, other techniques are also used to improve the cost and the recyclability like polymer blending, and the addition of fillers.

Nanocomposite coatings are considered a sustainable solution, due to their recyclability and the increasing interest in ecofriendly materials like clay[1], cellulose nanocrystals[2] or chitosan[3].

For nanocomposites, some affordable materials like clay, improves considerably the polymer properties even with adding low amounts, due to its high aspect ratio.[4] The dispersion and exfoliation of clay depend mainly on its interaction with the polymer and the applied process. Especially for melting and casting, high clay loading can't be reached due to its agglomeration that may deteriorate the barrier properties.[5] Coating, in the other hand, resulted in a better clay dispersion and intercalation.[6]

Among the coating techniques, Layer by Layer (LbL) was developed in the early 90's and consists in the alternate deposition of polymer layers.[7] The filler can be added whether directly to the polymer solution that will be deposited, or it can be deposited as a separate layer by dipping (for dip coating) the substrate in the filler solution. LbL has shown interesting results compared to conventional techniques by reducing oxygen permeability by up to 99.9%.[8] Obtained coatings have a tailored thickness that depends on the number of layers, the properties of the used materials (fillers and polymers) and the coating steps. To increase gas barrier and reduce the sensitivity to moisture, these coatings are usually chemically crosslinked.[9] For polymers with hydroxyl and amine functional groups, dialdehydes in particular are widely used. Their remarkable reactivity results in a high crosslinking density, reducing thus considerably the free volume in the film. Other than the gas barrier, crosslinking improves also the mechanical properties[10] due to the modification of the polymer structure with the established covalent bonds.[11] The acetal formation and crosslinking reaction is known to be reversible, which could be avoided with acidic conditions. Some studies

conducted this reaction under mild conditions and resulted in a non proportionality between the crosslinker concentration and the density of crosslinking.[12] Most of the crosslinking studies consider a homogeneous system in which the crosslinker solution is added to the polymer solution[11, 13] while heterogeneous reaction are not extensively studied.

To the best of our knowledge, this is the first thorough study of the variation of permeability with crosslinking time, the tracking of the acetal reaction reversibility and the correlation of permeability and FTIR absorption intensity for LbL coatings.

In this study crosslinking mechanism of a nanocomposite coating by glyoxal was investigated by comparing the impact of crosslinking time on the permeability of PVA-MMT and PVA coatings. To investigate the steps of a reversible reaction, both coatings were also crosslinked without the presence of an acid. The bonding variation in PVA based coatings was explored by FTIR characterization and a correlation was deduced between the permeability and the intensity of FTIR peaks. The hydrophobicity of their surface was also determined by water contact angle measurement.

7.1 Experimental

7.1.1 Materials

PVA (Mw=140 000 – 186 000 g. mol^{-1}) was purchased from Sigma Aldrich (Saint Louis, Missouri, USA) and Natural sodium montmorillonite (MMT) (Cloisite NA^{+}) with a density of 2.86 g/cm^3, supplied by BYK (Gonzales, Texas, United States), was used as received. Silicon wafers, purchased from EL-Cat Inc. (Ridgefield Park, New Jersey, United States) were also used as substrate. They were used for the FTIR characterization due to their transparency to infra-red. The selected substrate for permeability tests and the other characterizations, is a polyethylene terephthalate (PET) film, 16 μm, provided by ProAmpac (Terrebonne, Qc, Canada). The used primer is a polyethylene imine solution (PEI) (5% aqueous solution), purchased from MICA Corporation (Shelton, CT, USA). Glyoxal, the crosslinker, (40% aqueous solution) and Hydrochloric acid (37%) were purchased from Sigma Aldrich (Saint Louis, Missouri, USA).

7.1.2 Dip coating preparation

PVA solution was prepared with deionized (DI) water with continuous stirring for 2h and heating at 80 °C. MMT suspension in DI was stirred for at least 4 hours. Deposition of a coating by LbL is a repetition of three steps to deposit each layer: dipping of the substrate in the PVA or MMT solution, rinsing and drying. For the first bilayer (the first layers of PVA and MMT) the time for each step is higher to have a better coverage. Crosslinking the LbL coatings consists in dipping the coated substrate in the glyoxal solution (5%), twice: after the deposition of half the layers and at the end when all the bilayers are deposited. For crosslinking reaction with the presence of acid, hydrochloric acid (0.1 M) is added to the crosslinker solution.

7.1.3 Determination of the solubility and diffusion coefficients

To determine the solubility and diffusion coefficients of the coated substrate, the unsteady state is required. To achieve it, the tested films are first conditioned in the MOCON apparatus with nitrogen only for several hours, and then tested with nitrogen in order to remove all the oxygen trapped in the film. A test of the oxygen permeability is started directly afterwards without conditioning. With this unsteady state, Fick's second law can be applied, equation 7.1. Diffusion and permeability coefficients are determined with the solution to this law, equation 7.2, and the solubility is calculated with equation 7.3.

$$\frac{\partial C}{\partial t} = D\ \frac{\partial^2 C}{\partial x^2} \tag{7.1}$$

$$J(t) = \frac{Pp}{l}\left[1 + 2\sum_{n=1}^{\infty}(-1)^n\, exp\left(-\ \frac{D\pi^2 n^2 t}{l^2}\right)\right] \tag{7.2}$$

$$P = S.D \tag{7.3}$$

7.2 Characterization techniques

The interlayer spacing d(001) of MMT was determined according to Bragg's law, by using X-ray diffraction spectroscopy (Philips X'pert) in the wide-angle mode and copper CuKα radiation (λ =1.54056 Å) as a source. The coatings were scanned with a rate of 0.02 °/s in the range of 2 to 10 degrees. MOCON OXTRAN 2/21 (Minneapolis, USA) apparatus was used to measure the permeability to oxygen at 0% relative humidity, 25 °C, and 1 atm pressure, as described in the

ASTM standard, D-3985-81. For a higher relative humidity (70%), tests were conducted with a MOCON OXTRAN 10X apparatus (Minneapolis, USA), at 25°C.

The contact angle of the coated PET was determined with the sessile drop method by using a Goniometer OCA20 from dataphysics. Measures were done at room temperature and distilled water was the probe liquid. To determine the contact angle, the drop image to analyze is considered the one taken after 5 seconds from the deposition of the drop on the surface. The reported values are an average of five readings at different location of the sample's surface. Coatings thickness was measured with a Dektak 3030 stylus profilometer with silicon plates as substrate. Transparent to Infrared silicon plates constituted the substrate for FTIR testing. Coatings were scanned in transmission mode in the range 600 to 4000 cm^{-1} with a resolution of 4 cm^{-1}. The spectrum of the silicon substrate was subtracted afterwards from the analyzed spectra. To determine the percentage per weight of clay, thermogravimetric analysis was conducted with a TGA Q500 from TA instruments, by heating the sample up to 800 °C. At this temperature, the residual weight is the one of clay only.

7.3 Results and discussion

7.3.1 Crosslinking reaction of hydroxyls with glyoxal in a homogeneous system

Polymer crosslinking studies focused on extrusion and solution casting by adding the crosslinker solution to the melt or polymer solution, which are homogeneous reactions. Nonetheless, those studies differ from LbL coatings where the crosslinking is performed by the addition of the crosslinker solution to a LbL deposited film which was previously dried. As such, the crosslinking can be assumed as a heterogeneous reaction.

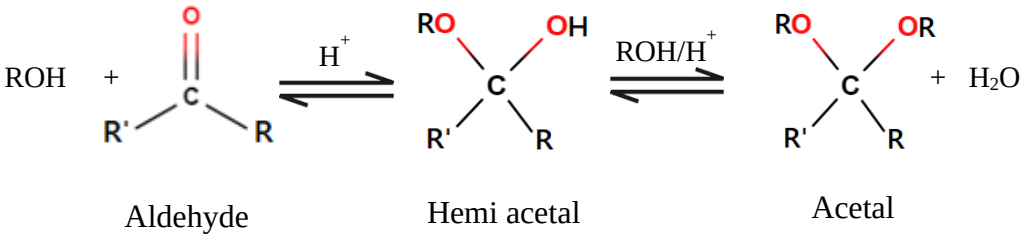

Figure 7.1 Crosslinking reaction of hydroxyl groups with dialdehydes

The reaction mechanism for some crosslinkers, e.g. glyoxal, can vary depending on the polymer functional group. For instance, for aldehydes crosslinkers the crosslinking mechanism with polymers containing hydroxyl groups in their structure, e.g. PVA, is based on two reactions occurring in an acidic environment. In the case of PVA, presented in Figure 7.1, it first reacts with Gly to result in an unstable intermediate, the hemi acetal, which then reacts with the PVA to form the acetal and water. Both reactions are reversible in the absence of acid. The kinetic study of the crosslinking of aliphatic alcohol with aldehydes to form acetals, for homogeneous systems, is presented as a second order reaction with two reactants (Equation 7.4)[14]:

$$-\frac{\mathrm{d}\,[\mathrm{Gly}]}{\mathrm{dt}} = \mathrm{k}.\,[\mathrm{Gly}].\,[\mathrm{PVA}] \tag{7.4}$$

According to a study conducted by Kormanovskaya et al.(1964), with PVA and formaldehyde, the second reaction involving the reaction of hemiacetal with PVA is the limiting step of the crosslinking reaction.[15] To make the reaction run in the forward direction, avoiding the reversibility of the crosslinking mechanism, the use of high initial concentration of PVA was suggested.

7.3.2 Mild conditions for PVA crosslinking

Most of the studies of the crosslinking of PVA with aldehydes consider a homogeneous system, in which the crosslinker solution is added to the PVA solution. This is not the case for LbL deposited film, as whether for spin, spray or dip coating, the crosslinker solution is applied to a dry film. For dipping, for instance, the LbL film is crosslinked by dipping it in the crosslinker solution. Crosslinking LbL deposited films is a heterogeneous reaction that implies a crosslinker diffusion with a simultaneous reaction.

The presence of acid in the acetal reaction is important for limiting the reversibility of both reaction steps, by pushing the reaction toward the formation of acetal, Figure 7.2.

The addition of acid can, however, be considered aggressive for some applications. Applying mild conditions by using the crosslinker only without acid, yields to a reversible reaction. The steps of this reversibility can be clearly identified when measuring the permeability of the coatings for different crosslinking times (Figure 7.2). This is an interesting observation as it allows to investigate the effect of the crosslinking on the reaction reversibility.

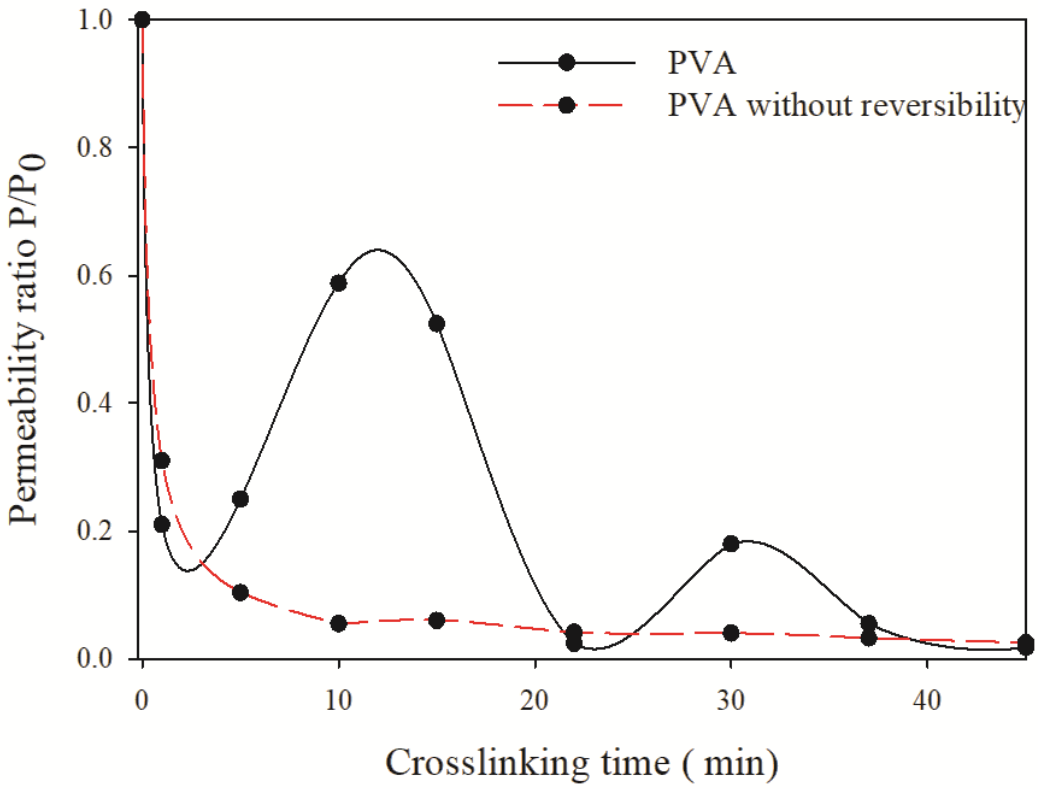

Figure 7.2 LbL assembly of PVA layers with and without acidic environment

The crosslinking reaction was studied for up to 60 min of reaction time. For the first 45 minutes of crosslinking there's two increases in the permeability at 15 and 30 min. For the first reached maximum of P/P_0, the value 0.6 is obtained whereas for the second, this value is lowered to 0.2. This can be explained by the fact that it's a reversible two steps reaction.

For the first step, one hydroxyl group reacts and for the second, both are linked to the polymer chain. The free volume is then different in both steps and induces a lower permeability for the acetal state. The permeability in function of the crosslinking time curve shows clearly the different crosslinking stages.

The two reached maxima are around 10-15min and 30 min with a permeability reduced three times for the second maximum compared to the first. The lowest permeabilities follow also the same trend as the highest, with first a minimum around 0.2 cc/ m^2.day.atm during the first 5 min and a second minimum with half the permeability of the first (0.1 cc/ m^2. day. atm) for 22 min crosslinking time. This reversibility is attenuated with longer crosslinking time, as permeability is lower than 0.06 cc/ m^2.day. atm for times higher than 37 minutes. It's clear that beyond this time,

the maximum reduction of free volume is achieved meaning the predominance of acetals in the film. Knowing that the possible states of crosslinked Gly are hemiacetal or acetal and that Gly may establish four covalent bonds or less, such gradual reduction in permeability may be related to the steps of the reversible crosslinking reaction. The 0.2 value is reached twice, between 1 and 5 min as a minimum and at 30 min as a maximum. As an intermediate value, this would correspond to a predominance of the hemi acetal state. This would also be explained by the fact that's in between two maxima in the first case and two minima in the second. The two maxima correspond to the non crosslinked state and a partly crosslinked state with hemi acetal whereas the two minima are due to the predominance of acetals in the coating. Even though, this reversibility has a more attenuated effect on the permeability with longer crosslinking time, with the presence of minima around 5 and 20 minutes, choosing the right crosslinking time can yield a high barrier film without the need to use an acidic environment or very long crosslinking times

7.3.3 Effect of fillers in the diffusion of the crosslinker

The nanocomposite PVA- MMT film has an intra and interchain hydrogen bonding as well as a bonding with the MMT. With the crosslinker, there is breakage of those bonds and a creation of a more solid and short ones, the covalent bonds. During this reversible reaction, there's a constant variation in the bonds type and as the length and intensity of these bonds is different, it contributes differently to the reduction of free volume in the coating. Hydrogen bonds between hydroxyl groups have a higher length than C-O covalent bond (1.85 Å[16] compared to 1.44 Å for a covalent bond).

As PVA-MMT assembly is based on hydrogen bonding and this affinity affects the clay properties, the interlayer spacing of MMT was determined for several crosslinking times and the result showed that crosslinking didn't affect considerably this spacing, Figure S.1.

MMT increases the tortuosity in the coating by increasing the path of diffusing molecules but it also affects the mobility of PVA chains,[17] which may hinder the diffusion of Gly, considering that MMT represents 60 wt% of the coating, Figure S.2. Plotting relative permeability in function of the crosslinking time for both coatings, with and without MMT, Figure 7.3, showed a better reduction in permeability for PVA coatings. Both types of coatings had a similar variation of P/P_0 with the crosslinking time, meaning that MMT didn't affect the different steps of the reaction and its reversibility. The only difference observed is the lower permeability ratio of PVA coating for

the first 30 min of crosslinking. Gly molecules diffuse through the coating while reacting with hydroxyl groups to establish covalent bonds which could slow the reaction rate, such assumption must be confirmed by a kinetic study.

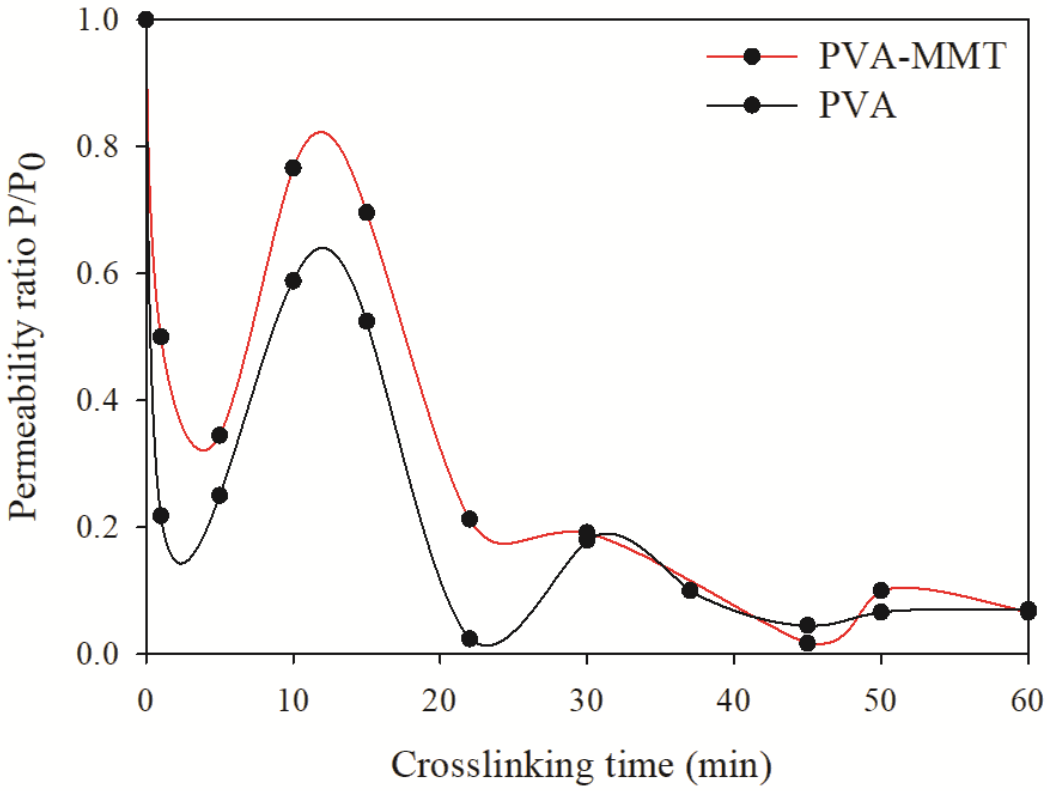

Figure 7.3 Permeability ratio in function of crosslinking time for LbL coated PET with PVA and PVA-MMT coatings

The lower permeability coefficients for nanocomposites compared to the neat polymers is often interpreted with the reduction of the diffusion of permeant gas molecules, making the free volume an important nanocomposite property to be considered. This latter has been described as having an exponential effect on the permeability. [17]

Permeability is, however, also a function of the solubility coefficient which is specific to the pair polymer- permeant molecule. Gas solubility is related to the static free volume and is independent of the polymer chains motions while its diffusivity is related to the dynamic free volume due to the motion of the polymer segments.

Table 7.1 Diffusivity and solubility coefficients for different PVA and PVA-MMT coatings

Coating	D (cm^2/s)	S (cm^3/ cm^3. atm)
15 PVA, Gly 5 min	3.18 e-9	10.88
15 PVA	2.4 e-9	50.44
15 PVA MMT, Gly 5 min	7.63 e-10	0.72
15 PVA MMT, Gly 50 min	8.47 e-10	0.079

Diffusion coefficient is thus a kinetic factor that gives an understanding of the mobility of permeant molecules in the polymer. Solubility coefficient, in the other hand, is a thermodynamic factor that depends on the affinity between gas molecules and the polymer.[18]

The presence of MMT in the LbL coating decreases both coefficients. The diffusivity coefficient decreases around 5 times for 5 min crosslinked coatings, due to the higher tortuosity in the nanocomposite and the reduction of the free volume. The solubility decreases considerably with the addition of MMT with a 15 times reduction. For both PVA and PVA-MMT coatings, crosslinking did not affect diffusion and had a more pronounced impact on solubility instead. A higher reduction is obtained with a longer crosslinking time, as a 50 min crosslinking time resulted in a 10 times lower solubility coefficient for the PVA-MMT coating than a 5 min crosslinking time.

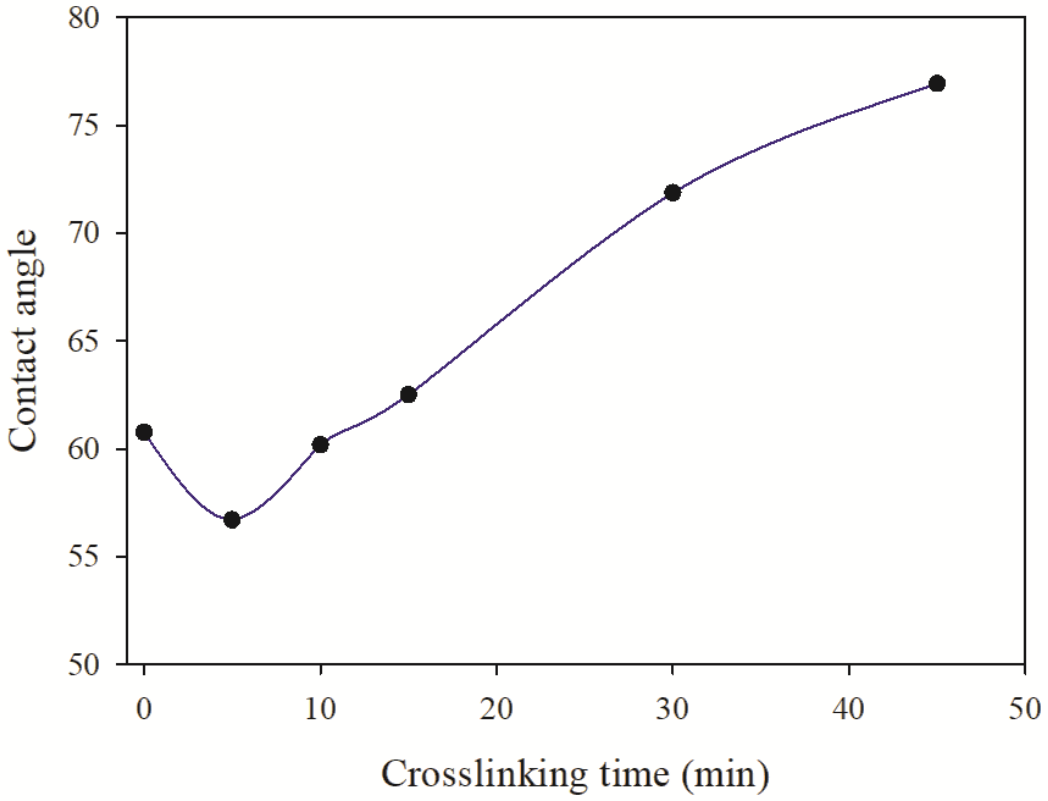

Figure 7.4 Water contact angle of PVA-MMT coatings at different crosslinking times

Contrary to the bulk, reversibility did not seem to affect the coatings surface hydrophilicity. The water CA varies according to the density of free hydroxyl groups at the surface as they can establish hydrogen bonds with the water. The lower the CA, the higher the surface hydrophilicity. For crosslinked PVA-MMT coatings without added acid, surface hydrophobicity increased proportionally to the crosslinking time. Crosslinking for a dipping process implies a reaction/diffusion mechanism. During the crosslinking, the coating is dipped in the crosslinker solution which keeps the surface in constant contact with the crosslinker molecules. Such availability of the crosslinker may explain the increase in the surface hydrophobicity with the crosslinking time despite the reversibility of the reaction.

7.3.4 **Investigation of the crosslinking reaction**

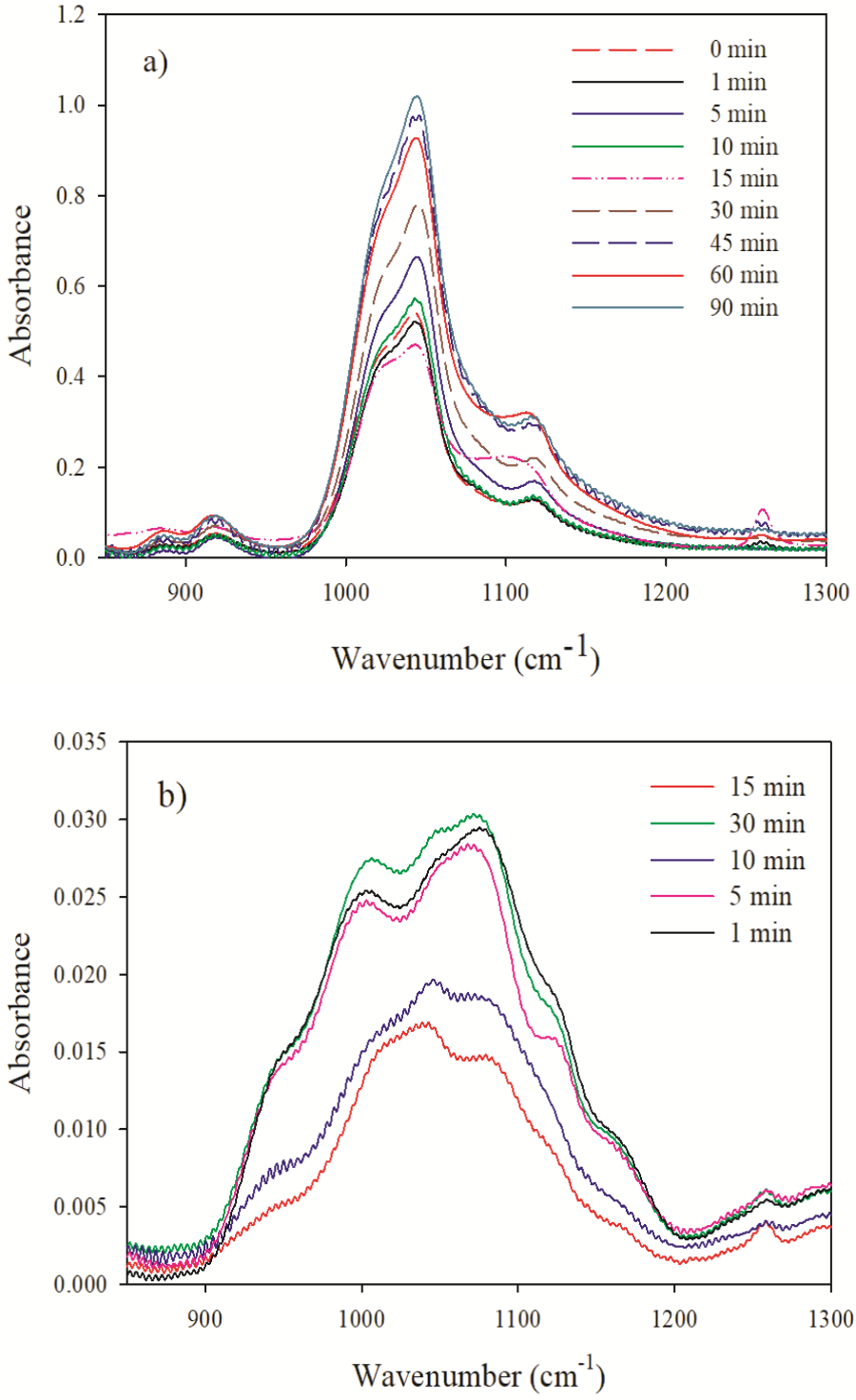

Figure 7.5 FTIR spectra of different crosslinking times for a) PVA-MMT coatings and b) PVA only coating

FTIR spectroscopy is a reliable characterization technique to investigate the variation in the bonding for the studied material. The spectra of PVA and PVA-MMT coatings with different crosslinking times were collected by transmission mode. The peak linked to the stretching of the C-O bond in the PVA-MMT coatings is at 1047 cm^{-1} whereas it is at 1076 cm^{-1} for PVA-coatings. This bond is usually at 1092 cm^{-1} for neat PVA but it shifted due to hydrogen bonding (for both coatings) and due to overlapping with MMT peak, in the case of the nanocomposite coating. As the C-O is the established bond by crosslinking, the variation of the peak intensity reflects the extent of crosslinking. Following Beer Lambert's law, the intensity of this peak should be proportional to the concentration of the C-O bond in the coating which means its proportionality to the crosslinking density.

For PVA coatings, a clear difference between the intensities of the C-O peak for the 10 and 15 min crosslinking times and the remaining crosslinking times is observed which corroborate their lower permeabilities. For PVA-MMT coatings, the 5 min time has an intermediate intensity between low permeability and high permeability coatings dividing them in two distinct groups. The high permeability group consists of 0,1,10 and 15 min and the low permeability one includes the 30, 45, 60 and 90 min crosslinking times. The 90 min crosslinking time was only characterized by FTIR to corroborate the obtained results, and according to the obtained spectra the permeability should be lower than 0.04 cc/ m^2.day .atm.

When plotting permeability results in function of the C-O peak intensities, for PVA and PVA-MMT coatings with and without reversibility, a linear correlation is obtained. Such correlation enables a different approach in interpreting the permeability results.

This linear relation between the permeability and the peak intensity means that the permeability is also linearly proportional to the crosslinked groups concentration. As the determined diffusion and solubility coefficients showed, solubility is more affected by the crosslinking than diffusivity. With such logic, solubility is thus linearly proportional to the concentration of crosslinked groups.

By establishing this correlation for the same material and coating technique, the permeability can be estimated, with only the coated samples needed for FTIR, cutting thus drastically the experimental time.

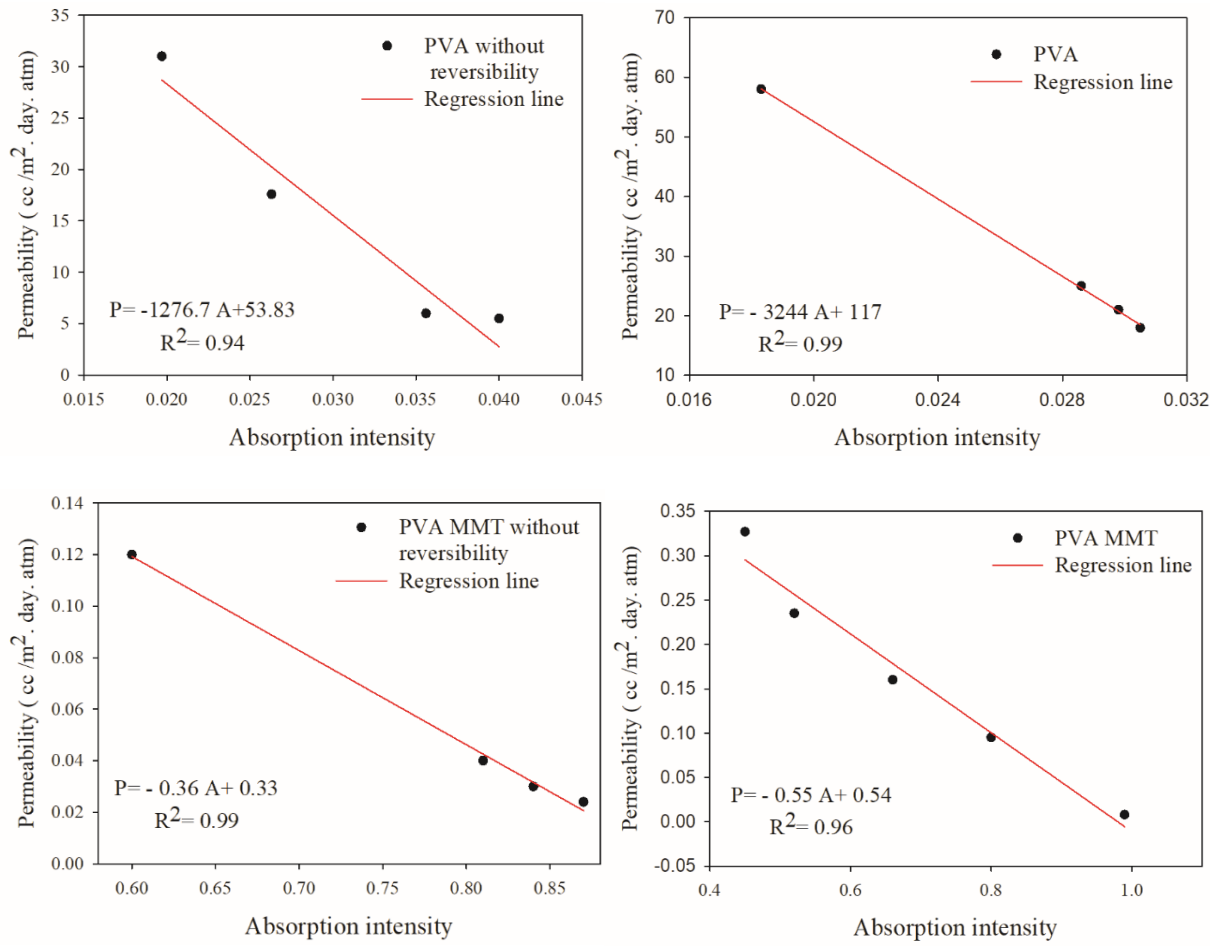

Figure 7.6 Correlation between the permeability coefficients and FTIR absorption intensity for PVA and PVA-MMT coatings with and without reversibility

7.3.5 **Reaction kinetic**

For a homogeneous crosslinking reaction, the considered reaction kinetic depends on both PVA and Gly with an order of 1 for each of them. In the case of LbL, two main differences exist, compared to the usually studied homogeneous reactions. On one hand, it is a heterogeneous reaction which affects the reaction kinetic, and on the other hand, for the crosslinking of LbL films, PVA is in excess compared to the crosslinker which simplifies equation 7.4 to equation 7.5. It must be mentioned that it is very difficult to determine the concentrations of both the PVA and the Gly in the LbL coating.

$$-\frac{d\,[Gly]}{dt} = k.[Gly]^{\alpha} \qquad (7.5)$$

with α, the reaction order. As discussed in Section 3.4, permeability is proportional to the FTIR absorption intensity corresponding to the C-O bond. According to Beer Lambert's law, this intensity is linearly proportional to the concentration of the crosslinker in the coating which makes this permeability proportional to concentration. Considering this linearity, the variation of the permeability with the crosslinking time was adopted to study the crosslinking kinetic of PVA. The crosslinking of PVA and PVA-MMT was elaborated with the presence of acid to avoid reversibility. Based on the FTIR correlation, the following reaction between the permeability and the Gly concentration is considered:

$$P = -a.[Gly] + b \qquad (7.6)$$

with a and b constants.

To find the reaction order, α, the Gly concentration in equation 7.5, is replaced by its expression in function of the permeability, deduced from equation 7.6:

$$-d\,.\left(\frac{P-b}{a}\right)/dt = k.\left(\frac{P-b}{a}\right)^{\alpha} \qquad (7.7)$$

To find the reaction order describing the crosslinking reaction, the linearity of the permeability equation related to each order with time was investigated (Figure 7.7). For the case of the first reaction order (logarithm of permeability) the linear regression was low (R^2=0.7) compared to second reaction order (R^2=0.97), which led to believe that the crosslinking reaction followed a second order reaction based on the Gly.

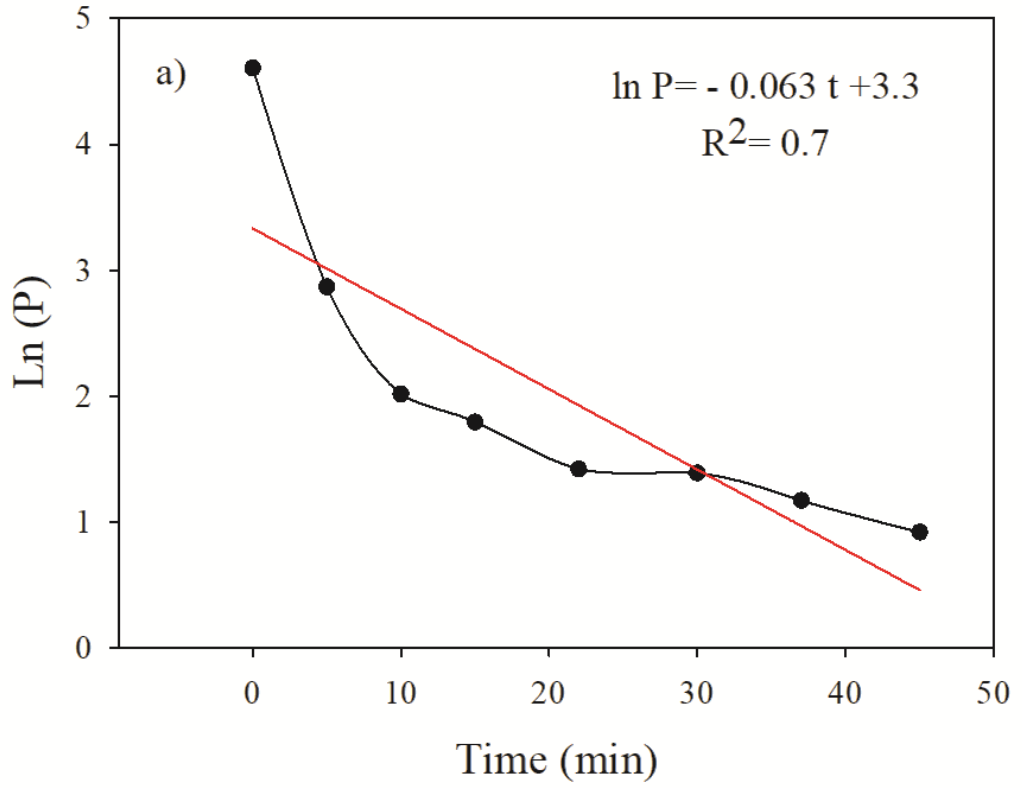

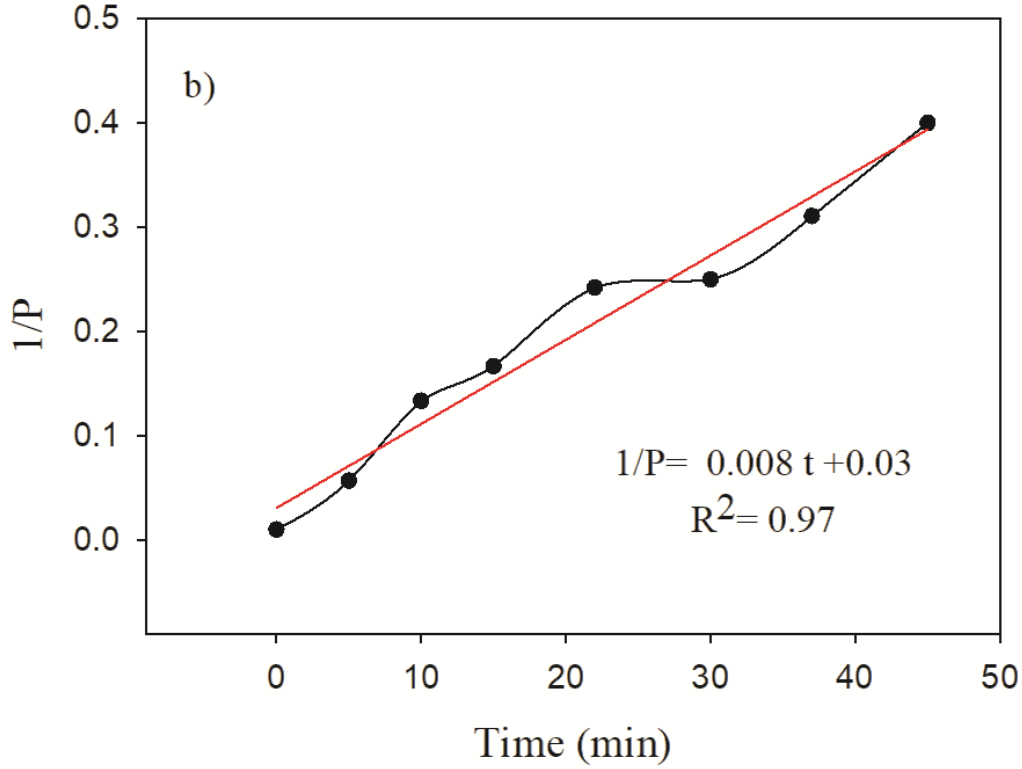

Figure 7.7 Kinetic evaluation of a crosslinking reaction: a) Order 1, b) Order 2

Integrating equation 7.7 while considering a reaction order of two, led to a perfect fit for both types of coating, with equation 7.8 that relates permeability values to the crosslinking time, Figure 7.8.

$$\frac{1}{P} = k_{app}.t + \frac{1}{P_0} \quad (7.8)$$

with k_{app} , the apparent reaction rate constant, as it is the ratio of the reaction rate constant k to the constant a (k/a).

The study of the correlation between permeability and FTIR absorption intensity, showed that the slope constants are not in the same range with a value of 1276.7 for PVA coatings and 0.365 for PVA-MMT coatings. This is mainly due to two reasons. In one side, the interfering of clay peaks with the peak of interest, and in the other side the thicker nanocomposite coatings (1µm compare to 0.2 µm for PVA coatings).

According to this second order fitting, the obtained k_{app} is 1.5 m^2.day.atm.$cc^{-1}$$min^{-1}$ for PVA-MMT coating and 0.01 m^2.day.atm.$cc^{-1}$$min^{-}$for PVA coatings. A straightforward multiplication $a * k_{app}$ to obtain k, can't be applied in this case, due to the consideration of the constant a in the integration as a slope of the correlation between the permeability and the Gly concentration whereas, only the correlation between the permeability and the FTIR absorption intensity was experimentally obtained.

To be able to compare those values, a correction of the FTIR absorption intensity of PVA-MMT coatings could also be conducted to deduct the effect of clay if needed.

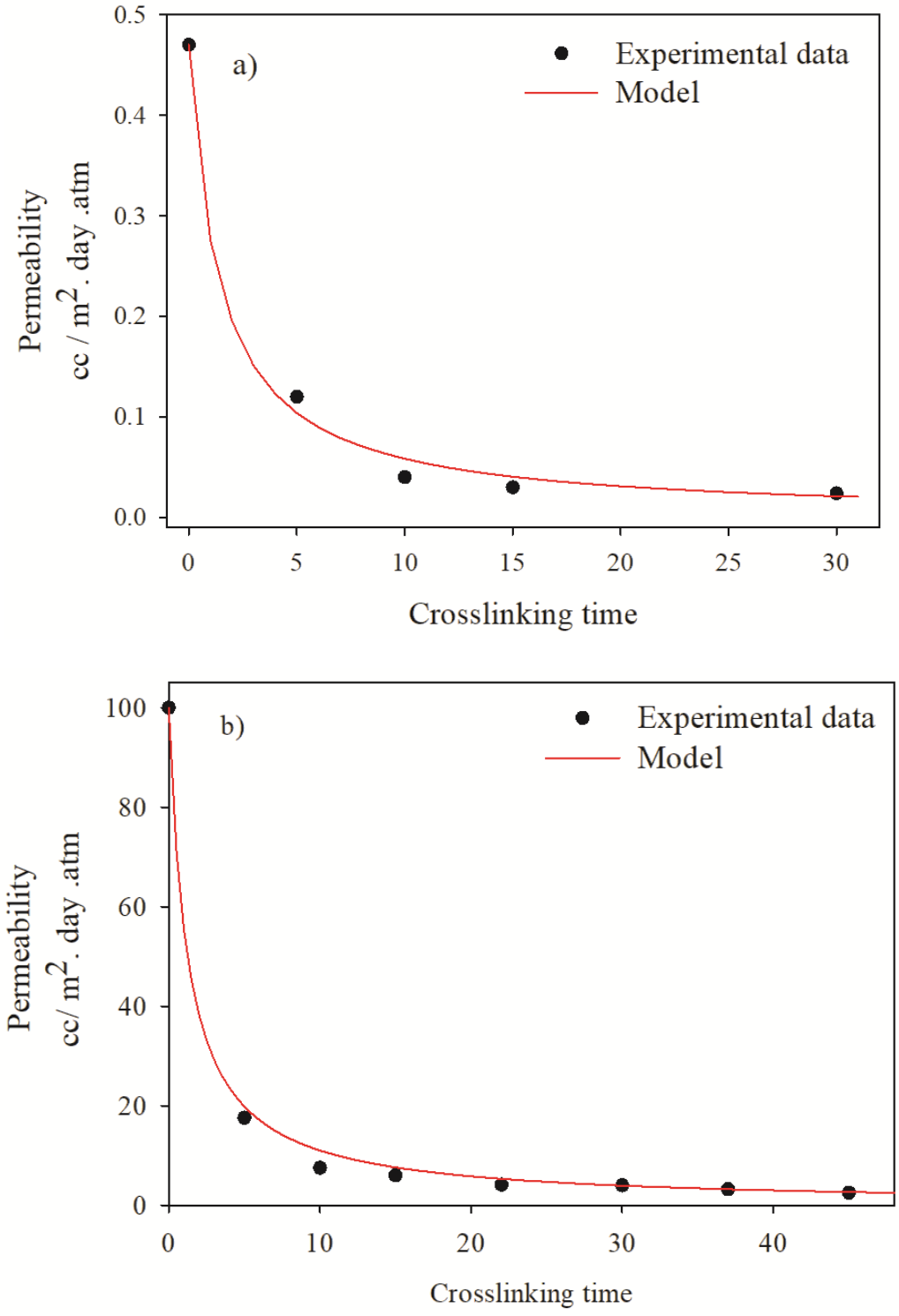

Figure 7.8 Reaction kinetic of a) PVA-MMT and b) PVA coatings without reversibility

7.4 Conclusion

Crosslinking reaction of PVA with Gly for a LbL deposited film, was studied in this work. It was proven that despite working in heterogeneous systems as LbL, the acetal reaction was still reversible. This reaction mechanism was evaluated by the variation of the coated film permeability at various crosslinking times, which allowed to determine the multiple reversibility steps. It was also noticed that the use of fillers in the LbL film did not affect the reaction mechanism since the reversibility was still proven by the permeability and the FTIR studies. To avoid the reversible reaction mechanism, acidic conditions were necessary for the PVA crosslinking.

During the crosslinking study, a strong correlation between the FTIR absorption intensity and the permeability was observed and was interpreted as the result of the proportionality between the solubility coefficient and the crosslinked group concentration.

To complete the study, a kinetic model describing the PVA-Gly crosslinking reaction was performed. As a result, a second order reaction with respect to the Gly was proposed to evaluate the evolution of the permeability with the crosslinking time. The kinetic study was developed assuming that in LbL the polymer is usually in excess compared to the crosslinker, and the linear correlation between the permeability and the concentration of crosslinker, i.e. FTIR measurements. The proposed model with apparent reaction rate constants based on the proposed correlations fitted perfectly the experimental data. It was observed that the use of fillers in the coatings, MMT, increased the apparent reaction rate.

7.5 Acknowledgement

The authors are grateful for the financial support of 3SPack NSERC Industrial Research Chair by the Natural Science and Engineering Council of Canada (NSERC) and ProAmpac Inc. Company.

7.6 Supporting information

TGA thermograms and XRD patterns for different crosslinking times.

REFERENCES

1. Laufer, G.; Kirkland, C.; Cain, A. A.; Grunlan, J. C., Clay-chitosan nanobrick walls: completely renewable gas barrier and flame-retardant nanocoatings. *ACS Appl Mater Interfaces* **2012,** *4* (3), 1643-9.
2. Yagoub, H.; Ma, S.; Yang, S.; Xu, J., Preparation and characterisation of cellulose nanocrystals thin films utilising layer-by-layer deposition. *Mater Res Innov* **2014,** *18* (sup4), S4-821-S4-824.
3. Luksiene, Z.; Buchovec, I., Impact of chlorophyllin-chitosan coating and visible light on the microbial contamination, shelf life, nutritional and visual quality of strawberries. *Innovative Food Science & Emerging Technologies* **2019**.
4. Ploehn, H. J.; Liu, C. Y., Quantitative analysis of montmorillonite platelet size by atomic force microscopy. *Industrial & Engineering Chemistry Research* **2006,** *45* (21), 7025-7034.
5. Ha Thuc, C. N.; Cao, H. T.; Nguyen, D. M.; Tran, M. A.; Duclaux, L.; Grillet, A. C.; Ha Thuc, H., Preparation and Characterization of Polyurethane Nanocomposites Using Vietnamese Montmorillonite Modified by Polyol Surfactants. *Journal of Nanomaterials* **2014,** *2014*, 1-11.
6. Cho, C.; Wallace, K. L.; Hagen, D. A.; Stevens, B.; Regev, O.; Grunlan, J. C., Nanobrick wall multilayer thin films grown faster and stronger using electrophoretic deposition. *Nanotechnology* **2015,** *26* (18), 185703.
7. Decher, G.; Ebler, F.; Hong, J. D.; Lowack, K.; Schmitt, J.; Lvov, Y., Layer-by-layer adsorbed films of polyelectrolytes, proteins or DNA. *Polymer Preprints, Division of Polymer Chemistry, American Chemical Society* **1993,** *34* (1), 745-745.
8. Cui, Y. B.; Kumar, S.; Kona, B. R.; van Houcke, D., Gas barrier properties of polymer/clay nanocomposites. *Rsc Adv* **2015,** *5* (78), 63669-63690.
9. Vartiainen, J.; Harlin, A., Crosslinking as an Efficient Tool for Decreasing Moisture Sensitivity of Biobased Nanocomposite Films. *Materials Sciences and Applications* **2011,** *02* (05), 346-354.
10. Patro, T. U.; Wagner, H. D., Influence of graphene oxide incorporation and chemical cross-linking on structure and mechanical properties of layer-by-layer assembled poly(Vinyl alcohol)-Laponite free-standing films. *Journal of Polymer Science Part B: Polymer Physics* **2016,** *54* (22), 2377-2387.
11. Zhang, Y.; Zhu, P.; Edgren, D., Crosslinking reaction of poly(vinyl alcohol) with glyoxal. *J Polym Res* **2009,** *237* (5), 725-730.
12. Figueiredo, K. C. S.; Alves, T. L. M.; Borges, C. P., Poly(vinyl alcohol) films crosslinked by glutaraldehyde under mild conditions. *Journal of Applied Polymer Science* **2009,** *111* (6), 3074-3080.
13. Rudra, R.; Kumar, V.; Kundu, P. P., Acid catalysed cross-linking of poly vinyl alcohol (PVA) by glutaraldehyde: effect of crosslink density on the characteristics of PVA membranes used in single chambered microbial fuel cells. *Rsc Adv* **2015,** *5* (101), 83436-83447.
14. Ogata, Y.; Okano, M.; Ganke, T., Kinetics of the Formation of the Formal of Polyvinyl Alcohol. *Journal of the American Chemical Society* **1956,** *78* (13), 2962-2964.
15. Kormanovskaya, G. N.; Vlodavets, I. N., Kinetics of the homogeneous interaction of polyvinyl alcohol with formaldehyde in aqueous solutions. *Russ Chem Bull* **1964,** *13* (10), 1661-1666.
16. Rumyantsev, M.; Zelentsov, S. V.; Gushchin, A. V., Retardation effect in acetalization of poly(vinyl alcohol) with butyraldehyde. *European Polymer Journal* **2013,** *49* (6), 1698-1706.
17. Wang, Z. F.; Wang, B.; Qi, N.; Zhang, H. F.; Zhang, L. Q., Influence of fillers on free volume and gas barrier properties in styrene-butadiene rubber studied by positrons. *Polymer* **2005,** *46* (3), 719-724.
18. Choudalakis, G.; Gotsis, A. D., Permeability of polymer/clay nanocomposites: A review. *Eur Polym J* **2009,** *45* (4), 967-984.

CHAPTER 8 GENERAL DISCUSSION

Sustainable packaging has nowadays become a major concern worldwide and particularly in Canada. Multilayers structure represents a considerable part of the packaging material and finding an alternative is a major challenge. One of the promising solutions is to replace the barrier layer by a coating. This, as was presented in this work, can be deposited by the LbL technique.

The choice of PET as substrate and the MMT as filler, for these coated substrates, was due to their availability in the laboratory. As we used a primer to enhance the adhesion of these coatings to the substrate, LbL coatings could also be deposited on other substrates and the choice of another clay with a different aspect ratio will induce different permeability results.

As this technique results in very thin coatings, its characterization was not always straightforward. To have a clear image of the microstructure, for example, TEM was used but didn't have satisfying outcome as the coating couldn't be localized in the mold. Also, to have thicker coatings suitable for mechanical testing more layers need to be deposited which is not possible for manual coating. Such structure (hundreds of layers) needs to be deposited with an automatic coater.

This coating would have been interesting to characterize separately from the substrate. Unfortunately, this was only possible for the FTIR characterization, as silicon plates transparent to infra red were used as substrates. For other types of characterization, however, the main problem was to detach the coating from the substrate without deteriorating it.

The deposition of LbL coatings by dipping technique allowed a better understanding of the interaction between the polymers and the filler. Since this technique requires a contact between the coated substrate and the polymer or clay solution, the volume of the deposited layer and its interdiffusion in the other layers is mainly governed by the affinity of these components and the extent of their bonding. This technique is interesting for fundamental study as the deposited amount of material depend only in the affinity between layers, however, it's time consuming due to the several hours needed to deposit one coating. In a try to reduce the experimental time, the clay was added first to the polymer solution and then deposited as a layer instead of depositing the clay separately from the polymer. This approach however, resulted in a higher permeability of deposited layers of the mix (10 layers of the mix compared to 10 bilayers). A preliminary sonication or longer

mixing time may improve this permeability but it wasn't investigated in this work and only the structure with separate layers of MMT was considered.

In the interpretation of the permeability results a reference was made to the rigidity and the cyclic structure of CS to explain the obtained permeability for the LbL structure with CS layer. This however should only be based on the rigidity of CS as this polymer doesn't have cyclic groups.

The characterization of the clay orientation shed light on the effect of the polymer structure on the clay orientation and intercalation. Orientation was similar for these polymers, with a better orientation for PVA-MMT bilayer. Due to the clay-polymer interaction, the effect clay may have on the polymer structure was also discussed. This interest in orientation is due to the general association of the reduction of permeability with the improvement of the tortuosity. This is the reason why many permeability models vary from one another by their representation of this tortuosity. In this work, we tried to interpret this tortuosity with the obtained results of the orientation and intercalation of the clay, but we didn't quantify this tortuosity.

Based on known permeability models, e.g. Cussler or Nielsen, the role of clay's interfacial region in reducing the permeability was considered. Due to the high loading of clay (>50 wt.%), the existing models were unable to properly fit the permeability of LbL coatings. Therefore, some models could be adapted by adding to the barrier of PVA and clay, the effect of the interfacial region (surrounding clay platelets), where PVA is denser. This region becomes considerable in the case of LbL coating due to the high loading of fillers. By including into Nielsen's model, a factor (β) to consider the increase of the impermeable region, the permeability model was able to fit better the LbL permeability.

We associated the good fitting to an increase of interfacial region, but we didn't quantify the thickness of this region, meaning that this improvement could also be due to another parameter that we didn't consider.

As a conclusion for the first part it was stated that other types of coating will be studied. That indeed was conducted but the results were not judged pertinent to report. As an example, the bilayer structure PEI-MMT was investigated and its permeability was higher than the one of PVA-MMT coating.

Other fillers were also investigated like Cellulose nanocrystals (CNC) and graphene oxide. A mix of these fillers with PVA resulted in a higher permeability than PVA-MMT mix which led to shift

the focus only on PVA-MMT. CNC and graphene oxide fillers may give interesting results with other polymers and with a prior preparation (sonication, grafting….).

Subsequently, the aim of this study of LBL deposited coatings is to extend its application to industry, which led to the use of blade coating as it's a faster and more prone to scale up technique than dipping. To evaluate the efficiency of this technique, a comprehensive comparison with dipping in terms of oxygen barrier was made for PVA-MMT coatings.

Both coatings (bladed and dipped) were crosslinked in a first place and their composition (PVA and clay concentration) was modified. Since the oxygen permeability at high relative humidity is a major concern in packaging, it was chosen as the main parameter to evaluate the performance of these coating techniques. The outcome of this study showed that increasing the hydrogen bonding in the coating gave lower permeability at high humidity than crosslinking or increasing clay concentration. Dipping resulted in better barrier at high relative humidity, nonetheless, its adaptability to industrial scale compared to blading is still a main concern.

Even though permeability results were different for these techniques, similar WVP results were obtained for crosslinked and non crosslinked coating for both dipping and blading, meaning that WVP is more affected by the coating structure than by the coating deposition technique.

This crosslinking has been conducted for a reasonable time (5 min) and a considerable decrease of the permeability was obtained. As the review of the literature showed a divergence in the reported crosslinking times, going from few minutes to several hours, a study of the kinetic of PVA crosslinking with Gly was performed to determine the optimum conditions.

The aim of this study was first to investigate the reversibility of this two-steps reaction by conducting the crosslinking under mild conditions. Following the changes in permeability in function of the crosslinking time, led to interesting results. The increase in permeability, due to the reverse reaction, was higher at first but then went to lower values with longer crosslinking times. This was explained by the different state of crosslinking and the predominance of a certain state (hemi acetal, acetal).

To investigate the kinetic of this reaction, reversibility was suppressed by the addition of acid. As determining the exact concentration of glyoxal was not possible, the kinetic study was based on a correlation between the FTIR absorption intensity and the permeability. This study was not complete as the reaction rate constant still to be determined.

For this reaction kinetic, an interesting parameter to investigate is the crosslinking temperature, by conducting this crosslinking at higher temperature, as it will affect the reaction rate constant, which was not studied in this work.

This work was mainly based on permeability testing which required days of testing. The used MOCON apparatus have two chambers allowing to test two films at a time. To test the permeability at high relative humidity, the main concern was to adjust the RH at 70% exactly, as even a value of 69% or 71% changed the permeability. For such low values of oxygen permeability, a preliminary testing cycle with nitrogen as permeant gas is required. Once this cycle done, a second cycle with oxygen as permeant gas is started. This procedure takes at least two days to have an accurate result. This long testing time and the dipping time needed to deposit the coatings, are the most time consuming steps of this work.

One of the main concerns when studying LbL technique is its upscale as the number of layers must be reduced and the drying optimized in order to keep a high-speed coating process.

Among the limits of this work is the lack of industrial trial and that all the deposited coatings were only deposited by LbL, with a thickness of individual layers lower than a 100 nm. Using a bench coater would have enabled the deposition of fewer layers with higher thickness. In such case depositing the polymer/ clay mix would probably result in a better barrier than LbL technique.

CHAPTER 9 CONCLUSION AND RECOMMENDATIONS

9.1 Conclusion

In this dissertation, nanocomposite coatings of MMT with different polymers (PVP, PVA, PEO and CS) were deposited on a PET substrate with the LbL technique. The oxygen permeability, the coating morphology and the clay properties were studied. The choice of polymers was based on the aimed type of bonding in the coating, which was hydrogen bonding. Results showed that the affinity of those polymers to the clay affects the clay intercalation and orientation as well as the coating morphology. As LbL deposition enables to reach high filler loading in the coating, the comparison of the obtained permeability coefficients of those coatings with permeability models led to the conclusion that for this type of nanocomposites, the interfacial region becomes considerable and should, thus, be taking into account when modeling the permeability. To do so, Nielsen's model was modified by introducing a constant to increase the volume fraction of the impermeable region and this modified model fitted better the experimental results.

In the second part of this work, the focus was on the blading technique as it's more similar to industrial coating techniques than dipping. PVA-MMT coatings were deposited by these two techniques on a PET substrate, and were crosslinked with two dialdehydes, glyoxal and glutaraldehyde. The permeability to oxygen of these coatings was determined for different values of relative humidity and the surface hydrophobicity was characterized. Crosslinking reduced considerably the permeability for high relative humidity, especially with glyoxal in the case of dipped coatings which is due to less free hydroxyl groups in the coating that can interact with water. In the case of blade coating, however, there was a sharp increase in the permeability at high relative humidity, for the coating crosslinked with glyoxal which was explained by a high amount of non reacted glyoxal molecules in the coating due to the short drying time. This was also confirmed by the surface hydrophobicity, as this coating had the highest hydrophilicity among crosslinked and no coating, due to a higher amount of hydroxyl groups. Beside crosslinking, tailoring the PVA and MMT concentrations in the coating to improve the oxygen barrier, was also studied. By increasing the concentration of the PVA solution, FTIR results showed that there was a higher amount of PVA deposited in the coating. The higher the concentration, the better was the barrier to oxygen at 0 and 70 % RH due to a denser hydrogen bonding. Increasing the concentration of the MMT solution increased the amount of MMT in the coating but improved the barrier only up to a certain

concentration beyond which permeability increased. A high filler loading in the coating may, at some point leads to agglomeration and can even disrupt the hydrogen bonding. Compared to crosslinking, increasing the concentration of PVA led to better results.

The better permeability results obtained by crosslinking with glyoxal, compared to glutaraldehyde, was the first motive for the third part of this work. In this study, crosslinking of two types of coatings, PVA and PVA -MMT with glyoxal was investigated. Mild conditions were first applied, in order to define the steps of this reaction. To do so, permeability of those coatings for different crosslinking times was determined. Plotting permeability in function of crosslinking time enabled a clear identification of the crosslinking steps. This reversibility caused a constant variation in the permeability as its values kept increasing and decreasing repeatedly. This fluctuation was only during the first 37 minutes of crosslinking, and the reached maxima of permeability were decreasing with longer times. Over 37 minutes, permeability was lower than 0.06 $cc/m^2.day.atm$. This was interpreted by the predominance of acetals in the coating. Characterizing those coatings with FTIR led to a correlation of the permeability coefficient and the absorption intensity. Based on this correlation and the fact that PVA is in excess for this heterogeneous reaction, the reaction kinetic was studied. To understand the kinetic of crosslinking, acid environment was used to avoid reversibility and the apparent reaction rate constant was determined. This constant was higher for nanocomposite coatings

9.2 Recommendations

In the previous section, the accomplished work during this thesis was briefly described and the main achievements were summarized. For future research and as a continuation of this work, the following subjects are recommended:

- the kinetic study of PVA crosslinking with glyoxal can be improved by determining the reaction rate constant.

- Reversibility of the PVA crosslinking reaction, can be further studied by determining the effect of high concentrations of PVA and Glyoxal in the steps and extent of reversibility.

- The FTIR-Permeability correlation can be investigated, in order to understand its variation with the polymer and clay concentrations. This would decrease the permeability characterization time

as well as the time needed to prepare the samples. This correlation can also be applied to other coating techniques.

- Based on the blade coating results, LbL coating can be scaled up. To deposit fewer layers, polymer and clay concentrations must be tailored. For this, the exact deposited volume and concentrations for each coating should be accurately characterized in order to compare it with industrial scale coater capacity.

REFERENCES

1. Cui, Y. B.; Kumar, S.; Kona, B. R.; van Houcke, D., Gas barrier properties of polymer/clay nanocomposites. *Rsc Adv* **2015,** *5* (78), 63669-63690.
2. Selke, S. E. M., *understanding plastics packaging technology*. Hanser publishers: Munich, 1997.
3. Susan E. M. Selke; Culter, J. D.; Hernandez, R. J., *Plastics Packaging: Properties, Processing, Applications, and Regulations*. 2004.
4. Hiltner, A.; Liu, R. Y. F.; Hu, Y. S.; Baer, E., Oxygen transport as a solid-state structure probe for polymeric materials: A review. *Journal of Polymer Science Part B: Polymer Physics* **2005,** *43* (9), 1047-1063.
5. *plastics extrusion technology*. Hanser Pub.: Munich, 1988.
6. Pauly, S., Permeability and diffusion data. In *Polymer Handbook*, J, B.; EH, I.; EA, G., Eds. JohnWiley&Sons,Inc. : New York, 1999.
7. Flodberg, G.; Hellman, A., Barrier Properties of Blends Based on Liquid CrystaI I ine PolIymers and Polyethylene. *Polymer Engineering and Science* **2000,** *40* (9), 1969-1978.
8. Hu, Y. S.; Prattipati, V.; Mehta, S.; Schiraldi, D. A.; Hiltner, A.; Baer, E., Improving gas barrier of PET by blending with aromatic polyamides. *Polymer* **2005,** *46* (8), 2685-2698.
9. Hedenqvist, M. S., Barrier Packaging Materials. In *Handbook of Environmental Degradation of Materials*, 2012; pp 833-862.
10. Nguyen, Q. T.; Baird, D. G., Preparation of polymer–clay nanocomposites and their properties. *Advances in Polymer Technology* **2006,** *25* (4), 270-285.
11. Nielsen, L. E., Models for the Permeability of Filled Polymer Systems. *Journal of Macromolecular Science: Part A - Chemistry* **1967,** *1* (5), 929-942.
12. MacKnight, W. J.; Karasz, F. E., Polymer Blends. In *Comprehensive Polymer Science and Supplements*, Allen, G.; Bevington, J. C., Eds. Pergamon: Amsterdam, 1989; pp 111-130.
13. Reichelt, K.; Jiang, X., The Preparation of Thin-Films by Physical Vapor-Deposition Methods. *Thin Solid Films* **1990,** *191* (1), 91-126.
14. Bieder, A.; Gruniger, A.; von Rohr, P. R., Deposition of SiOx diffusion barriers on flexible packaging materials by PECVD. *Surf Coat Tech* **2005,** *200* (1-4), 928-931.
15. Benmalek M; HM., D., Inorganic coatings on polymers. *Surf Coat Technol* **1995,** *76-77*, 821-826.
16. Bichler, C. H.; Langowski, H. C.; Moosheimer, U.; Seifert, B., Adhesion mechanism of aluminum, aluminum oxide, and silicon oxide on biaxially oriented polypropylene (BOPP), poly(ethyleneterephthalate) (PET), and poly(vinyl chloride) (PVC). *Journal of Adhesion Science and Technology* **1997,** *11* (2), 233-246.
17. Chatham, H., Oxygen diffusion barrier properties of transparent oxide coatings on polymeric substrates. *Surf Coat Tech* **1996,** *78* (1-3), 1-9.
18. Leterrier, Y., Durability of nanosized oxygen-barrier coatings on polymers - Internal stresses. *Progress in Materials Science* **2003,** *48* (1), 1-55.
19. Toor, A.; So, H.; Pisano, A. P., Improved Dielectric Properties of Polyvinylidene Fluoride Nanocomposite Embedded with Poly(vinylpyrrolidone)-Coated Gold Nanoparticles. *ACS Appl Mater Interfaces* **2017,** *9* (7), 6369-6375.
20. Vozar, S.; Poh, Y. C.; Serbowicz, T.; Bachner, M.; Podsiadlo, P.; Qin, M.; Verploegen, E.; Kotov, N.; Hart, A. J., Automated spin-assisted layer-by-layer assembly of nanocomposites. *The Review of scientific instruments* **2009,** *80* (2), 023903.
21. Seiji Kuroda; Jin Kawakita; MakotoWatanabe; Katanoda, H., Warm spraying—a novel coating process based on high-velocity impact of solid particles. *Sci. Technol. Adv. Mater.* **2008,** (9).
22. *Nanocoatings and ultra-thin films*. Woodhead Publishing Limited: 2011.

23. Burgués-Ceballos, I.; Stella, M.; Lacharmoise, P.; Martínez-Ferrero, E., Towards industrialization of polymer solar cells: material processing for upscaling. *J. Mater. Chem. A* **2014,** *2* (42), 17711-17722.
24. Nguyen-Tri, P.; Nguyen, T. A.; Carriere, P.; Ngo Xuan, C., Nanocomposite Coatings: Preparation, Characterization, Properties, and Applications. *International Journal of Corrosion* **2018,** *2018*, 1-19.
25. Kharlampieva, E.; Kozlovskaya, V.; Sukhishvili, S. A., Layer-by-Layer Hydrogen-Bonded Polymer Films: From Fundamentals to Applications. *Advanced Materials* **2009,** *21* (30), 3053-3065.
26. Patro, T. U.; Wagner, H. D., Influence of graphene oxide incorporation and chemical cross-linking on structure and mechanical properties of layer-by-layer assembled poly(Vinyl alcohol)-Laponite free-standing films. *Journal of Polymer Science Part B: Polymer Physics* **2016,** *54* (22), 2377-2387.
27. Bailey, L.; Lekkerkerker, H. N.; Maitland, G. C., Smectite clay--inorganic nanoparticle mixed suspensions: phase behaviour and rheology. *Soft matter* **2015,** *11* (2), 222-36.
28. Pavlidou, S.; Papaspyrides, C. D., A review on polymer-layered silicate nanocomposites. *Progress in Polymer Science* **2008,** *33* (12), 1119-1198.
29. Galgali, G.; Agarwal, S.; Lele, A., Effect of clay orientation on the tensile modulus of polypropylene-nanoclay composites. *Polymer* **2004,** *45* (17), 6059-6069.
30. Cole, K. C.; Perrin-Sarazin, F.; Dorval-Douville, G., Infrared spectroscopic characterization of polymer and clay platelet orientation in blown films based on polypropylene-clay nanocomposite. *Macromolecular Symposia* **2005,** *230* (1), 1-10.
31. Farmer, V. C., *The Infrared Spectra of Minerals* Mineralogical Society of Great Britain and Ireland: London, 1974; Vol. 4.
32. Cole, K. C.; Depecker, C.; Jutigny, M.; Lefebvre, J. M.; Krawczak, P., Biaxial deformation of polyamide-6: Assessment of orientation by means of infrared trichroism. *Polym Eng Sci* **2004,** *44* (2), 231-240.
33. j. brandrup; e. h. immergut; grulke, e. a., *Polymer Handbook (Fourth Edition)*. Wiley: New York, 1999.
34. Bartczak, Z.; Rozanski, A.; Richert, J., Characterization of clay platelet orientation in polylactide-montmorillonite nanocomposite films by X-ray pole figures. *European Polymer Journal* **2014,** *61*, 274-284.
35. Fereydoon, M.; Tabatabaei, S. H.; Ajji, A., Effect of Uniaxial Stretching on Thermal, Oxygen Barrier, and Mechanical Properties of Polyamide 6 and Poly(m-xylene adipamide) Nanocomposite Films. *Polymer Engineering and Science* **2015,** *55* (5), 1113-1127.
36. Priolo, M. A.; Holder, K. M.; Guin, T.; Grunlan, J. C., Recent Advances in Gas Barrier Thin Films via Layer-by-Layer Assembly of Polymers and Platelets. *Macromol. Rapid Commun.* **2015,** *36* (10), 866-79.
37. Corni, I.; Harvey, T. J.; Wharton, J. A.; Stokes, K. R.; Walsh, F. C.; Wood, R. J., A review of experimental techniques to produce a nacre-like structure. *Bioinspiration & biomimetics* **2012,** *7* (3), 031001.
38. de Villiers, M. M.; Otto, D. P.; Strydom, S. J.; Lvov, Y. M., Introduction to nanocoatings produced by layer-by-layer (LbL) self-assembly. *Advanced drug delivery reviews* **2011,** *63* (9), 701-15.
39. Elżbieciak-Wodka, M.; Kolasińska-Sojka, M.; Nowak, P.; Warszyński, P., Comparison of permeability of poly(allylamine hydrochloride)/and poly(diallyldimethylammonium chloride)/poly(4-styrenesulfonate) multilayer films: Linear vs. exponential growth. *Journal of Electroanalytical Chemistry* **2015,** *738*, 195-202.
40. Laufer, G.; Kirkland, C.; Cain, A. A.; Grunlan, J. C., Clay-chitosan nanobrick walls: completely renewable gas barrier and flame-retardant nanocoatings. *ACS Appl Mater Interfaces* **2012,** *4* (3), 1643-9.
41. Xiang, F.; Ward, S. M.; Givens, T. M.; Grunlan, J. C., Structural tailoring of hydrogen-bonded poly(acrylic acid)/poly(ethylene oxide) multilayer thin films for reduced gas permeability. *Soft matter* **2015,** *11* (5), 1001-7.
42. Jang, W. S.; Rawson, I.; Grunlan, J. C., Layer-by-layer assembly of thin film oxygen barrier. *Thin Solid Films* **2008,** *516* (15), 4819-4825.

43. Lutkenhaus, J. L.; Hrabak, K. D.; McEnnis, K.; Hammond, P. T., Elastomeric flexible free-standing hydrogen-bonded nanoscale assemblies. *J Am Chem Soc* **2005,** *127* (49), 17228-34.
44. Guin, T.; Krecker, M.; Hagen, D. A.; Grunlan, J. C., Thick growing multilayer nanobrick wall thin films: super gas barrier with very few layers. *Langmuir : the ACS journal of surfaces and colloids* **2014,** *30* (24), 7057-60.
45. Philipp, B.; Dautzenberg, H.; Linow, K.-J.; Kötz, J.; Dawydoff, W., Polyelectrolyte complexes - recent developments and open problems. *Prog. Polym. Sci.* **1989,** *14*, 91-172.
46. Yang, Y. H.; Haile, M.; Park, Y. T.; Malek, F. A.; Grunlan, J. C., Super Gas Barrier of All-Polymer Multilayer Thin Films. *Macromolecules* **2011,** *44* (6), 1450-1459.
47. Kim, D.; Tzeng, P.; Barnett, K. J.; Yang, Y. H.; Wilhite, B. A.; Grunlan, J. C., Highly size-selective ionically crosslinked multilayer polymer films for light gas separation. *Adv Mater* **2014,** *26* (5), 746-51.
48. Sung, C.; Vidyasagar, A.; Hearn, K.; Lutkenhaus, J. L., Effect of thickness on the thermal properties of hydrogen-bonded LbL assemblies. *Langmuir : the ACS journal of surfaces and colloids* **2012,** *28* (21), 8100-9.
49. Podsiadlo, P.; Kaushik, A. K.; Arruda, E. M.; Waas, A. M.; Shim, B. S.; Xu, J.; Nandivada, H.; Pumplin, B. G.; Lahann, J.; Ramamoorthy, A.; Kotov, N. A., Ultrastrong and stiff layered polymer nanocomposites. *Science* **2007,** *318* (5847), 80-3.
50. Cook, R.; Chen, Y.; Beall, G. W., Highly ordered self-assembling polymer/clay nanocomposite barrier film. *ACS Appl Mater Interfaces* **2015,** *7* (20), 10915-9.
51. Stern, S. A., Polymers for gas separations: the next decade. *Journal of Membrane Science* **1994,** *94*, 1-65.
52. Koros, W. J.; Paul, D. R., CO2 sorption in poly(ethylene terephthalate) above and below the glass transition. *J Polym Sci Polym Phys* **1978,** *16* (11).
53. Beall, G. W., A New Model for Interpreting Nanocomposite Behavior. In *59th Annual Technical Conference – Society of Plastics Engineers*, 2001; Vol. 2.
54. Bharadwaj, R. K., Modeling the barrier properties of polymer-layered silicate nanocomposites. *Macromolecules* **2001,** *34* (26), 9189-9192.
55. Ben Dhieb, F.; Dil, E. J.; Tabatabaei, S. H.; Mighri, F.; Ajji, A., Effect of nanoclay orientation on oxygen barrier properties of LbL nanocomposite coated films. *Rsc Adv* **2019,** *9* (3), 1632-1641.
56. Gusev, A. A.; Lusti, H. R., Rational design of nanocomposites for barrier applications. *Adv. Mater.* **2001,** *13* (21), 1641-1643.
57. Nielsen, L. E., Models for the Permeability of Filled Polymer Systems. *Journal of Macromolecular Science: Part A - Chemistry* **1967,** *1* (5), 929-942.
58. Chuanfang Yang; W.H. Smyrl; Cussler, E. L., Flake alignment in composite coatings. *Journal of Membrane Science* **2004,** *231* 1–12.
59. E.L.Cussler; Hughes, S. E.; William J. Ward, I.; Aris, R., barrier membranes. *Journal of Membrane Science* **1988,** *38*, 161-174.
60. Maxwell, J. C., *A Treatise On Electricity and Magnetism*. Dover Publications, Inc.: New York, 1881; Vol. 1.
61. Lape, N. K.; Nuxoll, E. E.; Cussler, E. L., Polydisperse flakes in barrier films. *Journal of Membrane Science* **2004,** *236* (1), 29-37.
62. Sorrentino, A.; Tortora, M.; Vittoria, V., Diffusion behavior in polymer-clay nanocomposites. *Journal of Polymer Science Part B: Polymer Physics* **2006,** *44* (2), 265-274.
63. Mauser, T.; Dejugnat, C.; Sukhorukov, G. B., Reversible pH-dependent properties of multilayer microcapsules made of weak polyelectrolytes. *Macromolecular Rapid Communications* **2004,** *25* (20), 1781-1785.
64. Spinu, C.; Kriza, A., Co(II), Ni(II) and Cu(II) complexes of bidentate Schiff bases. *Acta Chim Slov* **2000,** *47* (2), 179-185.

65. Meadows, G. W.; Darwent, B. D. B., The kinetics of the reactions of acetaldehyde with methanol. *Transactions of the Faraday Society* **1952,** *48*.
66. Rudra, R.; Kumar, V.; Kundu, P. P., Acid catalysed cross-linking of poly vinyl alcohol (PVA) by glutaraldehyde: effect of crosslink density on the characteristics of PVA membranes used in single chambered microbial fuel cells. *Rsc Adv* **2015,** *5* (101), 83436-83447.
67. Zhang, Y.; Zhu, P.; Edgren, D., Crosslinking reaction of poly(vinyl alcohol) with glyoxal. *J Polym Res* **2009,** *237* (5), 725-730.
68. Ogata, Y.; Okano, M.; Ganke, T., Kinetics of the Formation of the Formal of Polyvinyl Alcohol. *Journal of the American Chemical Society* **1956,** *78* (13), 2962-2964.
69. Kormanovskaya, G. N.; Vlodavets, I. N., Kinetics of the homogeneous interaction of polyvinyl alcohol with formaldehyde in aqueous solutions. *Russ Chem Bull* **1964,** *13* (10), 1661-1666.
70. Figueiredo, K. C. S.; Alves, T. L. M.; Borges, C. P., Poly(vinyl alcohol) films crosslinked by glutaraldehyde under mild conditions. *Journal of Applied Polymer Science* **2009,** *111* (6), 3074-3080.

Appendix A Supporting information of the first article

Effect of Nanoclay Orientation on Oxygen Barrier Properties of LbL Nanocomposite Coated Films

Fatma Ben Dhieb[1], Ebrahim Jalali Dil[1], Seyed H. Tabatabaei[2], Frej Mighri[3] and Abdellah Ajji[1*]

[1] *3SPack NSERC-Industry Chair, CREPEC, Chemical Engineering Department, Polytechnique Montreal, C.P. 6079, Succ. Centre ville, Montreal, QC, Canada H3C 3A7*

[2] *ProAmpac, Terrebonne, QC, Canada J6Y 1V2*

[3] *CREPEC, Chemical Engineering Department, Laval University, Quebec, QC, Canada*

(*) All correspondence should be addressed to: *abdellah.ajji@polymtl.ca*

a)

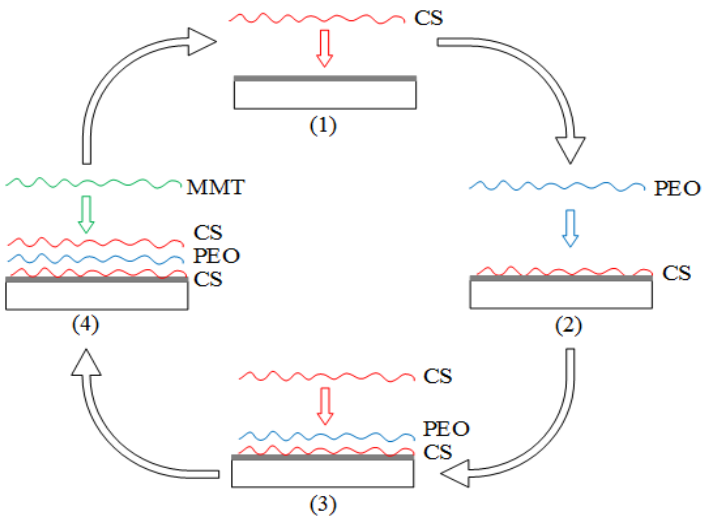

b)

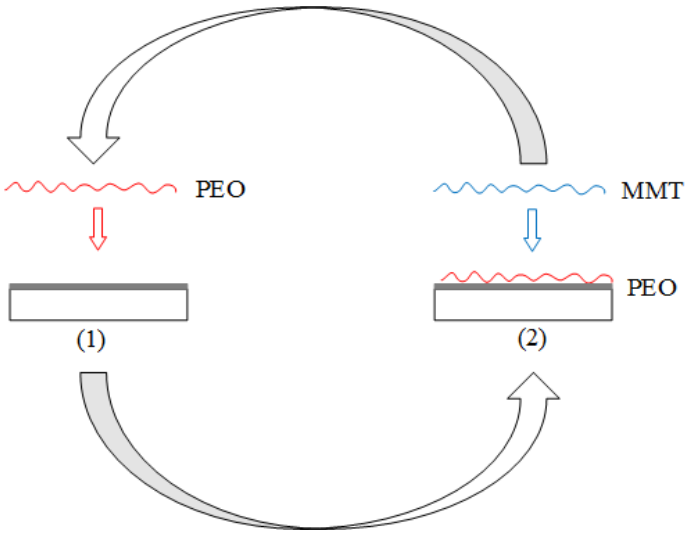

Figure S.1 Steps of the deposition of a) one quadlayer chitosan/PEO/chitosan/MMT and b) one bilayer PEO/MMT

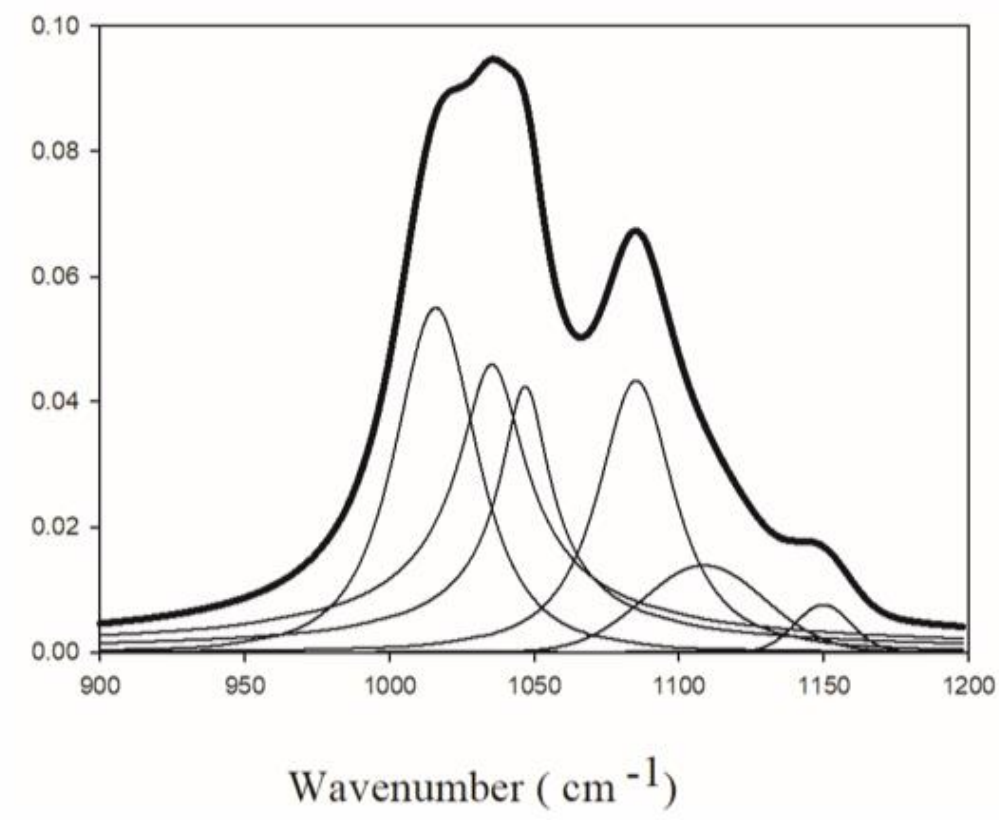

Figure S.2 Typical peak deconvolution of the S_0 spectrum for a PVA quadlayers

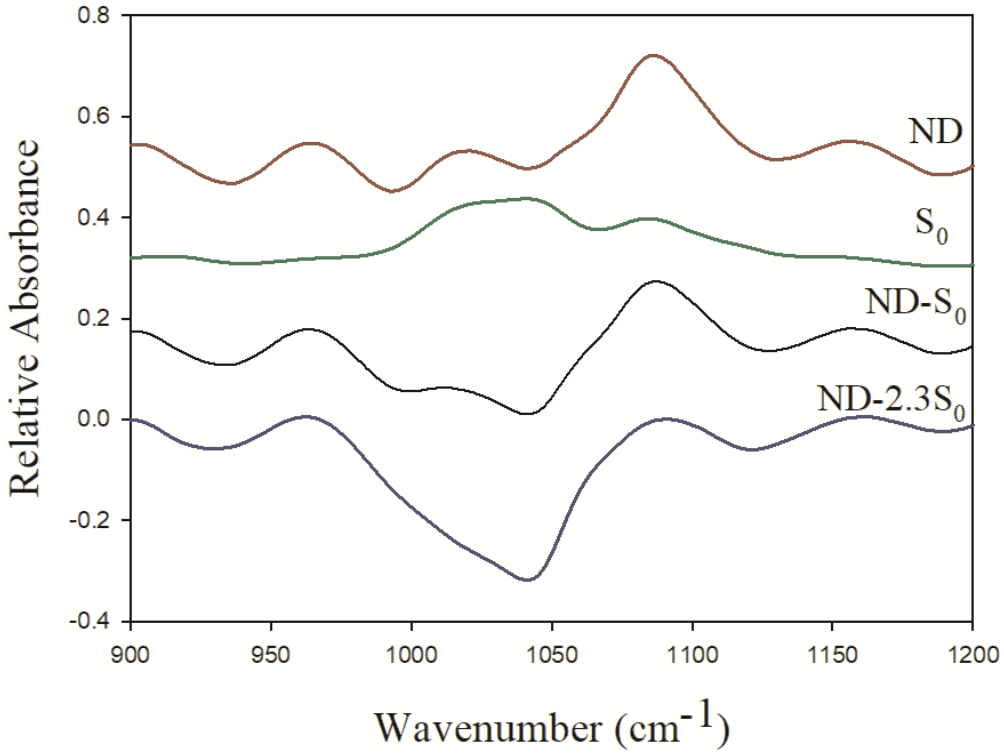

Figure S.3 Peak subtraction for a PVP quadlayers

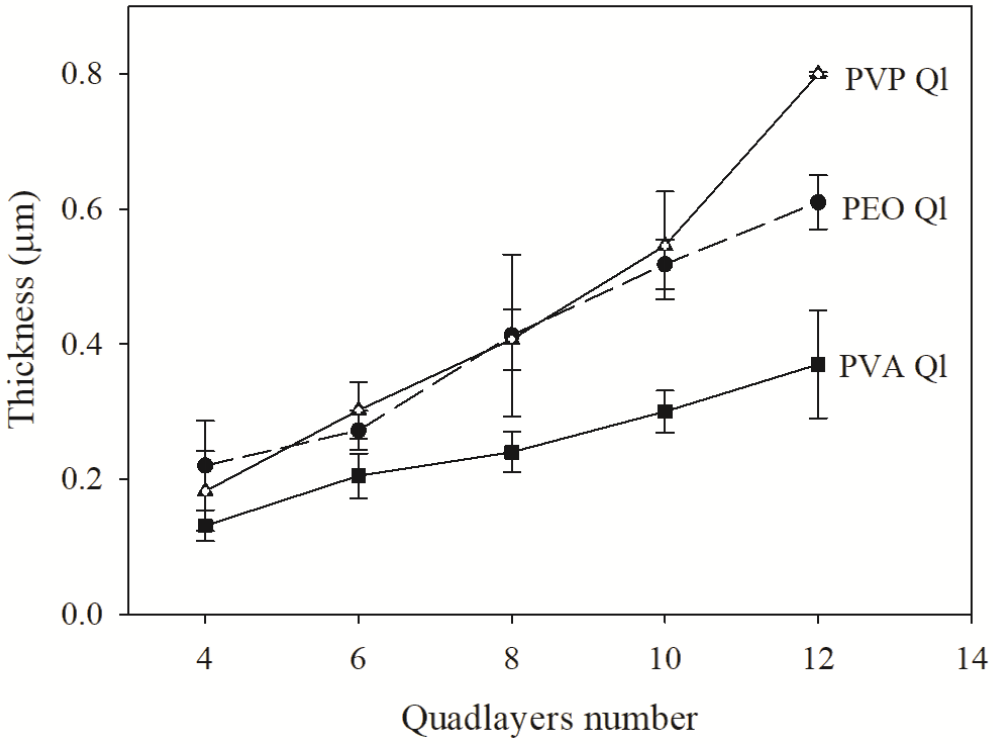

Figure S.4 Thickness variation with the number of layers for the three assemblies

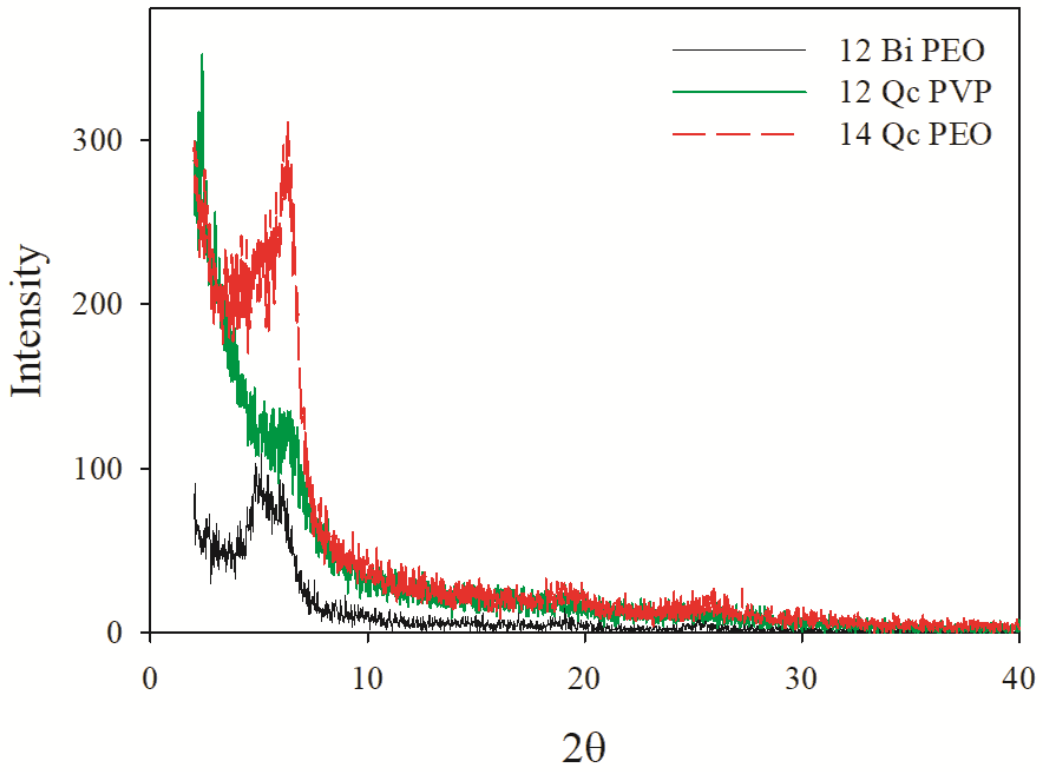

Figure S.5 XRD patterns of three of the studied assemblies

Appendix B Supporting information of the second article

Comparison of crosslinking efficiency in dip and roll deposited coatings on their oxygen barrier

Fatma Ben Dhieb[1], Seyed H. Tabatabaei[2], Frej Mighri[3] and Abdellah Ajji[1*]

[1] *3SPack NSERC-Industry Chair, CREPEC, Chemical Engineering Department, Polytechnique Montreal, C.P. 6079, Succ. Centre ville, Montreal, QC, Canada H3C 3A7*

[2] *ProAmpac, Terrebonne, QC, Canada J6Y 1V2*

[3] *CREPEC, Chemical Engineering Department, Laval University, Quebec, QC, Canada*

(*) All correspondence should be addressed to: *abdellah.ajji@polymtl.ca*

To determine the orientation of the nanoclay platelets in the coatings, infrared analysis was elaborated using a Spectrum 65 FTIR spectrometer from PerkinElmer (Waltham, MA) with a resolution of 4 cm^{-1} and a 32 scans accumulation within the wavenumber range of 900 to 1200 cm^{-1}. A Spectra-Tech zinc selenide wire grid polarizer from thermo Electron Corp was used to record three types of spectra; in the vertical machine direction, S_M, in the horizontal transverse direction, S_T and in the horizontal direction with a tilted film at an angle φ with respect to the machine direction (MD), S_{NT}. To avoid peaks saturation and overlapping, LDPE was used as substrate instead of PET. The Montmorillonite Si-O stretching bands are around 1080,1025, 1048,1120 cm^{-1} [30]. The peaks at 1025, 1048 and 1120 cm^{-1} correspond to the oxygen at the surface of the clay platelets (basal oxygen) and the peak at 1080 cm^{-1} is associated with the apical oxygen. This latter is the oxygen at the internal edge of the tetrahedral sheet, linked to Aluminum and having its Si-O bond perpendicular to platelet plane [31]. The spectrum in the normal direction, S_N, can be calculated with the following equation [32].

$$S_N = \frac{S_{NT}\left(1-\frac{sin^2\varphi}{n^2}\right)^{1/2} - S_T\left(1-\frac{sin^2\varphi}{n^2}\right)}{sin^2\varphi/n^2} \quad (1)$$

φ is equal to 45° and n, the refractive index of Montmorillonite has a value of 1.503 [33], S_0, a structurally independent spectrum, represent the arithmetic average of the 3 spectra, S_M, S_N and S_T. As the plane normal of the clay platelets can well characterize their orientation, the following Herman's orientation function [30], can be used to calculate this orientation:

$$f_{CN} = 0.5\left(\frac{A_N}{A_0} - 1\right) \quad (2)$$

Where, A_N and A_0 are the band intensities in the S_N and S_0 spectra corresponding to the peaks whose vibrational transition moment lies along the c-axis, normal to the platelets plane. The ratio $\left(\frac{A_N}{A_0}\right)$ is referred to as dichroic ratio, D. This function can also be written in function of the angle of orientation of clay:

$$f_{CN} = \frac{3\langle cos^2\theta\rangle - 1}{2} \quad (3)$$

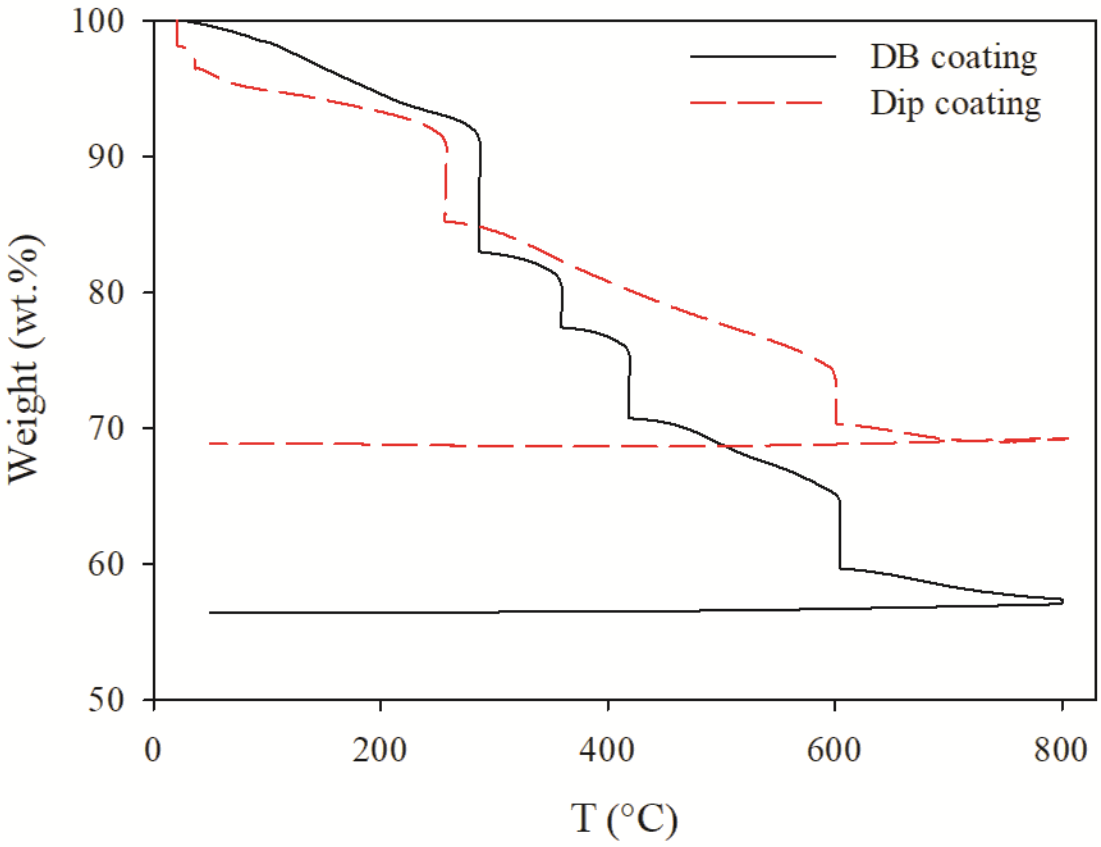

Figure S.1 TGA thermograms of dipped and bladed coatings

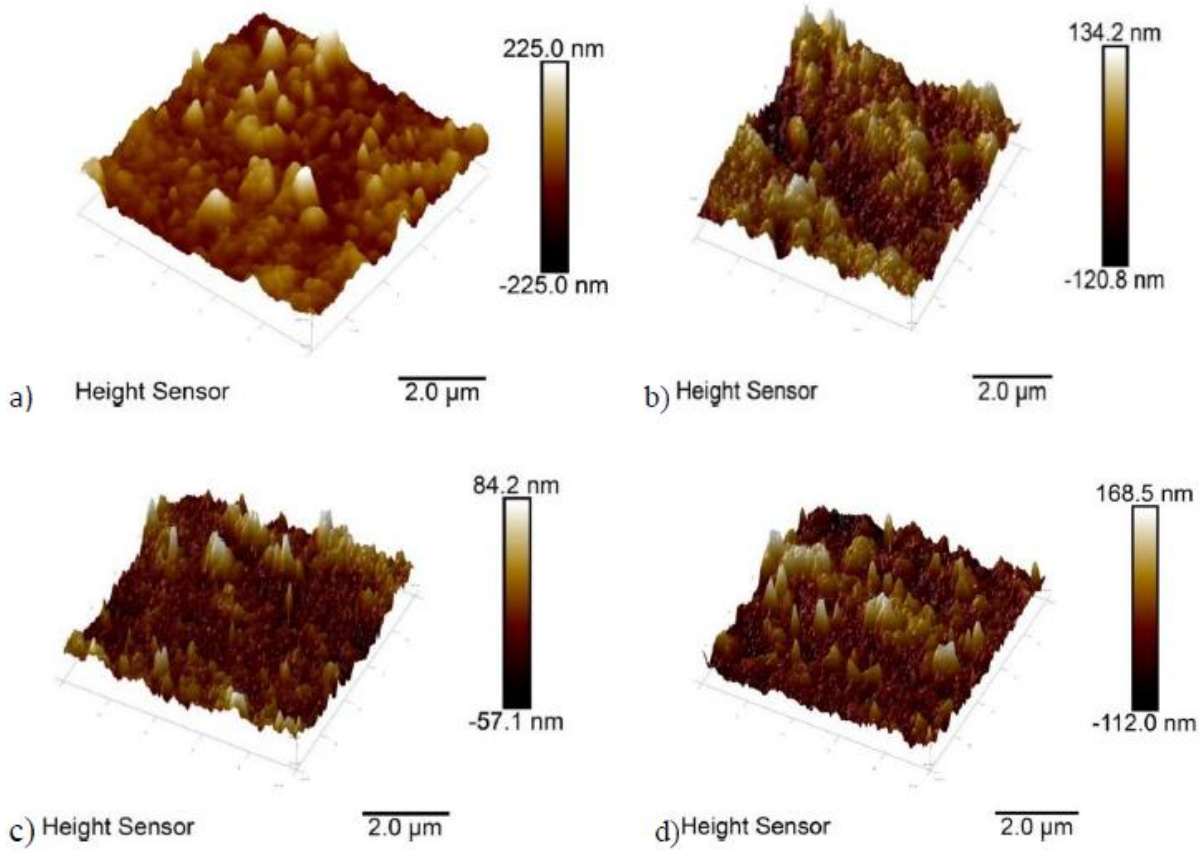

Figure S.2 AFM image of the surface roughness of a) Gly crosslinked dipped coating, b) Gly crosslinked bladed coating, c) bladed coating and d) dipped coating.

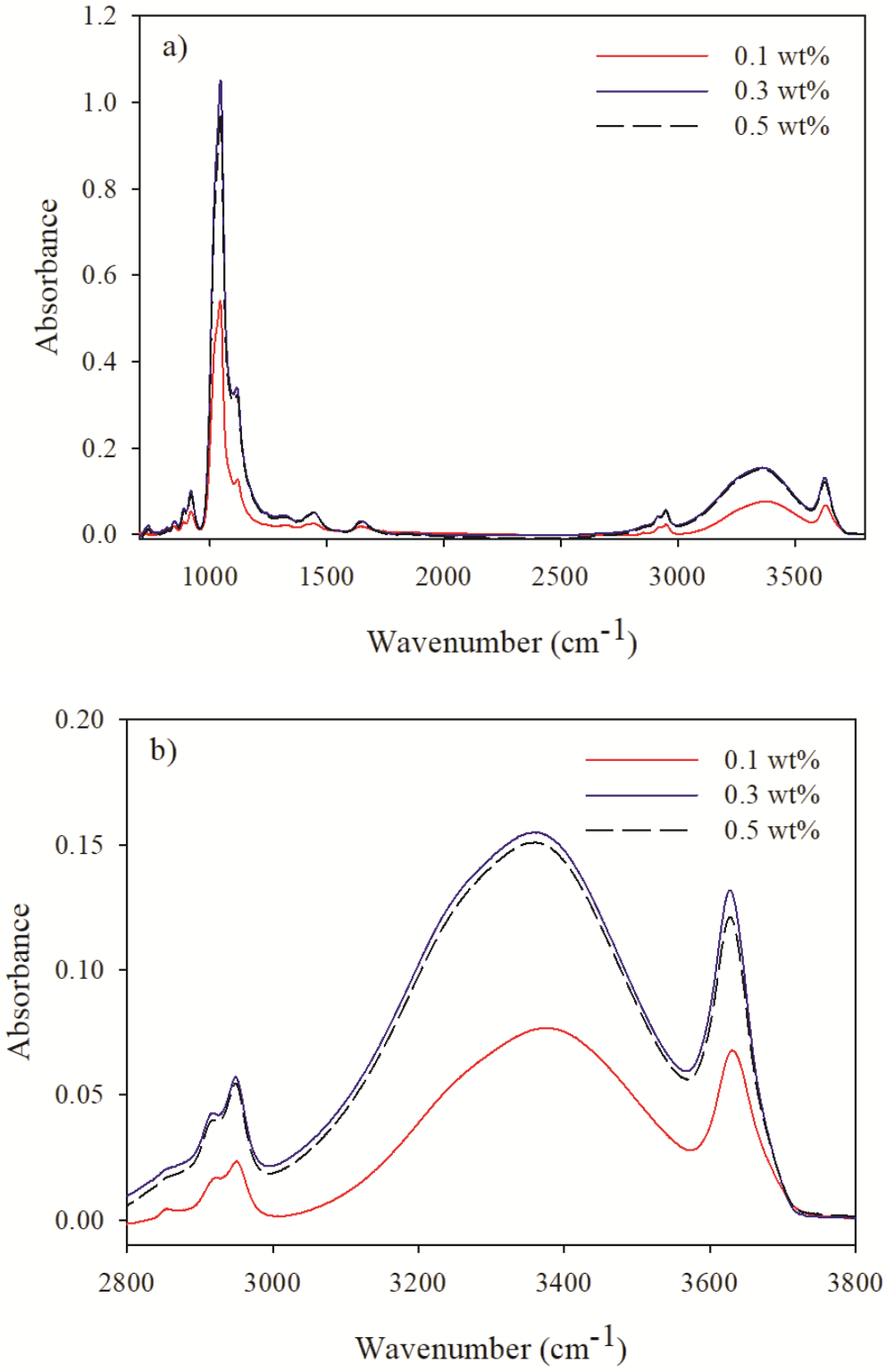

Figure S.3 FTIR spectra of PVA MMT coatings with different concentrations of PVA solution at different scales, a) from 600 to 3800 cm^{-1} and b) from 2800 to 3800 cm^{-1}.

Table S.1 Clay concentration, coating permeability and thickness for three different coating composition

coating	%MMT	Permeability ($cc.\mu m / m^2.day.atm$)	Thickness (μm)
PVA (0.1wt%)-MMT (0.5 wt%)	71	8.17	0.964
PVA (0.1 wt%)-MMT (3 wt%)	90	13.67	3.324
PVA (0.5 wt%)-MMT (0.5 wt%)	67	0.32	1.668

Appendix C Supporting information of the third article

Study of the crosslinking of PVA with glyoxal in LbL nanocomposites

Fatma Ben Dhieb[1], Adrián Carrillo García[2], Seyed H. Tabatabaei[3], Frej Mighri[4], Abdellah Ajji[1*]

1 3SPack NSERC-Industry Chair, CREPEC, Chemical Engineering Department, Polytechnique Montreal, C.P. 6079, Succ. Centre ville, Montreal, QC, Canada H3C 3A7

2 Chemical Engineering Department, Polytechnique Montreal, Montreal, QC, Canada

3 ProAmpac, Terrebonne, QC, Canada J6Y 1V2

4 CREPEC, Chemical Engineering Department, Laval University, Quebec, QC, Canada

(*) All correspondence should be addressed to: abdellah.ajji@polymtl.ca

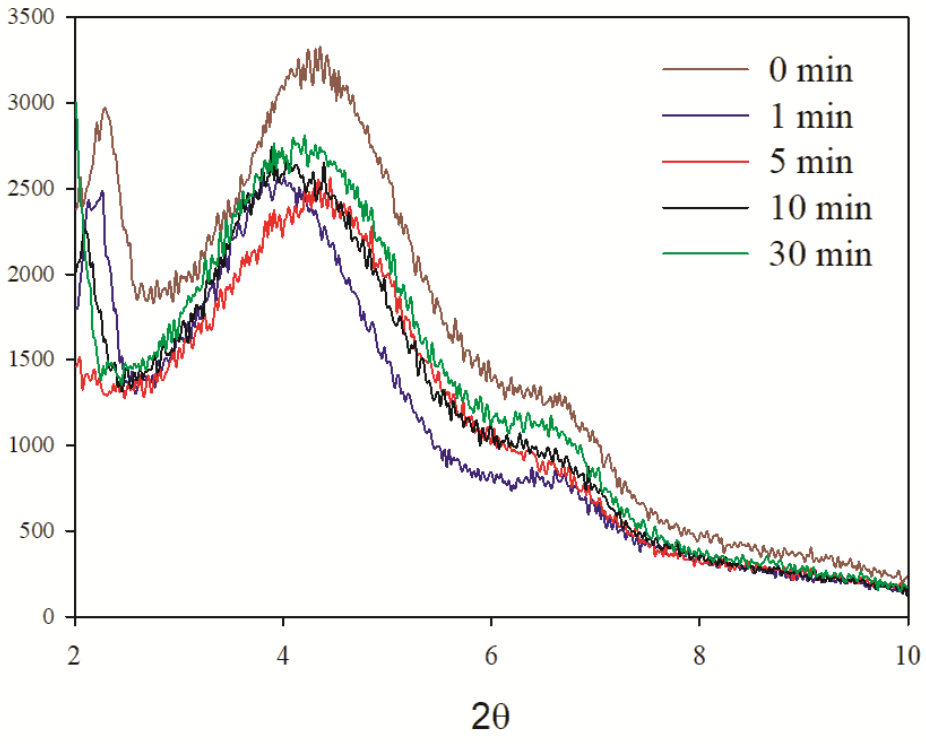

Figure S.1 XRD Patterns for different crosslinking times for a PVA-MMT coatings under mild conditions

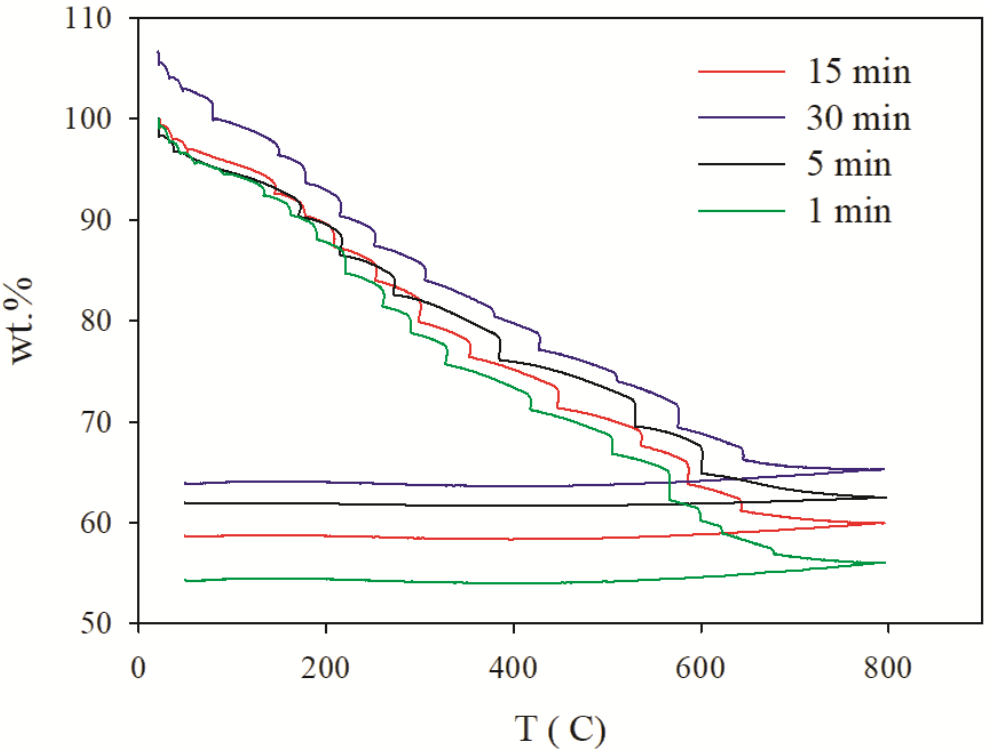

Figure S.2 TGA thermograms for crosslinked PVA-MMT coatings under mild condition